DISSERTATION

submitted to the

Combined Faculties for Natural Sciences and for Mathematics

of the Ruperto-Carola University of Heidelberg, Germany

for the degree of Doctor of Natural Science

presented by

Diplom-Ingenieurin (FH) Biologische Chemie, Sonja Zacherl

born in Pforzheim, Germany

Oral examination:

A Role for ATP1A1 in Unconventional Secretion of Fibroblast Growth Factor 2

Referees: Prof. Dr. Walter Nickel

Prof. Dr. Oliver Fackler

Table of Contents

Summary

Fibroblast growth factor 2 (FGF2) is a potent mitogen involved in many physiological processes such as cell proliferation, differentiation as well as angiogenesis and, therefore, has a prominent function in tumor growth. FGF2 is secreted via an unconventional pathway using a route that is independent from the endoplasmic reticulum and the Golgi apparatus. Secretion of FGF2 occurs by direct translocation across the plasma membrane in a folded state, which is initiated by binding to phosphatidylinositol-4,5-bisphosphate ($PI(4,5)P_2$) at the inner leaflet of the plasma membrane. In the extracellular space, membrane proximal heparan sulfate proteoglycans (HSPGs) are required to complete translocation as well as to store and protect FGF2 on cell surfaces. The interaction with $PI(4,5)P_2$ was shown to facilitate oligomerization of FGF2 leading to the formation of a lipidic membrane pore that has been interpreted as an intermediate structure in FGF2 membrane translocation. In addition, Tec kinase was discovered as a factor regulating FGF2 secretion by phosphorylating tyrosine 82 in FGF2. Recent evidence suggests that phosphorylation stabilizes the formation of FGF2 oligomers, which favors the arrangement of a transient hydrophilic pore constituted by FGF2 molecules in the plasma membrane.

Based on a genome-wide ribonucleic acid interference (RNAi) screen this study aimed for the identification of further proteinaceous components that regulate or facilitate FGF2 secretion. Pharmacological studies previously implicated the sodium potassium pump (Na^+/K^+-ATPase) as a potential factor involved in FGF2 secretion, which indeed was a major hit in the genome-wide RNAi screen described in this thesis. Therefore, the main goal of this study was to validate these findings and to obtain mechanistic insight into the role of the Na^+/K^+-ATPase in the overall process of FGF2 secretion.

Since the Na^+/K^+-ATPase is formed of a heterodimeric complex that consists of the α- and β-subunit, cell-based secretion experiments identified the α1-subunit (ATP1A1) as the component involved in FGF2 secretion. Furthermore, a direct interaction between the cytoplasmic domains of ATP1A1 with FGF2 could be demonstrated. In addition, both proteins were shown to co-localize at the plasma membrane in HeLa cells. Therefore, it is highly likely that a direct interaction of FGF2 and ATP1A1 occurs at the cytoplasmic leaflet facilitating export of FGF2 from cells.

Based on an alpha screening setup analyzing a large library of small molecules, compounds were identified that block the interaction between FGF2 and ATP1A1. Therefore, this study provides new tools for future investigations on the mechanism of FGF2 secretion as well as lead compounds with a high potential for the development of novel anti-angiogenic drugs.

Zusammenfassung

Fibroblastenwachstumsfaktor 2 (FGF2) ist ein potentes Mitogen, das diverse physiologische Prozesse wie Zellproliferation, Zelldifferenzierung und die Bildung von Blutgefäßen beeinflusst. Im pathophysiologischen Zusammenhang spielt FGF2 eine besondere Rolle, sowohl bei der Tumor-induzierten Angiogenese als auch bei der Resistenz von Tumorzellen gegenüber Chemotherapien. Deshalb ist FGF2 ein validiertes Zielmoleküle zur Entwicklung von Strategien zur Begrenzung von Tumorwachstum. Die Freisetzung von FGF2 durch Zellen verläuft unabhängig vom endoplasmatischen Retikulum und dem Golgi Apparat. Die unkonventionelle Sekretion von FGF2 erfolgt in gefaltetem Zustand durch eine direkte Translokation über die Plasmamembran. Bisher konnten zwei Faktoren identifiziert werden, die für diesen Sekretionsprozess essentiell sind. Zum einen das Phosphoinositid ($PI(4,5)P_2$) an der Innenseite der Plasmamembran, welches für die Rekrutierung von FGF2 zuständig ist. Zum anderen Heparansulfat-Proteoglykane, die für einen späten Schritt in der Translokation notwendig sind und FGF2 auf der Zelloberfläche präsentieren. Die Bindung an $PI(4,5)P_2$ induziert die Oligomerisierung von FGF2 und in der Folge die Bildung einer transienten Membranpore, die als Translokationsintermediat interpretiert wurde. Weiterhin ist die Tec Kinase eine wichtige regulatorische Komponente für die Sekretion von FGF2. Es wurde kürzlich gezeigt, dass eine Phosphorylierung von Tyrsoin 82 in FGF2 durch die Tec Kinase zu einer Stabilisierung der oligomeren Struktur von FGF2 führt und hierdurch die Entstehung einer Membranpore begünstigt wird.

Anhand einer genomweiten Analyse - basierend auf RNA Interferenz (RNAi) - sollten in dieser Studie weitere Faktoren ermittelt werden, die maßgeblich an der Sekretion von FGF2 beteiligt sind. Hierbei wurde die Natrium-Kalium ATPase (Na^+/K^+-ATPase) als eine essentielle Komponente der FGF2 Sekretion entdeckt. Diese Befunde bestätigen frühere pharmakologische Studien, in denen eine solche Rolle bereits diskutiert wurde. Im Zuge der vorliegenden Arbeit wurde diese Funktion validiert und einer mechanistischen Analyse unterzogen.

Die Na^+/K^+-ATPase besteht aus einem heterodimeren Komplex, zusammengesetzt aus einer α- und β-Untereinheit. In einem *in vivo* Sekretionsexperiment konnte gezeigt werden, dass ausschließlich die α1-Untereinheit (ATP1A1) an der Sekretion von FGF2 beteiligt ist. Biochemische Analysen deckten außerdem eine direkte Interaktion zwischen den zytoplasmatischen Domänen von ATP1A1 und FGF2 auf. Im zellulären Kontext konnte eine entsprechende Kolokalisation an der Plasmamembran von HeLa Zellen beobachtet werden. Dies deutet stark darauf hin, dass eine direkte Interaktion zwischen FGF2 und ATP1A1 notwendig ist, um die Sekretion von FGF2 zu ermöglichen.

Um diese Frage weiter molekular analysieren zu können, wurden im dritten Teil dieser Arbeit kleine Moleküle identifiziert, die die Interaktion von ATP1A1 und FGF2 blockieren. Hierzu wurde ein Alpha Screening Ansatz etabliert und eine Bibliothek von etwa 4000 Molekülen nach Inhibitoren durchsucht. Die identifizierten Moleküle können nun in vielfältiger Weise eingesetzt werden, sowohl zur weiteren Analyse des molekularen Mechanismus der FGF2 Sekretion als auch zur Entwicklung von Wirkstoffen, die die Inhibierung der Tumor-induzierten Angiogenese anstreben.

1 Introduction

A eukaryotic cell is characterized by the presence of an elaborated membrane system that is defined by highly organized membrane compartments known as organelles. It is surrounded by the plasma membrane, which forms a biological barrier between the extracellular and intracellular environment and is essential for maintaining cell integrity. The genome is found in the nucleus and is encoded by deoxyribonucleic acid (DNA). Once, genes are translated into newly synthesized polypeptides they have to reach their final destination. This can either be a subset of organelles, the plasma membrane, or the extracellular space. Here, the organelles fulfill specific functions during the process of protein biogenesis, modification, sorting and secretion. The vast majority of secretory proteins are secreted via the classical secretory pathway through the ER and Golgi apparatus *en route* to the plasma membrane. However, there is a growing list of proteins that follow a distinct pathway and are externalized independent of the ER and Golgi apparatus.

1.1 The classical secretory pathway

Proteins that enter the secretory pathway are synthesized on free ribosomes in the cytoplasm. Soon after the amino terminal (N-terminal) hydrophobic signal sequence emerges from the nascent polypeptide chain a signal-recognition particle (SRP) recognizes the sequence to target the ribosomal-nascent chain complex to the ER (Blobel and Dobberstein, 1975). This is mediated in a guanosine triphosphate (GTP) dependent manner through the binding of the SRP to the SRP-receptor that is located on the ER membrane. Concomitant with GTP hydrolysis and SRP release the nascent polypeptide is handed over to the translocon, a trimeric Sec61 complex, that forms a protein conducting channel that allows the polypeptide to cross the ER membrane. The signal sequence of the polypeptide chain is cleaved immediately after the entry into the ER by a signal peptidase, while the ribosome completes the synthesis of the protein (Corsi and Schekman, 1996; Dalbey and von Heijne, 1992; Görlich et al., 1992; Lee et al., 2004; Rapoport, 1992; Walter et al., 1981). Soluble proteins are completely transferred into the ER lumen. In contrast transmembrane proteins laterally diffuse with their hydrophobic transmembrane segment into the lipid bilayer of the ER (Shao and Hegde, 2011). The ER itself provides an environment for protein folding, maturation and assembly into multisubunit complexes. Proteins are subjected to asparagine-linked glycosylation (N-glycosylation), modifications, that serve as substrates for a variety of chaperones that facilitate protein folding (Bukau and Horwich, 1998).

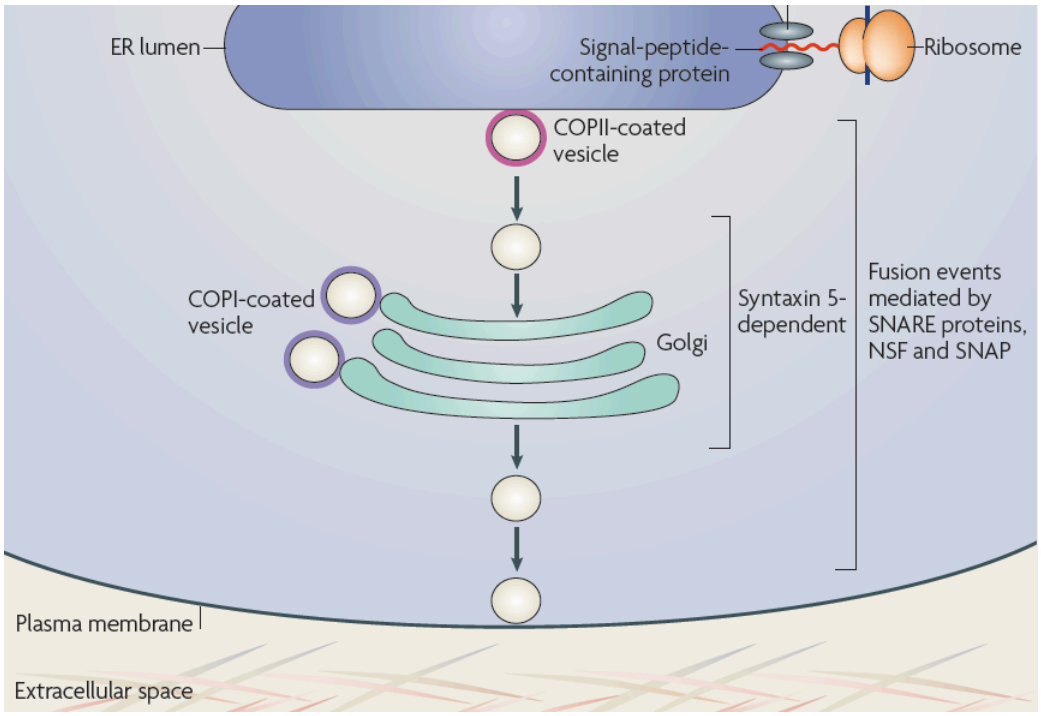

Figure 1: The classical secretion pathway. Adapted from Nickel and Rabouille, 2009. Nature Review Molecular Cell Biology 2009, 10:148-55

The three dimensional structure of proteins is further determined by the formation of disulfide bonds, which are mainly formed in the oxidative milieu of the ER (Freedman, 1995). A complex quality control system ensures that abnormally folded proteins are removed from the ER. The ER-associated degradation (ERAD) system delivers misfolded proteins back to the cytosol where they undergo ployubiquitinylation and finally degradation by the proteasome (Ellgaard and Helenius, 2001, 2003; Taxis et al., 2002). Properly folded proteins leave the ER at specific landmarks, the ER exit sites, where cargo is packed into Coat-protein-complex II (COPII) vesicles (Kuge et al., 1994; Orci et al., 1991; Pagano et al., 1999). COPII vesicles mediate anterograde transport, from the ER to the Golgi, where the cargo arrives and fuses with the *cis*-Golgi network (CGN). Retrograde transport from the CGN to the ER occurs via Coat-protein-complex I (COPI)-coated vesicles to recycle proteins that have to be retrieved in the ER. The CGN is a vesicular tubular cluster of ER derived vesicles that subsequently build up the *cis*-cisterna of the Golgi. The Golgi apparatus is a polarized organelle where proteins move in a sequential manner from the *cis*- to the *medial*- and *trans*- cisternae (Glick, 2000). Each compartment contains a subset of specific enzymes, glycosyl transferases that gradually modify N-glycans added in the ER to produce more complex oligosaccharide chains (Roth, 2002). Furthermore, the Golgi apparatus is the place where glycosylation occurs to hydroxyl groups of serine or threonine (O-linked glycosylation) and where glycosaminoglycan chains are added to proteins to form proteoglycans (Prydz

and Dalen, 2000). The *trans*-Golgi network (TGN) sorts the proteins according to their final destination. These can be lysosomes (via endosomal compartments) regulated by clathrin-coated vesicles (Le Borgne and Hoflack, 1998a, 1998b), delivery to secretory vesicles for regulated secretion and constitutive secretion to the cell surface (Burgess and Kelly, 1987).

1.2 Unconventional secretion

Beside the transport along the classical secretory route, which is an ER/Golgi-dependent pathway, eukaryotic cells employ various alternatives for cell surface delivery of both soluble and membrane proteins. There are common features that account for almost all proteins that are secreted via unconventional means. This is the absence of a N-terminal signal peptide and their secretion is not affected by the treatment with brefeldin A (BFA). The latter is an inhibitor of anterograde protein transport from ER to Golgi apparatus, which interferes with vesicular trafficking, thus, resulting in protein accumulation inside the ER (Lippincott-Schwartz et al., 1989). In general, there are two types of unconventional protein secretion that involve non-vesicular or vesicular mechanisms. The former are based on direct translocation of cytoplasmic proteins across the plasma membrane and are subsequently deposited on cell surfaces or released into the extracellular space (Nickel and Rabouille, 2009). On the other hand, vesicular mechanisms of unconventional protein secretion depend on intracellular membrane-bound intermediates (such as secretory lysosomes, microvesicular bodies or autophagosomes), which need to fuse with the plasma membrane in order to enable cargo release into the extracellular space. Just lately, a more defined categorization was made (Rabouille et al., 2012). Here, unconventional secreted proteins were classified into four different subgroups from Type I to Type IV. Type I resembles proteins that follow the non-vesicular pathway and are secreted by direct translocation across the plasma membrane. Type II secretion proteins are released through an ABC-transporter system and lipidated proteins or peptides. Type III pathway comprises proteins that are secreted via a vesicular intermediate. Finally, proteins that bypass the Golgi apparatus are assigned to type IV secretion (Rabouille et al., 2012). The following table gives an overview of some proteins that are transported by unconventional means and categorizes them according to their different subgroups. In the next section proteins of each class will be described in more detail.

Table 1: Overview of unconventionally secreted proteins classified according to their secretion mechanisms. Modified table was from Rabouille et al., 2012. Journal of Cell Science 2012,125:5251-5255.

	Mechanism	Cargo and Reference	
Non-vesicular	**Type I** Self-sustained membrane translocation	FGF1 (Prudovsky et al., 2013) FGF2 (Engling et al., 2002; Nickel et al., 2009) Tat (Ensoli et al., 1990; Rayne et al., 2010a, 2010b) Annexin A2 (Deora et al., 2004; Rescher and Gerke, 2008)	**Cytoplasmic proteins**
	Type II ABC transporter-based secretion (Lipidated proteins and peptides)	Yeast a-factor mating pheromone, prenylated polypeptide (McGrath and Varshavsky, 1989; Michaelis, 1993) *Leishmania* hydrophilic acylated surface protein B (HASPB) protein (Denny et al., 2000; Maclean et al., 2012; Stegmayer et al., 2005) *Plasmodium falciparum* acylated protein kinase (PfCDPK1) (Möskes et al., 2004)	
Vesicular	**Type III** Autophagy and vesicular based secretion	Acb1/AcbA (Cabral et al., 2010; Duran et al., 2010; Manjithaya et al., 2010) Interleukin1-β (IL1β) (Dupont et al., 2011; Keller et al., 2008; Lopez-Castejon and Brough, 2011) High mobility group box 1 (HMGB1) protein (Bonaldi et al., 2003; Gardella et al., 2002)	
	Type IV Golgi bypass	CFTR (Gee et al., 2011; Yoo et al., 2002) αPS1 integrin (Schotman et al., 2008) Connexin 26 and 30 (George et al., 1999; Qu et al., 2009) Pannexin 1 and 3 (Penuela et al., 2007) Tyrosine phosphatase (CD45) (Baldwin and Ostergaard, 2001)	**Transmembrane proteins**

1.2.1 FGF1 and FGF2 – examples for Type I secretion

Fibroblast growth factor (FGF) 1 and 2 are both absent of a signal peptide and are released from cells without entering the ER or Golgi compartment. They have in common that they pass the plasma membrane by direct translocation and are subsequently immobilized on the cell surface on HSPGs (Cao and Pettersson, 1993; Zehe et al., 2006).

Secretion of FGF1 is mainly induced due to cellular stress conditions such as heat shock (Jackson et al., 1995), hypoxia (Mouta Carreira et al., 2001), and serum starvation (Shin et al., 1996). Secretion is facilitated by a multiprotein complex, in which FGF1 is associated with sphingosine kinase 1, p40 synaptotagmin 1, and S100A13 (Mohan et al., 2010; Prudovsky et al., 2013). It is believed that the assembly of the complex occurs prior to secretion in the cytosol close to the inner plasma membrane leaflet (Mohan et al., 2010). A prerequisite for FGF1 secretion is the formation of a FGF1 homodimer, which is part of the multiprotein complex. Dimer formation occurs intermolecular between the cysteines 30 mediated through oxidative conditions of copper (Cu^{2+}), which is tightly associated to shingosine kinase 1 and p40 synaptotagmin 1 of the multiprotein complex (Engleka and Maciag, 1992; Landriscina et al., 2001). Furthermore, it has been shown that FGF1, p40 synaptotagmin 1, and S100A13 can bind to acidic phospholipids leading to a destabilization of liposomes. Therefore, it is believed that binding of the multiprotein complex at the inner side of the plasma membrane to acidic phospholipids plays a major role in externalization of FGF1, which might involve a flipping mechanism after binding to the phospholipids (Graziani et al., 2009; Prudovsky et al., 2008). However, a detailed mechanism on how FGF1 can traverse the plasma membrane being released at the extracellular space is currently unknown.

Constitutive secretion of FGF2 from cells is dependent on several components (Nickel, 2010). FGF2 is recruited to the inner plasma membrane leaflet by binding to $PI(4,5)P_2$ (Temmerman et al., 2008), which has been shown to induce the formation of FGF2 oligomers. These oligomers stimulate the formation of a lipidic pore through which FGF2 can traverse the plasma membrane. In addition, phosphorylation of FGF2 at the cytoplasmic side contributes to the stabilization of such FGF2 oligomers. This is mediated by Tec kinase an essential regulatory component of this secretion process (Ebert et al., 2010; Steringer et al., 2012). To date the structure of such a FGF2 pore is still under investigation. A detailed description of the FGF2 secretion mechanism will be revisited in section 1.4.4.

1.2.2 Tat – an example for Type I secretion

Tat stands for “trans-activator of transcription” and is a protein with a molecular weight of 11 kDa that is encoded from the human immunodeficiency virus type 1 (HIV-1). In the replication cycle of HIV-1, Tat plays a crucial role to enhance transcription of viral genes, acting as a transactivating protein (Jeang et al., 1999). Despite the lack of a signal sequence it has been reported that Tat is secreted from HIV-1 infected CD4 positive T cells (Ensoli et al., 1990) and does not pass the ER or Golgi compartment (Chang et al., 1997; Rayne et al., 2010b). The extracellular role of Tat is not fully understood but different studies point to the direction that it is involved in the development of acquired immune deficiency syndrome and Kaposi’s sarcoma (Barillari et al., 1999; Campbell et al., 2004). Tat is recruited to the inner leaflet of the plasma membrane by binding to $PI(4,5)P_2$ with its basic domain (residues arginine (R) 49, lysine (K) 50 and K51. Interestingly, a tryptophan (W) at position 11 is needed to stabilize this interaction between Tat and $PI(4,5)P_2$, which subsequently leads to membrane insertion (Rayne et al., 2010a). Concomitantly, such an insertion is required for secretion of the protein since a mutant where W 11 is replaced by tyrosine (Y) is strongly impaired to be detected in the supernatant (Rayne et al., 2010a; Yezid et al., 2009). Details of the secretion mechanism are currently unknown. On the cell surface Tat is able to interact with multiple receptors such as lipoprotein receptor-related protein (Liu et al., 2000), chemokine receptor 4 (CXCR4) (Ghezzi et al., 2000) and HSPGs (Tyagi et al., 2001) to fulfill its biological function.

1.2.3 The a-factor mating pheromone – an example for Type II secretion

The second secretion pathway describes a non-vesicular pathway that makes use of an energy-dependent transport mediated through a superfamily of proteins termed adenosine triphosphate (ATP)-binding cassette (ABC) transporters. Evolutionary ABC-transporters are well conserved from bacteria to eukaryotes. They consist of two homolog transmembrane domains that both have the ability to bind ATP (Ketchum et al., 2001). With the help of ATP hydrolysis they transport a variety of substrates ranging from ions, carbohydrates, amino acids, phospholipids, and peptides across extra- and intracellular membranes (Bauer et al., 1999). One example is the Ste6p ABC-transporter, which was discovered in the yeast *Saccaromyces cerivisiae*. It is required for the export of a-factor mating pheromone (Kuchler et al., 1989). Mating in yeast occurs when two haploid cells of the two opposite mating types a and α fuse to form a diploid cell. This is achieved through the secretion of either a-factor or α-factor mating pheromone from a haploid cell. Neighboring cells can sense their corresponding opposite mating type, from an outgrowth, and fuse with each other (Cross et al., 1988). Interestingly, secretion of a-factor was still maintained when the classical

secretory pathway of yeast was blocked by growing temperature-sensitive secretion-defective (sec) mutants (Schekman, 1985) at restrictive temperature, whereas α-factor secretion of the opposite mating type was inhibited (Kuchler et al., 1989). Pro-a-factor is synthesized in the cytosol as a 36 or 38 amino acid precursor peptide lacking any N-terminally hydrophobic signal sequence. On the C-terminus a farnesyl moiety and a methyl group is attached to the cysteine 33, which is needed for its biological activity. Subsequently, the precursor protein is processed on its N-terminus to form the mature lipopeptide (12 amino acid in length) that is secreted via the Ste6 ABC-transporter by active transport across the plasma membrane (Michaelis, 1993).

1.2.4 Acb1/AcbA – an example for Type III secretion

Another example for a protein that lacks a N-terminal secretion signal is the acyl-coenzyme A (CoA)-binding protein (Acb1) in yeast. Homolog proteins are expressed in humans (ACBP) and *Dictyostelium discoideum* (AcbA). All proteins are very small in size (10 kDa). In *Dictyostelium discoideum* secretion of AcbA was found to be dependent on the Golgi reassembly and stacking protein (GRASP) (Kinseth et al., 2007), which is in mammalian cells required for Golgi stacking of the cisternae (Feinstein and Linstedt, 2008). During the development of *Dictyostelium discoideum,* AcbA is getting secreted from pre-spore cells. Once secreted, AcbA will be proteolytically cleaved into a 34 amino acid spore differentiation factor-2 peptide that can induce sporulation (Anjard and Loomis, 2005). The secretion mechanism was further investigated by two different studies in yeast (Duran et al., 2010; Manjithaya et al., 2010). The major findings revealed that secretion of Acb1 is not only dependent on Grh1 (yeast homolog of GRASP) but also on autophagosomal structures that subsequently fuse with endosomal compartments, finally being directed for vesicular fusion with the plasma membrane. The onset of secretion in yeast is initiated by nutrition starvation giving raise to a concerted release of the biological active (34 amino acids) peptide after 3 h (Duran et al., 2010). Concomitant with the starvation process it has been reported that punctuated structures form near the ER exit sites, so called compartments for unconventional protein secretion (CUPS) (Bruns et al., 2011). This compartment is enriched of phosphatidylinositol 3-phosphate and proteins such as Grh1. Moreover, autophagy related proteins (Atg-8 and Atg-9) and Vps23 are recruited to it, all of them being essential factors for Acb1 secretion (Bruns et al., 2011). Vps23 might be required for the fusion of CUPS with endosomal compartments, such as multivesicular bodies. Vps23 is a component of the endosomal sorting complex-I (ESCRT-I), which is needed for sorting of proteins into multivesicular bodies (Katzmann et al., 2003). To date it is not clear how these vesicles can escape the multivesicular bodies to be directed to the plasma membrane.

However, a plasma membrane specific t-SNARE (soluble N-ethylmaleimide sensitive factor attachment protein receptor on the target membrane) Sso1 was identified as a factor mediating the fusion of vesicles to the plasma membrane and thus, allowing the release of Acb1 into the extracellular space (Malhotra, 2013).

1.2.5 CFTR – an example for Type IV secretion

The last secretion pathway describes proteins that typically enter the ER but during the following secretion process are absent from the Golgi apparatus. One of the best-studied members in this group is the cystic fibrosis transmembrane conductance regulator (CFTR), which is a cyclic adenosine monophosphate (cAMP)-activated anion channel involved in transport of chloride throughout epithelia. Mutations in the CFTR gene lead to the development of a very severe disease named cystic fibrosis. The perturbation of the epithelial electrolyte transport gives rise to sticky mucus that most critically affects the lungs, pancreas and intestines (Quinton, 2010). In mammalian cells CFTR is found in two different states, as a core-glycosylated immature form (band B) in the ER and as a fully glycosylated protein (band C) (Amaral, 2004). Under normal growth conditions the glycosylated form is found on the plasma membrane. Yoo and colleagues could show that dominant negative mutants of Sar1 a component of the COPII complex and Arf1 a component of the COPI complex blocked the maturation of CFTR, which remains in the band B form. This was also observed when syntaxin 5 was overexpressed in cells. Syntaxin 5 is a N-ethylmaleimide-sensitive factor that is involved in fusion of COPII vesicles with Golgi membranes (Yoo et al., 2002). However, the effect of Arf1 and sytaxin 5 seemed to be cell type specific. Interestingly, under these conditions when the ER to Golgi pathway was blocked, suddenly the core-glycosylated version of CFTR appeared to be on the plasma membrane. Measuring chloride currents showed that the protein was still functional (Gee et al., 2011). It could be shown that this unconventional route of secretion was triggered by ER-stress, during which a signaling cascade was activated leading to the phosphorylation of GRSP55 (mammalian homolog of GRASP) in HEK293T cells. In addition, CFTR can directly bind to a specific PDZ-domain region of GRSP55 that is absolutely essential for the delivery of CFTR to the plasma membrane (Gee et al., 2011). This is another example where unconventional protein secretion is linked to GRASP, which was already suggested to be involved in the secretion of Acb1/AcbA (see section 1.2.4).

1.3 Fibroblast growth factor (FGF) gene family

In vertebrates, the FGF gene family consists of 22 genes with an overall identity of 30-60% of their amino acid sequence and a conserved 120 amino acid core region (Itoh and Ornitz, 2004). They range in size from 17-34 kDa (Ornitz and Itoh, 2001) and contribute to a wide variety of biological functions. FGFs have a high affinity for extracellular HSPGs present in close proximity on the cell surface. Binding to HSPGs protects FGFs from proteolysis and it is essential to form a ternary complex with high-affinity FGF tyrosine kinase receptors (FGFR 1-4) to activate the signaling cascade (Nugent and Iozzo, 2000; Pellegrini et al., 1998). The conserved core region provides a stretch of 10 amino acids that interact with the FGF receptors (Plotnikov et al., 2000). Considering their extracellular roles, most of the FGFs contain a signal peptide that targets them to the classical ER/Golgi-dependent secretory pathway (FGFs 3-8, 10, 17-19, 21-23). Another class of FGFs lacking the signal peptide (FGFs 11-14) has exclusively an intracellular localization. In contrast, even though FGF 1, 2, 9, 16 and 20 lack an obvious signal peptide, they are still secreted (Itoh and Ornitz, 2004). Regarding their mode of secretion FGF1 and FGF2 are the best-characterized growth factors. Both of them are released from cells by means of an ER/Golgi-independent pathway. The underlying secretion mechanism of FGF2 will be discussed in detail in the following sections.

1.4 Fibroblast growth factor 2 (FGF2)

1.4.1 FGF2 isoforms

As described above FGF2 belongs to the family of heparin binding proteins. In vertebrates, five different isoforms were found, all of them lacking a N-terminal signal sequence. The 18 kDa form is often referred as basic or low molecular weight (LMW) FGF2. Its translation is initiated from the AUG start codon of the mRNA. Four additional alternative CUG initiation codons are present upstream of the canonical AUG. This results in the translation of four high molecular weight (HMW) isoforms with electrophoretic mobility of 22, 22.5, 24 and 34 kDa (Delrieu, 2000; Prats et al., 1989). The HMW isoforms carry a nuclear localization signals (NLS) and are predominantly found in the nucleus where they fulfill their biological functions such as cell proliferation and differentiation (Couderc et al., 1991; Dini et al., 2002; Dvorak et al., 2005; Renko et al., 1990). The LMW FGF2 is found in the nucleus and the cytoplasm (depending on the cell line) but is also secreted from cells (Florkiewicz et al., 1995a; Sheng et al., 2004). Upon secretion FGF2 can interact with HSPGs and the high affinity receptors (FGFR1-4) to exert its function in an autocrine and paracrine manner

(Turner and Grose, 2010). The expression patterns of FGF2 isoforms are largely dependent on the cell type, developmental stage and can also be influenced in response to heat shock or oxidative stress (Giordano et al., 1992; Vagner et al., 1996). In the following parts of this thesis the 18 kDa, LMW will be referred to as FGF2.

1.4.2 Biological function of FGF2

FGF2 is a potent mitogen that plays a major role in various cellular processes that involve cell migration, proliferation and differentiation (Bikfalvi et al., 1997). For example, it has been reported that expression of endogenous FGF2 is required for the migration of bovine capillary endothelial cells and human fibroblast cells (Sato and Rifkin, 1988) and also has an impact on cell growth (Neufeld et al., 1988; Sasada et al., 1988). In addition, FGF2 is involved in many physiological and pathological processes such as tumor angiogenesis and tumor growth (Presta et al., 2005; Wang and Becker, 1997), vasculogenesis (Murakami and Simons, 2008), wound healing (Barrientos et al., 2008) and neural development (Giordano et al., 1992; Vescovi et al., 1993). Angiogenesis supports the formation of new blood vessels from a pre-existing vascular system. It has been reported that FGF2 is needed for the stimulation of vascular endothelial growth factor (VEGF) expression, which is one of the most critical growth factors that induce angiogenesis (Seghezzi et al., 1998). The growth of new blood assures the supply of oxygen and nutrition and concomitantly, supports tumor growth.

1.4.3 Structural aspects of FGF2

The 18 kDa form of FGF2 consists of 155 amino acids that are arranged in a trigonal pyramid of 12 antiparallel β-sheets of which 6 form a β-barrel (Ago et al., 1991; Eriksson et al., 1991, 1993; Zhang et al., 1991; Zhu et al., 1991). Later on high-resolution nuclear magnetic resonance (NMR) spectroscopy experiments revealed only 11 β-sheets and a helical structure in the region of 131 - 136 amino acids, which replaces the β-sheet 11 (Figure 2) (Moy et al., 1996). This is also the major region involved in heparin binding. Co-crystallization of FGF2 with heparin (hexasaccharide) as well as in a ternary complex with heparin and FGFR revealed the following residues involved in heparin binding: asparagine (N) 36, R129, threonine (T) 130, lysine (K) 134, K138, glutamine (Q) 143, K144 and alanine (A) 145 (the numbering was chosen starting with methionine at position 1) (Faham et al., 1996; Schlessinger et al., 2000). Interestingly, the co-crystallization experiments demonstrate that FGF2 can simultaneously bind to FGFR and heparin on the cell surface. In agreement with different studies, the first 28 amino acids are largely unstructured indicating a high flexibility (Kastrup et al., 1997; Moy et al., 1996).

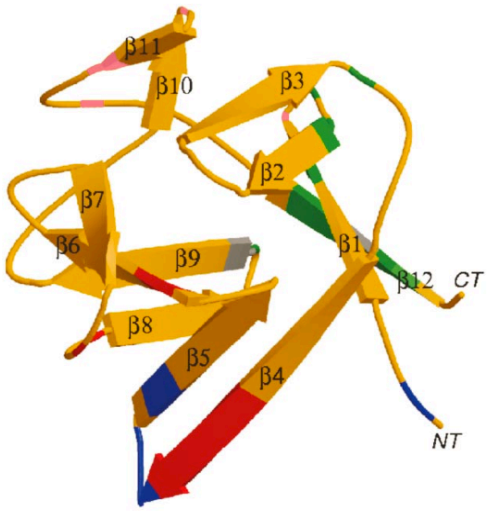

Figure 2: Three-dimensional structure of human FGF2. The protein backbone of FGF2 consists of 12 antiparallel β-sheets organized in a pyramidal structure. The pink regions between β-sheet 1 and 2 as well as between β-sheet 11 and 12 representing binding regions to heparin. In green, red and blue contacted sites to FGFR are shown. The N-terminus and C-terminus is labeled with NT and CT, respectively. According to Eriksson *et al.,* this structure is lacking the first 19 amino acids (Eriksson et al., 1991). Adapted from Ornitz and Itoh, 2001. Genome Biol. 2001; 2(3): reviews3005.1-12, copyright BioMed Central Ltd, 2001

1.4.4 Unconventional secretion of FGF2

Even though FGF2 lacks a classical signal peptide, it is still released from cells but it does not follow the ER/Golgi-dependent export route (Abraham et al., 1986; Mignatti et al., 1992; Muesch et al., 1990; Nickel, 2005). This was demonstrated by treatments of cells with the drug BFA, which commonly blocks the classical secretory pathway and hence had no effect on FGF2 secretion (Florkiewicz et al., 1995b; Mignatti et al., 1992). Furthermore, subcellular fractionation experiments primarily localized FGF2 in the cytosolic fractions that were not associated with secretory vesicles (Renko et al., 1990). Early studies proposed a mechanism by which FGF2 is released from dead or injured cells (McNeil et al., 1989; Schweigerer et al., 1987). In contrast to these findings, it could be clearly demonstrated that FGF2 is secreted from intact cells in a constitutive manner without compromising cell integrity (Engling et al., 2002; Florkiewicz et al., 1995b). This points towards a specific mechanism of non-classical protein release from cells. Different models of secretion mechanisms have been proposed so far. This is (i) membrane blebbing and shedding of the vesicles to the extracellular space (Schiera et al., 2007; Taverna et al., 2003) (ii) release by multivesicular bodies (iii) and direct translocation of FGF2 across the plasma membrane. Release of FGF2 by membrane shedding (i) was observed from hepatocarcinoma and fibroblast cells that were subjected to serum starvation followed by the onset of FGF2 secretion stimulated by the addition of serum

(Taverna et al., 2003). It remains questionable if serum starvation reflects the physiological conditions of FGF2 secretion. In contrast, inhibition of the Rho kinase a critical factor, which blocks plasma membrane blebs had no influence on the secretion efficiency of FGF2-GFP from CHO cells and FGF2-GFP was not found in plasma membrane-bound vesicles (Seelenmeyer et al., 2008). Ceccarelli and colleagues observed that the oncogene latent membrane protein 1 (LMP1) of Epstein-Barr virus could induce export and release of FGF2 from cells (Ceccarelli et al., 2007). This study argues for a distinct unconventional pathway of secretion mediated through exosomes (ii), which were derived from multivesicular bodies. There are controversial findings describing FGF2 secretion. However, secretion routes might vary with different cell types and conditions such as transfection with Epstein-Barr virus or with different treatments of cells as described for serum starvation. To date, the third model (iii) of direct translocation across the plasma membrane is believed to be the most probable one. A key finding was that in a cell free system using inside-out vesicles derived from plasma membrane FGF2 was able to pass through the membrane into the lumen of these vesicles. This translocation occurred in an ATP independent manner and did not require an electrochemical gradient (Schäfer et al., 2004a).

Current findings supporting this mechanism (iii) are summarized in Figure 3. FGF2 is synthesized on free ribosomes in the cytoplasm and subsequently recruited to the inner leaflet of the plasma membrane by binding to the phosphoinositide $PI(4,5)P_2$. Externalization of FGF2 is controlled by the binding of FGF2 to Translokin, which functions as a molecular shuttle. Translokin itself can interact with a motor protein, a member of the type II kinesin family (KIF3A), which in turn can move along microtubules and can deliver FGF2 to the periphery of the cell. Translokin is also believed to facilitate retrograde transport of FGF2 from the cell surface after internalization to the nucleus (Bossard et al., 2003; Meunier et al., 2009).

At least one posttranslational modification of FGF2 is required for FGF2 secretion and occurs presumably at the plasma membrane after binding to $PI(4,5)P_2$. It has been shown that this interaction to $PI(4,5)P_2$ is crucial for secretion. Mutation of the $PI(4,5)P_2$ binding site at residue K128 and R129 impaired both FGF2 binding to $PI(4,5)P_2$ containing liposomes and export from cells. Interestingly, the lipid background also influenced binding of FGF2. It was shown that a lipid mixture that resembles plasma membranes, containing cholesterol and sphingomyelin, favors $PI(4,5)P_2$ dependent binding of FGF2 (Temmerman et al., 2008). This might be due to a local enrichment of $PI(4,5)P_2$ through the formation of cholesterol and sphingomyelin dependent microdomains (Pike, 2008; Temmerman et al., 2008). To date, it is not entirely clear how FGF2 can traverse the plasma membrane. One possibility could be a protein-conducting channel. Well-characterized transporter systems are already known.

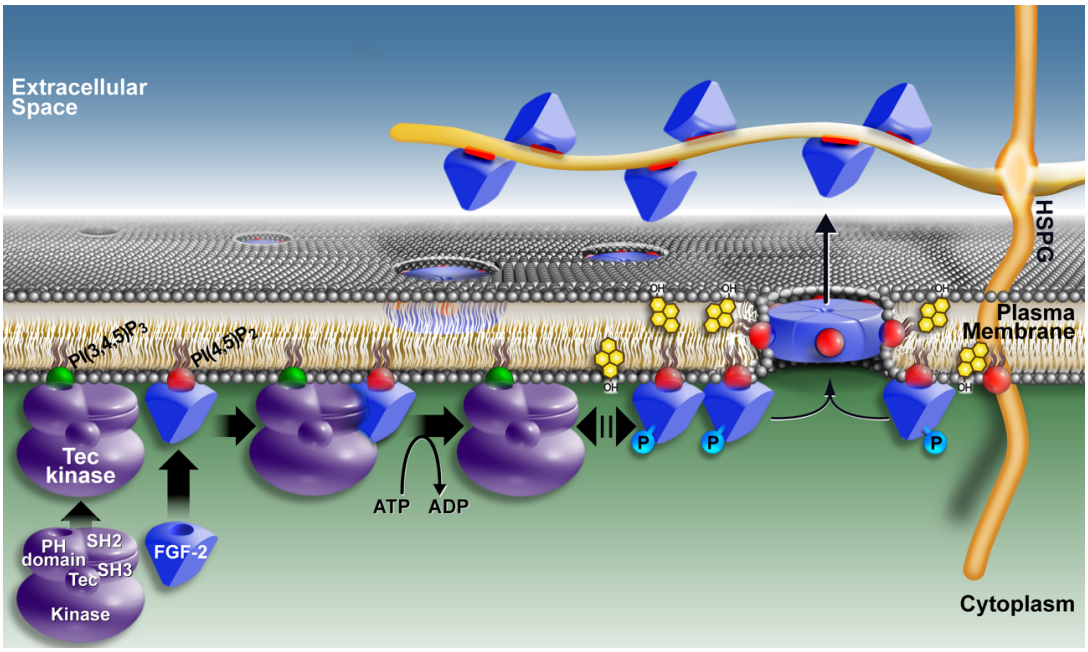

Figure 3: Molecular secretion mechanism of FGF2. Modified from Nickel, 2010. Current Opinion in Biotechnology 2010, 21:621-626

For example the Sec61 protein-conducting channel or the TIM/TOM complex that ensures protein import into mitochondria (Neupert and Herrmann, 2007; Rapoport, 1992). However, these systems have in common that the cargo protein has to be unfolded during translocation. None of these factors or transporters could be identified with the genome-wide RNAi screen that was carried out lately to reveal new components involved in FGF2 secretion (doctoral thesis, Antje Ebert 2009). However, recent data could clearly demonstrate that FGF2 is translocated across the plasma membrane in a folded state (Backhaus et al., 2004; Torrado et al., 2009). Arguing for an intrinsic quality control mechanism to assure that only correctly folded and biologically active FGF2 molecules can be secreted (Torrado et al., 2009).

A study of Ebert and co-workers identified the Tec kinase in a genome-wide RNAi screen. It was demonstrated that Tec kinase phosphorylates FGF2 at tyrosine 82, which is a prerequisite for FGF2 secretion (Ebert et al., 2010). Tec kinase is a non-receptor tyrosine kinase that is recruited to membranes through binding to phophatidylinsoitol-3,4,5-triphosphate ($PI(3,4,5)P_3$) with its pleckstrin homology (PH) domain. Complete activation of Tec kinase occurs after binding to $PI(3,4,5)P_3$ and phosphorylation by Src family kinases followed by subsequent auto-phosphorylation (Schaeffer and Schwartzberg, 2000).

Interestingly, a recent study of Steringer and colleagues could demonstrated that binding of FGF2 to a plasma membrane like lipid background, containing $PI(4,5)P_2$, induced the formation of FGF2 oligomers. In addition, binding of FGF2 to model membranes enriched in $PI(4,5)P_2$ allowed for the passage of a small tracer molecules (~1 kDa) into the vesicles (Steringer et al., 2012). This indicates that a stable structure or lipidic pore is formed after binding of FGF2 to the lipid bilayer. More precisely, data from a transbilayer diffusion assay indicated the formation of a toroidal pore (Steringer et al., 2012). This means that after FGF2 induced pore formation lipids can freely diffuse between the two leaflets of the lipid bilayer (Qian et al., 2008). In addition to these findings it was shown that a phosphomimetic protein of FGF2 (tyrosine 82 was replaced by the unnatural amino acid *p*-carboxyl-methylphenylalanine) exerted a much higher membrane activity (Steringer et al., 2012; Young et al., 2010). A possible mechanism could be that the phosphate stabilizes the oligomeric structures, which in turn enhances the process of pore formation. More recent results point to the direction that surface localized cysteines of FGF2 have the ability to form inter-disulfide bridges, which might provide the building block of such oligomeric structures (personal communication, Dr. Hans-Michael Müller). However, the defined molecular structure of such a lipidic FGF2 pore remains elusive.

It is well-established that on the extracellular space membrane proximal HSPGs act as a molecular trap to extract FGF2 from the plasma membrane and subsequently, immobilize FGF2 molecules on the cell surface since it is not released into the medium (Engling et al., 2002; Trudel et al., 2000). Neither truncation mutants of FGF2, lacking the HSPG binding region, nor HSPG deficient cells were able to secrete FGF2. A rescue of the secretion defect in HSPG deficient cells was achieved by co-cultivation with HSPG positive cells. This was only observed when co-cultured cells had close contact to HSPG deficient cells. Therefore, HSPGs are absolutely essential for the secretion mechanism of FGF2 and their close proximity to the plasma membrane is necessary to maintain FGF2 secretion (Nickel, 2007; Zehe et al., 2006).

Many years ago, pharmacological studies implicated the sodium potassium ATPase (Na^+/K^+-ATPase) as a potential factor involved in FGF2 secretion. It was shown that inhibition of the Na^+/K^+-ATPase by ouabain impaired FGF2 release from cells (Dahl et al., 2000; Florkiewicz et al., 1998). In contrast, an ouabain insensitive mutant was able to reverse this phenotype. However, these studies were lacking functional data and furthermore a direct interaction between FGF2 and the Na^+/K^+-ATPase was not clearly demonstrated.

1.5 Sodium potassium ATPase (Na^+/K^+-ATPase)

The Na^+/K^+-ATPase is an integral membrane protein found in most of the higher eukaryotes and is located in the plasma membrane of cells. It was first described by Skou in 1957 as a membrane bound ATPase that facilitates cation transport (Skou, 1957). Since then, many studies were carried out to understand its physiological function in cells. Beside its main role in transport of sodium and potassium ions across the plasma membrane it was implemented in cellular processes such as signal transduction after binding of cardiotonic steroids.

1.5.1 P-type ATPase family

The Na^+/K^+-ATPase belongs to a large family P-type ATPases comprised of more then 300 members. Among those, the well-characterized sarco(endo)plasmatic Ca^{2+}-ATPase (calcium pump) and H^+/K^+-ATPase (proton pump) are listed (Scarborough, 1999). All of them are enzymes that function in ion transport to maintain the electrochemical gradient across cellular membranes and undergo auto-phosphorylation during their catalytic cycle. The electrochemical gradient is a driving force to control many physiological processes in mammalian cells such as absorption and secretion of molecules, signal transduction, nerve impulse transmission, excitation and contraction of muscle cells as well as growth and differentiation (Scarborough, 1999). Characteristics that are shared among the P-type ATPases are their ability to form a transient high-energy aspartyl-phophoanhydride intermediate. Phosphorylation of the aspartate takes place at a highly conserved amino acid region (DKTGT), which is homologues in almost all P-type pumps (Kaplan, 2002). In general P-type ATPases cycle between two different conformational states shown in Figure 4B and C, which corresponds to E1 and E2 state, respectively. The alteration between these two states is necessary to facilitate binding, occlusion and release of the transported ions. The energy of this process is utilized by the hydrolysis of ATP. The P-type ATPases have been classified into five different subgroups according to their cationic and lipid substrates. The Na^+/K^+-ATPase is assigned to the subgroup P_{IIC} together with the H^+/K^+-ATPase (Axelsen and Palmgren, 1998; Tang et al., 1996). The catalytically active subunit (termed α-subunit) is an integral membrane protein usually comprised of 6-12 α-helices. Among the P-type ATPases these α-subunits have very similar domain architecture. They commonly consist of the N-domain (nucleotide binding domain), the P-domain (phosphorylation domain), and the A-domain (actuator domain), needed for ATP hydrolysis (see Figure 4A; Bublitz et al., 2010).

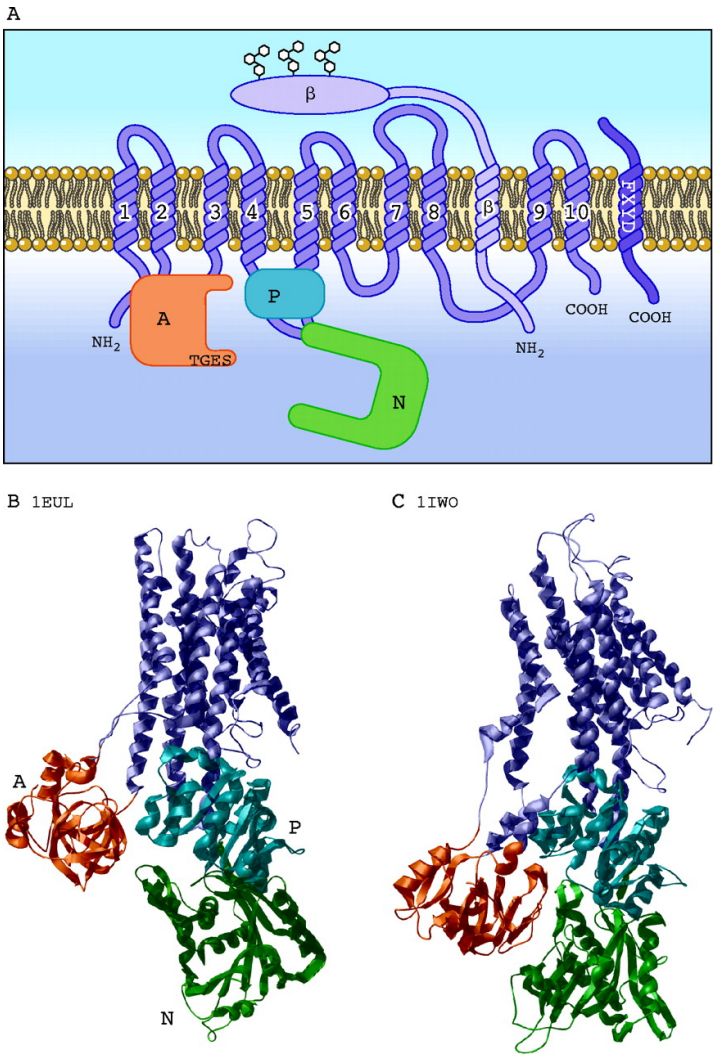

Figure 4: General structure of P-type ATPases. (A) Illustration of the Na^+/K^+-ATPase with the 10 transmembrane segments of the α-subunit that carries all the catalytically domains (Domain A, P, and N) for ion transport. The α-subunit is closely bound to the glycosylated single pass membrane protein β-subunit and the accessory FXYD that is mostly associated with the Na^+/K^+-ATPase. In **(B)** and **(C)** the crystal structures of the Ca^{2+}-ATPase in a Ca^{2+} occluded E1 state and a Ca^{2+} free E2 state are depicted. This represents the common domain architecture of P-type ATPases that also accounts for the Na^+/K^+-ATPase. Adapted from Horisberger 2004. Journal of Physiology 2004;19:377-387.

To carry out their catalytic activity some P-type ATPases have to be assembled in a heterodimeric complex. This concerns members of the P_{IIC} and P_{IV} subgroups where the α-subunit is assembled with the β-subunit or CDC50 subunit, respectively (Poulsen et al., 2008; Scheiner-Bobis and Farley, 1994). In contrast, the sarco(endo)plasmatic reticulum Ca^{2+}-ATPase (subgroup P_{IIA}) exists as a monomeric ATPase (Olesen et al., 2007).

1.5.2 Structural and catalytically aspects of the Na^+/K^+-ATPase

As mentioned above, the α-subunit is the catalytic subunit of the enzyme. It consists of 10 transmembrane α-helices (M1-M10) and has a molecular weight of about 100 kDa. The C- as well as the N-terminus are localized to the cytoplasmic side. The main catalytically active domains are positioned in two loop regions that face towards the cytoplasmic side. This is the A-domain between M2-M3 and the P- and N-domain, which are enclosed by the transmembrane domains M4-M5 (see schematic drawing of the Na^+/K^+-ATPase in Figure 2A). The α-subunit is tightly associated with the β-subunit in a 1:1 stoichiometry. The β-subunit interacts with the α-subunit at the extracellular loop region between M7-M8 (Chow and Forte, 1995; Lemas et al., 1994).

The β-subunit consists of only one transmembrane segment and a rather small N-terminal cytoplasmic domain in comparison to its C-terminal extracellular glycosylated portion. Furthermore, it has 6 cysteines that form 3 disulfide bonds on its extracellular side. The positioning of the cysteines is very conserved in all the β-subunits that belong to the P-type ATPase family, arguing that the structural arrangement of this subunit is very important for the enzyme function (Beggah et al., 1997; Noguchi et al., 1994). The β-subunit has a molecular weight of approximately 34 kDa but due to its glycosylation it appears as a diffuse band migrating between 50-70 kDa on a SDS-PAGE. It has been shown that the β-subunit is critically important for the maturation of the enzyme because it is required for the correct insertion of the transmembrane regions M5-M10 into the ER membrane and the subsequent delivery to the plasma membrane (Beggah et al., 1999; Hasler et al., 2001). Furthermore, it has also been observed that the association of the β-subunit with the α-subunit stabilizes the α-subunit, protects it from intracellular degradation (Chen et al., 1998) and is also involved in K^+ occlusion of the enzyme (Lutsenko and Kaplan, 1993). It is generally accepted in the field and also early studies in *Xenopus* oocytes could demonstrate that the α-subunit has to be assembled with the β-subunit in a heterodimeric complex to form a fully active pump (Noguchi et al., 1987). However, the role of glycosylation of the β-subunit seems to be unclear. It has been reported that the sites of glycosylation of the β-subunits can vary within different species and even in different isoforms of the enzyme (Chow and Forte, 1995) but the removal of the glycosylation sites had no influence on the biogenesis and activity of the pump (Zamofing et al., 1988).

Additionally, the Na^+/K^+-ATPase as a heterodimeric complex is associated with an accessory FXYD protein, a small hydrophobic polypeptide with a molecular weight of 8-14 kDa (see Figure 4A). This family consists of 7 members and is expressed in a tissue specific manner (Sweadner and Rael, 2000). It has been reported, that it can modulate the activity of the

Na^+/K^+-ATPase by increasing the affinity of K^+ or Na^+ to the ATPase (Crambert et al., 2002). This is regulated on the basis of the physiological requirements of the tissue (Geering, 2005).

To balance sodium and potassium concentrations inside and outside of the cell the Na^+/K^+-ATPase has to transport constantly ions against a steep concentration gradient. This is achieved by the active transport of 3 Na^+ exported from the cell in exchange of 2 K^+ that are taken in. During this catalytic cycle the Na^+/K^+-ATPase undergoes various conformational changes that will be described in the following section referring to the illustration depicted in Figure 5.

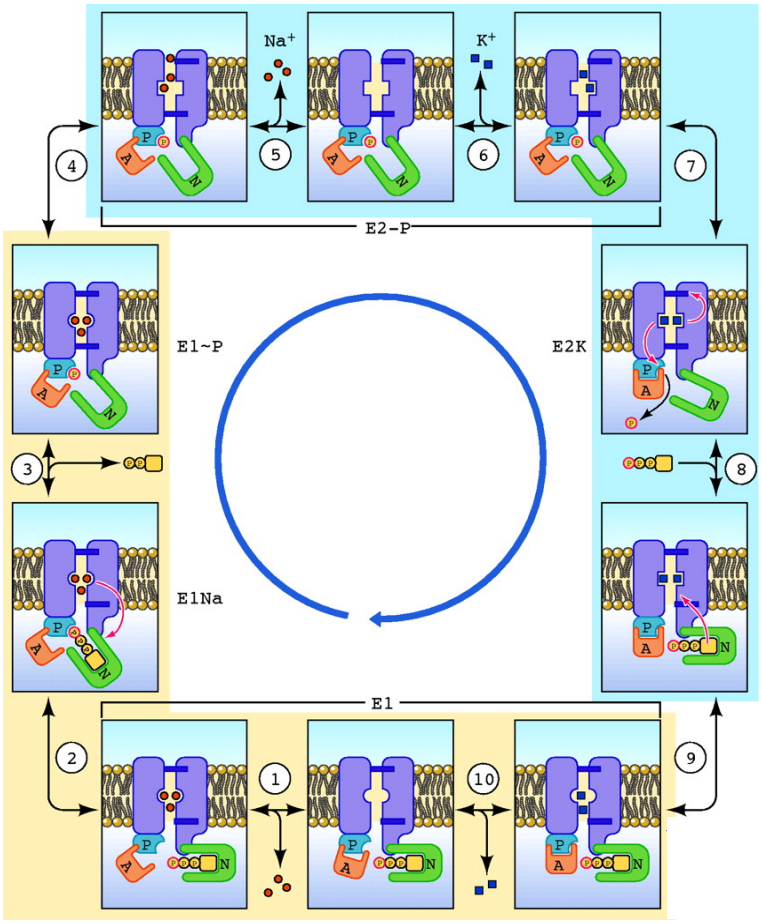

Figure 5: Catalytic cycle of the Na^+/K^+-ATPase. Adapted from Horisberger 2004. Journal of Physiology 2004;19:377-387.

In the E1 state the Na^+/K^+-ATPase has a high affinity for ATP and Na^+ (1). Once the ATP and Mg^{2+} are bound to the N-domain 3 Na^+ can enter (2). Subsequently, the N-domain undergoes a rotation to be in close proximity to the P- and A-domain. Auto-phosphorylation takes place at a conserved amino acid sequence (DKTGT) located on the P-domain, which gives rise to a phorphrylated aspartate (D376) and the E1P state of the ATPase (3). With this

phosphorylation a conformational change is induced in the enzyme that opens the extracellular gate (4) to release the Na^+ towards the extracellular space (5). This E2-P state has now a high affinity for K^+ (6). Two K^+ bind (7) and after dephophorylation, (8) the extracellular gate can close causing a conformational change leading to the original state of the pump. Phosphorylation occurs with the help of the A-domain. The glutamate at the TGES motive can position a water molecule for hydrolysis to release the phosphoryl group. ATP can bind again and 2 K^+ are released to the cytoplasmic side (9-10), giving the possibility to initiate a new reaction cycle.

1.5.3 Isoforms of the Na^+/K^+-ATPase

The expression pattern of the α- and β-isoforms is regulated in a tissue-specific manner. In humans four isoforms of the α-subunit (α1-α4) have been discovered. The α1-isoform is ubiquitously expressed in almost all tissues and is the predominant version found in the kidney together with β1-subunit. The α2-isoform is mostly expressed in adipocytes (Lytton, 1985), in the brain (McGrail et al., 1991), vascular smooth muscles (Zhang et al., 2005) skeletal and heart muscles (Hundal et al., 1992; Lavoie et al., 1997; Zahler et al., 1992). The α3-isoform is a primary source in neurons (Hieber et al., 1991) whereas the α4-isoform is only expressed in the testes (Shamraj and Lingrel, 1994). For the β-subunit, commonly three isoforms have been suggested (β1, β2, and β3) (Blanco and Mercer, 1998; Morth et al., 2011). However, there is evidence for a fourth (β4) isoform in humans but its existence is not clearly linked to be a part of the Na^+/K^+-ATPase (Okamura et al., 2003; Pestov et al., 1999). The β-isoforms are reflecting a similar distribution as the α-subunits. Also here the β1-isoform is found in almost all tissues, β2 is mainly expressed in neurons and skeletal muscle (Lavoie et al., 1997; Peng et al., 1997). The β3-isoform is present in a variety of tissues like kidney, lung, stomach, colon, spleen, and liver (Malik et al., 1996). Different Isoform combinations have been discovered in mammalian tissue and a study in insect cells could demonstrate that various combinations of the α- and β-isoforms can still form a functional enzyme (Blanco et al., 1995a, 1995b). This indicates that there is a wealth of possibilities for the regulation of the Na^+/K^+-ATPase that is certainly not completely understood so far.

1.5.4 Physiological role of the Na^+/K^+-ATPase

By regulating the Na^+ and K^+ balance in the cell and the extracellular milieu the Na^+/K^+-ATPase is essential to guarantee the cellular homeostasis. This involves regulation of osmosis (Sáez et al., 2009), maintenance of the electrochemical gradient and resetting of the membrane potential after neuronal excitation (Brodie et al., 1987) as well as skeletal muscle

contractility (Clausen, 2003). In addition to these functions it plays a crucial role in the renal tubular epithelial cells to maintain the sodium gradient for continuous reabsorption of Na^+ from the glomerular filtrate (Bagrov et al., 2009). Furthermore, the energy stored in the Na^+ gradient drives a secondary transport system to move molecules across the plasma membrane leading to the uptake of nutrition such as amino acids and glucose into cells (Blanco and Mercer, 1998).

The Na^+/K^+-ATPase and more precisely the extracellular side of the α-subunit serves as a specific target for cardiotonic steroids. Binding of cardiotonic steroids to the α-subunits results in an inhibition of the Na^+/K^+-ATPase (Palasis et al., 1996). Extracts from plants or dried skin of toads, enriched in cardiotonic steroids, were already known for a long time in traditional medicine and used for the treatment of heart dysfunctions. In 1875 the first pure cardiotonic steroids called “digitoxin” was isolated from the foxglove plant (*Digitalis purpurea*) and was pharmacologically used for the treatment of congestive heart failure (Diefenbach and Meneely, 1949). Later on, it was replaced by a slightly modified cardiotonic steroid “digoxin” from *Digitalis lanata* (Gheorghiade et al., 2006). Binding of digoxin to the Na^+/K^+-ATPase exerts a positive ionotrophic effect. Partial inhibition of the Na^+/K^+-ATPase in the heart increases the intracellular Na^+ concentration and couples the increase of intracellular Ca^{2+} concentration by the activation of the Na^+/Ca^{2+}-exchanger. In turn Ca^{2+} influx affects the strength of the myocardial contractility to overcome congestive heart failure (Langer, 1977). However, nowadays there are more effective drugs on the market for the treatment of this disease (Belz et al., 2001). It is important to note that cardiotonic steroids have shown to differ in their binding affinities to various α-subunit isoforms and between mammalian interspecies (Abeywardena et al., 1984; Crambert et al., 2000).

In vertebrates also endogenous cardiotonic steroids are produced such as ouabain, which is one of the best-studied inhibitor of the Na^+/K^+-ATPase (Hamlyn et al., 1991). Noteworthy, under physiological conditions ouabain levels are very low. In addition, it has been shown that these concentrations cannot cause a perturbation of the overall ion concentration in cells. In contrast, binding of ouabain initiates a signaling cascade. Studies of Liu and colleagues could show that there is a subpopulation of the Na^+/K^+-ATPase, which resides in caveolae (Liu et al., 2005). In these regions the Na^+/K^+-ATPase is found to be closely associated with the non-receptor tyrosine kinase Src, a known protein acting in cell signaling (Liang et al., 2006). Binding of ouabain leads to a conformational change in the α-subunit and activates the Src kinase. This results in further transactivation of epidermal growth factor receptor (EGFR) that relays its signal to the mitogen-activated protein (MAP) kinase signaling pathway (Haas et al., 2002). It was indeed observed that binding of ouabain to the Na^+/K^+-ATPase could influence multiple cellular functions. It can alter gene expression that

leads to the formation of tight junctions, proliferation, differentiation, and migration in epithelial cells (Contreras et al., 2006).

1.6 Aim of this thesis

The current working hypothesis is that FGF2 directly translocates across the plasma membrane in a folded state. This process is highly dependent on $PI(4,5)P_2$ for recruitment of FGF2 to the inner plasma membrane leaflet followed by the induction of FGF2 oligomers. This leads to the subsequent formation of a toroidal lipidic pore through which FGF2 can traverse the plasma membrane. On the extracellular side membrane proximal HSPGs drive directional export of FGF2 and immobilize FGF2 molecules on the cell surface (Nickel, 2010; Steringer et al., 2012). Recently, Tec kinase was discovered in a genome-wide siRNA screen. It was shown that post-translational modifications of FGF2 such as phosphorylation of the tyrosine residue 82 mediated by the Tec kinase is crucial for FGF2 secretion (Ebert et al., 2010). Based on the genome-wide RNAi screen, this thesis aimed at the identification of further proteinaceous factors involved in FGF2 secretion.

One candidate, which was discovered during the RNAi screen, was the α1-subunit of the Na^+/K^+-ATPase acting as a potential positive regulator of FGF2 secretion. In addition to these findings, the Na^+/K^+-ATPase was already mentioned years ago being involved in FGF2 export from cells. However, these studies were solely based on pharmacological evidence and, ever since, have not been validated by independent methods (Dahl et al., 2000; Florkiewicz et al., 1998). The main goal of this study was to characterize the role of the Na^+/K^+-ATPase in regard to FGF2 secretion on a molecular level. For this purpose, the first step was to validate the initial screening hit with several independent siRNAs in a cell-based (fluorescence-activated cell sorting) FACS assay to monitor FGF2 secretion after knockdown. The FACS assay was also applied to control pleiotropic effects that could compromise cellular functions as a result of siRNA-mediated knockdown of the Na^+/K^+-ATPase.

In the second part, interaction studies of the α1-subunit and FGF2 were carried out. This involved an *in vivo* approach using a conventional immunofluorescence assay as well as a Duolink assay to assess their compartments of interaction in HeLa cells. Furthermore, *in vitro* experiments were applied to identify in more detail their region of interaction. For this reason the cytoplasmic domains of the α1-subunit of the Na^+/K^+-ATPase were expressed and purified to test for their ability to bind to FGF2 in pull-down assays. In addition, binding constants of this interaction were determined. In order to characterize the interaction

interface more closely deuterium exchange experiments as well as mutational analysis were conducted.

The last part of this study aimed at the identification of small molecules that could interfere with the interaction of FGF2 and the cytoplasmic region of the α1-subunit of the Na^+/K^+-ATPase. This offers a huge potential to regulate this interaction and will allow for more detailed studies to investigate the molecular mechanism of FGF2 secretion. Furthermore, the identification of small inhibitory molecules may lead to the development of anti-angiogenic drugs.

2 Materials and Methods

2.1 Materials

2.1.1 Chemicals and consumables

1 kb DNA ladder	New England Biolabs
100 bp DNA ladder	New England Biolabs
35 mm optical dish (∅ 1 cm gals bottom)	MatTek corportation
35 mm optical dish (∅ 2 cm gals bottom)	Ibidi GmbH
Acetic acid	Sigma-Adrich
Acetone	Merck
Acetonitrile	Sigma
ACQUITY UPLC C18 BEHcolumn	Waters Corporation
Agarose	Life Technologies
AlphaScreen® Glutathione Donor Beads	PerkinElmer
AlphaScreen® Histidine (Nickel Chelate Acceptor Beads) Detection Kit	PerkinElmer
Amicon Ultra-4 Centrifugal Filter (3K, 30K)	Millipore
Ammonium hydroxide	J.T.Baker
Ampicillin sodium salt	Gebru
Bacto Agar	BD (Becton Dickinson)
Bacto Tryptone	BD (Becton Dickinson)
Benzamidine hydrochloride	Applichem
Bovine serum albumin (BSA)	Roth
Bromphenol blue	Serva
Cell culture plates (10cm)	Corning Incorporated
Cell Dissociation Buffer Enzyme-Free PBS-based	Gibco (Life Technologies)
Chloramphenicol	Roth

Chloroquine	Sigma-Adrich
Collagen R	Serva Electrophoresis GmbH
Cryotrubes Cryo S	Greiner bio-one
Cuvette 10 x 4 x 45 mm	Sarstedt
Deionized water, TKA X-CAD	TKA
Deoxycholic acid sodium salt	Fulka
Diethylaminoethyldextran (DEAE-Dextran)	Sigma-Aldrich
Dimethyl sulphoxide (DMSO)	Sigma-Aldrich
dNTP-Mix (10 mM each)	PeQLab
Doxycycline	Clontech
DTT (1,4-Dithio-D,L-threitol)	Gebru
Dulbecco's Modified Eagle Medium (DMEM) low glucose	Biowest
Ethanol absolute	VWR
Ethidium bromide (EtBr)	Roth
Ethylenediaminetetraacetic acid (EDTA)	AppliChem
Fetal Calf Serum (FCS)	Biochrom AG
Formic acid	Merck
FuGene® HD	Promega
Glycerol 99 %	VWR
Glycine	AppliChem
GSH column (GSTrap™ FF, 5ml)	GE Healthcare
Guanidine hydrochloride	Sigma
Heparin column (HiTrap™ Heparin HP, 5 ml)	GE Healthcare
Heparin sodium salt from porcine intestinal mucosal	Sigma
His column (HisTrap™ FF crude, 5 ml)	GE Healthcare
InstantBlue, protein stain	Expedeon
isopropyl β-D-1-thiogalactopyranoside (IPTG)	Gebru
Kanamycin sulfate	Gebru

L-Glutathione reduced	Sigma
Magnesium chloride ($MgCl_2$)	AppliChem
Methanol	Sigma
MicroAmp Optical 96 well plate (0.1 ml)	Applied Biosystems
MOPS running buffer	Life Technologies
Multiwell culture plates (6-, 12-, 24, 96-well)	Greiner bio-one
Nonidet P40 (NP-40)	Roche
Nuclease-free water	Ambion
NuPAGE 4-10 % Bis-Tris Gel	Life Technologies
NuPAGE Antioxidant	Life Technologies
Oligofectamine Transfection Reagent	Life Technologies
Opti-MEM	Life Technologies
PageRuler prestained, protein ladder	Fermentas
PBS	Biochrom AG
PCR tubes (strip 8 x 0.2 ml)	G. Kisker GbR
PD-10 columns	GE Healthcare
Penicillin/Streptomycin	Biochrom AG
Petri dish 94 x 16 mm, sterile	Greiner bio-one
Pipette tip, Gilson, 200 µl and 1000 µl	Greiner bio-one
PMSF (phenylmethylsolfonyl fluorid)	Roche
Porozyme pepsin cartridge	Applied Biosystems
Potassium chloride (KCl)	AppliChem
Potassium dihydrogen phosphate (KH_2PO_4)	AppliChem
Primer and Oligonucleotides	Thermo Scientific
Protease Inhibitor tablets (complete, EDTA free)	Roche
ProxiPlate™-384 Plus, white 384-shallow well micorplate	PerkinElmer
qPCR Seal (Optical foil)	PeQLab
Reaction tube 1.5 ml	Sarstedt

Reaction tube 2 ml	Greiner bio-one
Reaction tube, sterile, 15 ml and 50 ml	Greiner bio-one
Silencer Select siRNA	Life Technologies
Sodium azide (NaN_3)	Roth
Sodium chloride (NaCl)	AppliChem
Sodium dodecyl sufate (SDS)	BioRad
Sodium hydrogen phosphate (Na_2HPO_4)	AppliChem
Superdex^{TM} 200 pg, Hiload^{TM} 16/600	GE Healthcare
Syringe filter (45 µm)	Sartorius
SYTOX green	Life Technologies
TaqMan Gene Expression Master Mix	Applied Biosystems
Tris base	Roth
Trypsin/EDTA	Biochrom AG
Tween 20	Roth
Wester blot transfer membrane, Immobilon-FL	Millipore
Whatman 3 MM paper	Whatman
Xylene cyanol FF	Serva
Yeast extract	Roth
β-Mercaptoethanol	Merck

2.1.2 Technical devices

Äkta purifier	GE Healthcare
Blotting chamber, MiniPreotean Trans Blot	BioRad
Centrifuge 5417R	Eppendorf
Chamber for agarose gels	BioRad
Confocal Microscope LSM 510	Zeiss
Direct Detect Spectrometer	Merck Millipore
FACSAria cell sorter	BD (Becton Dickinson)

FACSCalibur	BD (Becton Dickinson)
Gel-Doc 2000 System	BioRad
High-pressure homogenizer	Avestin
Incubator for bacteria plates	Heraeus
Incubator for eukaryotic cells	Heraeus
Laminar flow hood, Herasafe KS12	Thermo Scientific
Magnetic stirrer MR 3000	Heidolph
nanoACQUITY UPLC HDX ManagerTM	Waters Corporation
ND-1000 Spectrophotometer	NanoDrop Technologies
Odysee imaging system	LI-COR
Power supply to run gels; Power Pac 200	BioRad
Rosys Anthos 2001 plate reader	Anthos labtech
StepOne Plus Real-Time PCR System	Applied Biosystems
Thermo cycler, Primus 96 advanced	PeQLab
Thermomixer comfort	Eppendorf
Ultracentrifuge Optima L-90K	Beckman Coulter
Waters XEVO G2 TOF with ESI source	Waters Corporation
XCell SureLock (chambers for SDS-PAGE)	Invitrogen (Life Technologies)
EnVision 2101 Multilabel Plate Reader	PerkinElmer

2.1.3 Kits and assays

BCA protein assay	Pierce
DNA Ligation Kit	Takara
Duolink Kit	Olink Bioscience
DuolinkII Detection Reagent Red (92008-0030)	Olink Bioscience
ImProm-II Reverse Trascription System	Promega
MBS Mammalian Transfection Kit	Stratagene
NucleoSpin Plasmid Kit	Macherey-Nagel
pGEM-T Vector System I Kit	Promega

Plasmid Midi Kit	Qiagen
QIAquick Gel Extraction Kit	Qiagen
QIAquick PCR Purification Kit	Qiagen
RNeasy Mini Kit	Qiagen
Zero BluntII TOPO PCR Cloning Kit	Life Technologies

2.1.4 Enzymes

High-Fidelity DNA Polymerase, Precisor	BioCat
Phosphatase, alkaline (AP)	Roche
Restriction endonucleases	New England Biolabs
Thrombin 500 units	GE Healthcare

2.1.5 Antibodies

Primary Antibodies	
anti-ATP1A1 (α1-subunit) mouse monoclonal	Abcam (ab7671)
anti-ATP1B1 (β1-subunit) mouse monoclonal	Thermo Scientific (MA3-930)
anti-Cadherin mouse monoclonal	Abcam (ab6528)
anti-FGF2 rabbit polyclonal	RG Nickel
anti-FLAG mouse monoclonal	Sigma (F1804)
anti-GAPDH mouse monoclonal	Life Technologies (AM4300)
anti-GFP rabbit polyclonal	RG Nickel
anti-GM130 mouse monoclonal	RG Wieland
anti-HA mouse monoclonal	RG Wieland
anti-transferrin receptor; mouse monoclonal	Life Technologies (13-6800)
anti-COPB1 (βCOP) B1.2 rabbit polyclonal	RG Wieland
anti-tubulin (alpha) rabbit polyclonal	Abcam (ab18251)

Secondary Antibodies	
Alexa Flour 488 goat anti-rabbit	Life Technologies (A11034)
Alexa Fluor 546 goat anti-mouse	Life Technologies (A11030)
Alexa Flour 633 goat anti-rabbit	Life Technologies (A21071)
Alexa Fluor 680 goat anti-rabbit	Life Technologies (A21076)
Allophycocyanin (APC) goat anti-rabbit	Life Technologies (A10931)
IRDye 800 CW goat anti-mouse	Odyssey (926-32210)
DuolinkII PLA MINUS anti-mouse	Olink Bioscience (92004-0030)
DuolinkII PLA PLUS anti-rabbit	Olink Bioscince (92002-0030)

2.1.6 Plasmids

Plasmid	Application	Resistance	Origin
pRevTre2 SP-GFP-CD4	Mammalian vector stable expression	Ampicillin	Thesis
pUC57 CD1-3	Bacterial vector amplification	Ampicillin	Eurofins /synthetic gene
pGEM-T	Bacterial vector amplification	Ampicillin	Promega
pCR-BluntII-TOPO	Bacterial vector amplification	Kanamycin	Life Technologies
pGex2mod	Bacterial vector recombinant expression	Ampicillin	Thesis
pGex2mod	Bacterial vector recombinant expression	Ampicillin	Hans-Michel Müller
pGex2mod GST-CD1	Bacterial vector recombinant expression	Ampicillin	Hans-Michel Müller
pGex2mod GST-CD2	Bacterial vector recombinant expression	Ampicillin	Hans-Michel Müller
pGex2mod GST-CD3	Bacterial vector recombinant expression	Ampicillin	Hans-Michel Müller

pGex2mod GST-CD2-3	Bacterial vector recombinant expression	Ampicillin	Hans-Michel Müller
pGex2mod GST-CD1-3	Bacterial vector recombinant expression	Ampicillin	Hans-Michel Müller
pQE30 hisFGF2-wt	Bacterial vector recombinant expression	Ampicillin	Hans-Michel Müller
pGex2T GST-FGF2	Bacterial vector recombinant expression	Ampicillin	Claudia Seelenmeyer
pGex2T GST-Δ28 FGF2	Bacterial vector recombinant expression	Ampicillin	Thesis
pQE30 hisFGF2 K27E/D28K	Bacterial vector recombinant expression	Ampicillin	Thesis
pQE30 hisFGF2 D99R	Bacterial vector recombinant expression	Ampicillin	Thesis
pQE30 hisFGF2 K138E	Bacterial vector recombinant expression	Ampicillin	Thesis
pQE30 hisFGF2 T121R	Bacterial vector recombinant expression	Ampicillin	Thesis

2.1.7 Oligonucleotides and primer sequences

Primer	Sequence (5'-3')	Origin
S-21 eGFP_*SalI HindIII*	GC*gtcgac*GGC*aagctt*GTGAGCAAGGGCGAGGAGCTG	Thesis
AS-22 eGFP_*NotI BamHI*	CG*gcggccgc*C*ggatcc*CTTGTACAGCTCGTCCATGCCG	Thesis
S-23 CD4_*BamHI*	GC*ggatcc*GACGTCATCAAGGTTCTGCCCA	Thesis
AS-24 CD4_*NotI*	*GCgcggccgc*TCAGTTTGTTGCTGCGAATGTCTCC	Thesis
S-50 alpha1 hATP1A1	GCTGGATCAACGATGTGGAAG	Thesis
AS-51 alpha1 hATP1A1	CACCAGGTAGGTTTGAGGGG	Thesis
S-52 alpha2 hATP1A2	CCATCCCACTCCACTATGTTG	Thesis
AS-53 alpha2 hATP1A2	CCAGTCTCAGGCTCTTGCAC	Thesis
S-54 alpha3 hATP1A3	GCCCGGCAACCTGGTGGGCATCC	Thesis

AS-55 alpha3 hATP1A3	GGACAGGAAGGCAGCCAGGGCCG	Thesis
S-56 alpha4 hATP1A4	CAGTGGACCTATGAGCAACG	Thesis
AS-57 alpha4 hATP1A4	TGACGGATGAGGAGTTTTCTG	Thesis
S-68 beta1 hATP1B1	CCGTTTTCAGGGACGTTTTG	Thesis
AS-69 beta1 hATP1B1	CAGTAAAAATGGGCACGTCC	Thesis
S-70 beta2 hATP1B2	CGTGAGCCACCGCGCCCGGC	Thesis
AS-71 beta2 hATP1B2	GGTGGGGGCAGATCTGGGCTCAGGGG	Thesis
S-72 beta3 hATP1B3	AGTTATGTTCAAAATCACAGCACG	Thesis
AS-83 beta3 hATP1B3	CCTACATGTTTGGAATCAGGTG	Thesis
S-84 beta4 hATP1B4	TGTATTTTTGGCGGAGACAG	Thesis
AS-85 beta4 hATP1B4	CAGTCTTGATCAACAATGTCACC	Thesis
S-147 Δ28 FGF2_*BglII*	GGG*agatct*CCCAAGCGGCTGTACTGCAAAAACG	Thesis
AS-134 FGF2_*XhoI*	CTTCCAATGTCTGCTAAGAGCTAG*ctcgag*CCGG	Thesis
AS-151 FGF2_*EcoRI*	CCC*gaattc*TCAGCTCTTAGCAGACATTGGAAGAAAAAG	Thesis
S-156 FGF2 K27E/D28K	CGCCCGGCCACTTCGAGAAGCCCAAGCGGCTGTA	Thesis
AS-157 FGF2 K27E/D28K	TACAGCCGCTTGGGCTTCTCGAAGTGGCCGGGCG	Thesis
S-158 FGF2 D99R	ATTACTGGCTTCTAAATGTGTTACGCGTGAGTGTTTCTTTTTTG AACGATTG	Thesis
AS-159 FGF2 D99R	CAATCGTTCAAAAAAGAAACACTCACGCGTAACACATTTAGAAG CCAGTAAT	Thesis
S-160 FGF2 T121R	ACAATACTTACCGGTCAAGGAAATACAGGAGTTGGTATGTGGC	Thesis
AS-161 FGF2 T121R	GCCACATACCAACTCCTGTATTTCCTTGACCGGTAAGTATTGT	Thesis
S-162 K138E	GCAGTATAAACTTGGATCCGAGACAGGACCTGGGCAGAAAG	Thesis
AS-163 K138E	CTTTCTGCCCAGGTCCTGTCTCGGATCCAAGTTTATACTGC	Thesis

Oligonucleotides	Sequence (5'-3')	Origin
S-109 **Flag**_*AgeI PacI*	*ccggt***GATTACAAGGATGACGACGATAAG**TGA*ttaat*	Thesis
AS-110 **Flag**_*AgeI PacI*	*taa*TAATCA**CTTATCGTCGTCATCCTTGTAATC***a*	Thesis
S-109 **Yes**_*HindIII SalI*	*aagctt*GCCACC**ATGGGCTGCATTAAAAGTAAAGAAAACAA AAGTCCAGCCATTAAATACAGACCT***aagctt*	Thesis

AS-110 **Yes**_*HindIII SalI*	*agctt***AGGTCTGTATTTAATGGCTGGACTTTTGTTTTCTTTACTTTTAATGCAGCCCAT**GGTGGC*a*	Thesis
S-122 **Tom**_*AgeI PacI*	*ccggt***ATGGTGGGTCGGAACAGCGCCATCGCCGCCGGTGTATGCGGGGCCCTTTTCATTGGGTACTGCATCTACTTCGACCGCAAAAGACGA***ttaat*	Thesis
AS-123 **Tom**_*AgeI PacI*	*taa***TCGTCTTTTGCGGTCGAAGTAGATGCAGTACCCAATGAAAAGGGCCCCGCATACACCGGCGGCGATGGCGCTGTTCCGACCCACCAT***a*	Thesis

2.1.8 Small interfering RNAs (siRNAs)

Gene Product	Gene ID	siRNA ID	Sense sequence (5'-3')	Company
Human Na/K-ATPase α1-chain ATP1A1	476	s1718	CUCGCUCACUGGUGAAUCAtt	Ambion
Human Na/K-ATPase α1-chain ATP1A1	476	s1719	GAUUCGAAAUGGUGAGAAAtt	Ambion
Human Na/K-ATPase α1-chain ATP1A1	476	s1720	CAUCCAAGCUGCUACAGAAtt	Ambion
Human Na/K-ATPase β1-chain ATP1B1	2597	s1734	GAAAGAACGAGGAGACUUUtt	Ambion
Human Na/K-ATPase β3-chain ATP1B3	481	s1741	GGAUGAUCGUGACAAGUUUtt	Ambion
Human coatomer complex, subunit β1 COPB1	1315	s3371	GGUCUGUCAUGCUAAUCCAtt	Ambion
Human glyceraldehyde-3-phosphate dehydrogenase GAPDH	483	s5574	CUCAUUUCCUGGUAUGACAtt	Ambion
Human fibroblast growth factor 2 FGF2	2247	Custom designed	GGAGUGUGUGCUAACCGUUtt	Ambion
Green fluorescence protein GFP		Custom designed	CAAGCUGACCCUGAAGUUCtt	Ambion

All siRNAs were ordered as a validated version with a silencer select modification from Ambion/ Applied Biosystem (belongs to Life Technologies)

2.1.9 TaqMan gene expression assays

TaqMan primer and probes	Gene ID	Company
Hs 00167556_m1	Human ATP1A1 ID: 476	Applied Biosystems
Hs 00426868_g1	Human ATP1B1 ID: 2597	Applied Biosystems
Hs 0074857_mH	Human ATP1B3 ID: 481	Applied Biosystems
Hs 0074857_mH	Human GAPDH ID: 483	Applied Biosystems

2.1.10 Bacteria and media

Bacteria and media used for molecular cloning and plasmid amplification:

Eschericia coli (E. coli) DH5α (Life Technologies)

LB-Medium:	10 g	NaCl
	10 g	Tryptone
	5 g	Yeast extract
	ad 1 l	deionized water

For LB agar plates 1 l of LB-Medium was supplemented with 16 g of Agar and the solution was boiled until the Agar was dissolved. Antibiotics for bacterial selection were added at 60°C followed by casting the plates.

Bacteria and media used for protein expression:

E. coli BL21-(DE3)-RIL codon plus (Agilent Technologies) expression of proteins from pGex2T and pGex2mod vector *E. coli* W3110Z1 provided from Bukau (derivate of W3110, Hoffmann-La Roche AG) expression of proteins from pQE30 and pQE60 vector.

2YT-Medium:	5 g	NaCl
	16 g	Tryptone
	10 g	Yeast extract
	ad 1 l	deionized water

To select for bacteria resistance the corresponding antibiotics were used:

Ampicillin	final concentration of 100 µg/ml
Kanamycin	final concentration of 25 µg/ml
Chloramphenicol	final concentration of 36 µg/ml

2.1.11 Mammalian cell lines

Cell line	Expression of doxycycline induced proteins	Origin
$HeLa_{MT}$	-	RG Schwappach
$HeLa_{GFP-CD4}$	GFP-CD4	Thesis
HeLa $S3_{MT}$	-	RG Nickel
HeLa $S3_{FGF2\_IRES\_GFP}$	FGF2 and GFP	Sabine Wegehingel

2.2 Molecular biological methods

2.2.1 Polymerase chain reaction (PCR)

The polymerase chain reaction (Mullis and Faloona, 1987; Saiki et al., 1988) is a well-established method that allows for the amplification of specific DNA fragments.

PCR reaction:
1 µl template DNA (10-50 ng)
1 µl dNTPs (10 mM each)
1 µl Sense Primer (100 pmol)
1 µl Antisense Primer (100 pmol)
10 µl 5x High fidelity buffer
0.5 µl High-Fidelity Polymerase (1 Unit, BioCat)
35.5 µl deionized water

Cycle Steps	Temperature	Time	Cycle(s)
Initial denaturation	98°C	2 min	1
Denaturation	98°C	30 s	30
Annealing	X = 2-5°C below the melting temperature (Tm) of the lower primer	30 s	
Extension	72°C	30 s/kb	
Final extension	72°C	10 min	1
Cooling	8°C	10 min	1

The annealing temperature (X) was calculated according to the following formula, where N represents the number of base pairs of a primer:

$$Tm = 81.5+0.41\ (\%\ GC)- \frac{675}{N}$$

2.2.1.1 Site-directed mutagenesis

This method was used to introduce site-specific mutations for amino acid changes. As a template the pQE30 hisFGF2-wt was used and the PCR reaction was set up as described above. Primes were designed with the help of QuikChange Primer Design program from Agilent Technologies. And the PCR program was set as follows:

Cycle Steps	Temperature	Time	Cycle(s)
Initial denaturation	94°C	4 min	1
Denaturation	94°C	45 s	
Annealing	60°C	30 s	18
Extension	72°C	6 min	
Final extension	72°C	10 min	1
Cooling	8°C	10 min	1

17 µl of the PCR reaction were used to perform a DpnI digestion (section 2.2.2.1) to remove residual template DNA. This reaction was in total transformed (section 2.2.2.7) into DH5α *E. coli* cells. As a control 17 µl of undigested PCR reaction was transformed. Mutagenesis was verified by DNA sequencing (section 2.2.2.10).

2.2.2 Cloning procedure

The general procedure usually starts with the amplification of a specific gene product by PCR. The PCR fragment is then ligated into a replication vector and transformed into DH5α *E. coli* cells. After selection of antibiotic resistant colonies on LB agar plates the plasmids were isolated and a control digestion verified the insert. At this step, further modification can be conducted, for example the insertion of sequences by oligonucleotides. The construct can be cut out of the replication vector and inserted into the final vector. After an additional transformation, selection and control digestion are performed and the plasmid DNA is sequenced for verification.

2.2.2.1 DNA Digestion

Endonucleases are used to cut double stranded DNA fragments of interest. Endonucleases are enzymes that recognize a specific DNA sequence for digestion generating either sticky or blunt-ended DNA. The DNA fragment of interest and the vector have to be treated with the same enzymes for directional cloning. All digestions were performed with enzymes from New England Biolabs according to manufacture's instructions to ensure the right buffer conditions for optimal enzyme activity. Per 2 µg DNA, 2-4 units of each enzyme were used. The digestion reaction was incubated for 1-2 h at 37°C. Digested vectors were treated with an alkaline phosphatase (Roche). The digestion reaction was treated with 1 µl of the enzyme and appropriate amounts of buffer and further incubated for 30 min at 37°C. With this treatment, the 5' phosphate of the DNA will be removed to prevent re-ligation of the vector.

2.2.2.2 Hybridization of oligonucleotides

This procedure was performed to ligate small double stranded DNA fragments with a size of ≤150 bp into a predigested and phosphate-removed vector. Complementary single stranded oligonucleotides with a 5' phosphate were hybridized. A dilution of 1:1000 of each oligonucleotide stock (100 pmol/µl) of sense and antisense sequence was prepared in water. An amount of 10 µl of each dilution was mixed with 1 µl of 25 mM $MgCl_2$ and added to the reaction. The mixtures were incubated for 2 min at 95°C in a thermomixer. The reaction was slowly cooled down to room temperature (RT). Only 1 µl of double stranded oligonucleotides was used for a typical ligation reaction (section 2.2.2.6).

2.2.2.3 Agarose gel electrophoresis

Electrophoresis is used for separation of DNA bands of different sizes. The negatively charged nucleic acid molecules can move in an electric field. The molecules are loaded onto an agarose matrix with a defined pore size. Due to the size and conformation of the DNA, smaller molecules can migrate faster than larger molecules, thus leading to a separation of DNA fragments. For the preparation of 1% agarose gel, 1 g of agarose was heated up in a microwave with 100 ml of 1x TAE buffer until it was solved completely. After cooling, EtBr was added at a final concentration of 0.5 µg/ml and the agarose solution was poured into a tray. The agarose was cooled with a comb until it was solid. Finally, the comb was removed and the DNA samples with 1x sample buffer could be loaded into the wells. The agarose gel containing samples was covered with 1 x TAE buffer and electrodes were placed at each end of the chamber (120 V, 20-30 min). EtBr can intercalate between the base pairs of the DNA, making the bands on the gel visible while illuminating the gel with UV light (Gel-Doc 2000 System, BioRad). To estimate the size of the DNA fragment a marker was loaded on the gel.

50x TAE buffer:	242 g	Tris
	57.1 ml	Acetic acid
	100 ml	EDTA (0.5 M; pH 8)
	ad 1 l	deionized water
5x sample buffer:	0.25% (w/v)	Bromphenol blue
	0.25% (w/v)	Xylene cyanol FF
	30%	Glycerol, in deionized water

2.2.2.4 Gel extraction

Gel extraction is used to recover and purify DNA fragments from an agarose gel. In this way a DNA band with a certain size can be cut out from the gel, with ultraviolet (UV) light used for visualization. The obtained gel slice was treated according to manufacturer's instructions of the QIAquick Gel Extraction kit (Qiagen). The DNA was eluted with 30 µl of elution buffer. The isolated DNA can be used in a ligation reaction.

2.2.2.5 PCR purification

PCR fragments were purified prior to the ligation reaction with the QIAquick PCR Purification kit (Qiagen) according to manufacturer's instruction.

2.2.2.6 Ligation reaction

This method is employed to insert a desired DNA fragment into a vector. Therefore, the DNA fragment and vector have to be treated with the same restriction enzymes. Once the fragment is inserted into the vector a ligase catalyzes the formation of a covalent phosphodiester bond to join the two DNA strands together. To calculate the appropriate molar ratios of insert and vector, the following equation was used:

$$\frac{\text{amount of vector (ng)} \times \text{size of insert (bp)}}{\text{size of vector (b)}} = \text{insert (ng)} \quad \text{(molar ratio 1:1)}$$

For each ligation reaction different molar ratios of vector:insert were chosen (1:1, 1:3 and 1:6). Vector alone served as a control to estimate the background of the reaction. In general, 50 ng of vector were used for the reaction.

Ligation reaction performed with the DNA Ligation kit (Takara):

Desired molar ratios of vector and insert were mixed to a total volume of 5-10 µl. The same volume of solution I was added and the reaction was incubated in a thermomixer for 1 h at 16°C. Transformation (section 2.2.2.7) was performed by combining the whole reaction with 80 µl of competent *E. coli* cells.

Ligation of PCR products

The High-Fidelity polymerase was used for amplification with a 5'-3' proofreading exonuclease activity. Here, the blunt ended PCR products were ligated into pCR-BluntII-TOPO vector. The instructions from the manual Zero BluntII TOPO PCR Cloning Kit (Life Technologies) were followed. Alternatively, the PCR product can directly be cut with appropriate restriction enzymes and ligated into the final vector (section 2.2.2.6).

2.2.2.7 Transformation into *E. coli*

Calcium-competent cells were thawed on ice and 80 µl of cells were combined with the ligation reaction and gently mixed followed by an incubation time of 3 min on ice. In order for the cells to take up the DNA a heat shock was performed. The cells were placed in a water bath for 40 s at 42°C and again cooled down for 1 min on ice. With addition of 750 µl LB-Medium the cells were kept for 1 h at 37°C with gentle agitation at 450 rounds per minute (rpm) in a thermomixer. Finally, the cells were pelleted at 2500 relative centrifugal force (rcf) for 2 min and the pellet was gently resuspended in 70 µl medium and plated on an antibiotic selective agar.

2.2.2.8 Preparation of Plasmid DNA

To recover plasmid DNA from transformed *E. coli* cells, single colonies from an agar plate were picked and grown over night (o/n) in liquid LB-Media at 37°C with the addition of antibiotics. Extraction can be performed using different volumes of bacteria o/n culture according to the amount and purity of plasmid DNA that needs to be obtained. Plasmid purification kits were used according to manufacture's instructions.

Miniprep: NucleoSpin Plasmid (Macherey-Nagel); 6 ml of o/n culture

Midiprep: Plasmid Midi Kit (Quiagen); 100 ml of o/n culture

2.2.2.9 Determination of nucleic acid concentration

The DNA concentration can be measured photospectrometrically using a NanoDrop ND-1000 spectrophotometer. Absorbance is measured at an absorbance maximum of 260 nm for nucleic acids and the concentration calculated following the Lambert-Beer equation: $c = \frac{A}{E \times b}$

c = nucleic acid concentration [ng μl^{-1}] E = 50 for double stranded DNA

b = path length [cm] E = 50 for double stranded DNA

A = absorbance (no units) E = 40 for RNA

(E = wavelength dependent extinction coefficient [µl ng^{-1} cm^{-1}])

2.2.2.10 Sequencing of DNA

To confirm the correctness of the cloned DNA constructs, the purified plasmids were sent with an appropriate sequencing primer to GATC biotech company. Sequences were verified by using the ClustalW alignment algorithm from the European Bioinformatics Institute.

2.2.2.11 Overview of constructs created in this thesis

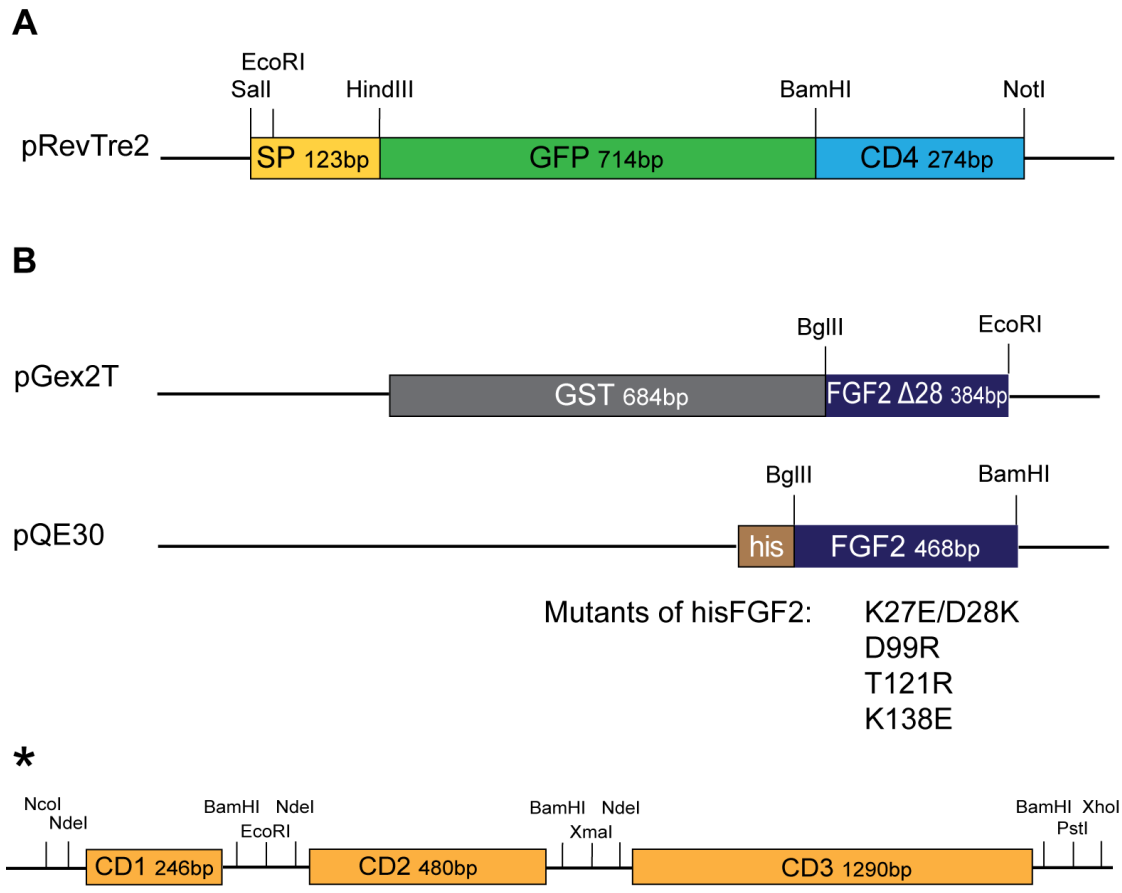

Figure 6: Schematic overview of constructs generated in this work. For **A)** Generation of stable mammalian cell lines and **B)** protein expression. The construct indicated with an asterisk was ordered as a synthetic gene from Eurofins, it was re-cloned by Hans-Michel Müller to generate N-terminal fusion constructs to GST and his, respectively. The following constructs were generated: GST-CD1-3 (full-length); GST-CD1 (domain CD1), GST-CD2 (domain CD2), GST-CD2-3 (domain CD2 and CD3), GST-CD3 (domain CD3) in pGex2mod vector and hisCD1-3 (full-length) was cloned into pQE30.

2.2.3 Isolation of total RNA

Total ribonucleic acid (RNA) was isolated from HeLa S3 cells after 48 h of siRNA transfection (section 2.3.2). Cells were grown in a 12-well or 6-well format to about 80% confluency. The isolation of total RNA was performed with the RNeasy Mini Kit from Qiagen according to manufacturer's manual.

2.2.4 Reverse transcription PCR (RT-PCR)

For reverse transcription of mRNA the ImProm-II Reverse Transcription System (Promega) was used according to the manufacturer's manual. Using this procedure makes it possible to generate single-stranded DNA (complementary DNA, cDNA) from an mRNA template. Primer annealing was performed in a reaction volume of20 µl. Amounts of 2 µl oligo dTPrimer and 1 µg of total RNA were added and incubated for 10 min at 70°C using a thermomixer followed by an additional incubation for 5 min on ice. The following components were mixed and the reaction was transferred to a thermocycler to perform the reaction:

5 µl $MgCl_2$ (25 mM)
8 µl 5 x buffer
1 µl RNAse inhibitor (1 unit)
4 µl dNTPs (10 mM each)
1 µl reverse transcriptase (1 unit)
1 µl RNAse free H_2O
add 20 µl of the previous annealing reaction

25°C	10 min
42°C	60 min
95°C	5 min
8°C	storage

The cDNA can be used as a template for quantitative real-time PCR (section 2.2.5) or PCR (section 2.2.1).

2.2.5 Quantitative real-time PCR (qRT-PCR)

Using quantitative real-time PCR, low amounts of cDNA can be amplified exponentially. This allows the relative amounts of mRNA transcripts to be quantified. For this purpose a gene-specific TaqMan Expression Assay (Life Technologies) (section 2.1.9) was used. Every assay is delivered with a gene-specific forward and reverse primer and probes that are labeled with a FAM™ dye that consists of a reporter and quencher. Primers and probes bind to the region that has to be amplified. The probe itself is quenched when intact. During the process of elongation mediated by the polymerase its exonuclaese activity removes the probe nucleotide by nucleotide. This leads to a dequenching effect and allows for measuring the emission of the fluorophore. The signal intensity of the emission directly correlates with the amount of template derived from the cDNA and concomitant of the messenger RNA (mRNA). The samples were measured in an optical 96 well plate that were sealed with an optical foil to avoid evaporation. The StepOne Plus Real-Time PCR System (Applied Biosystems) was operated according to manufacture's manual using the standard protocol for 2 hours.

Sample preparation for the TaqMan Gene Expression Assay in a 96 well plate:

TaqMan Gene Expression Assay (Primer & Probe) 20x mix	1 µl
TaqMan Gene Expression 2x Master Mix	10 µl
cDNA (from previous section 2.2.4, from a 1:4 dilution)	4 µl
	5 µl RNAse free H_2O

Cycle Steps StepOne System:	Temperature	Time	Cycle(s)
Complete denaturation of cDNA	95°C	2 min	1
Polymerase activation	95°C	10 min	1
DNA denaturation	95°C	15 s	
Annealing of primer and probes and elongation	60°C	1 min	40

The amount of mRNA detected from a certain gene of interest was normalized to an internal endogenous control such as mRNA levels from *glyceraldehyde 3-phosphate dehydrogenase* (GAPDH). The relative differences of mRNA levels from the gene of interest, of Mock and knockdown conditions were calculated and plotted.

2.3 Cell biological methods

2.3.1 Cell culture techniques

2.3.1.1 Cultivation of mammalian cells and medium

HeLa and HeLa S3 were grown on cell culture plates whereas HEK293T cells were grown on collagenated plates. All cell lines were cultured in DMEM complete medium and were kept in a carbon dioxide ($CO_{2)}$ incubator at 5% CO_2 and 37°C. Depending on the experimental format cells were seeded on various sizes of cell culture dishes.

Table 2: Overview of cell culture dishes

Plate format	Amount of medium
10 cm plate	10 ml cell culture medium
6-well plate	2 ml cell culture medium
12-well plate	1 ml cell culture medium
24-well plate	0.5 ml cell culture medium
48-well plate	300 µl cell culture medium
96-well plate	100 µl cell culture medium
35 mm optical dish (∅ 1 cm glass bottom)	2 ml cell culture medium
35 mm optical dish (∅ 2 cm glass bottom)	2 ml cell culture medium

Preparation of complete medium:

The DMEM cell culture medium was supplemented with 10% FCS, Penicillin (100 u/ml) and Streptomycin (100 µg/ml).

2.3.1.2 Collagenation of plates

Tissue culture plates were bathed with sterile collagen solution at a concentration of 0.02% and dried under a laminar flow hood.

2.3.1.3 Splitting of cells

Cells were passaged every 3-4 days when confluent. Old medium was aspirated and the cells were washed with PBS to remove old traces of medium. To adhere the cells 1-2 ml of

Trypsin/EDTA was added to the plate and the cells were resuspended in fresh medium and transferred into a new dish at the desired density.

PBS (Biochrom):	136.9 mM	NaCl
	2.7 mM	KCl
	8.3 mM	Na_2HPO_4 x H_2O
	1.5 mM	KH_2PO_4

2.3.1.4 Freezing and thawing of mammalian cells

For freezing, cells were detached from a 10 cm plate as described above (section 2.3.1.1) and resuspended in 1.4 ml of freezing medium that was transferred to a cryotube. After 48 h of incubation at -80°C in cryoboxes (ensuring a slow cooling process) the tubes were stored in liquid nitrogen.

For thawing, cryotubes with cells were removed from liquid nitrogen and rapidly thawed at 37°C. The cells were transferred to a 10 cm plate with complete medium until they adhere followed by subsequent change of medium.

Freezing medium:	DMSO 10% (v/v)
	FCS 20% (v/v)
	Complete medium 70% (v/v)

2.3.2 Small interference RNA (siRNA) transfection of mammalian cells

Transient transfection describes the transfer of genetic material such as siRNAs that are introduced into mammalian cells by passing through the cell membrane. In this case transfection reagents with cationic lipids were used, which fuse with the cell membrane and subsequently transfer the material into the cytosol.

2.3.2.1 Liquid phase transfection of siRNA

Transfection of siRNA was performed in 48-well plates. Prior to transfection 30,000 cells per well (HeLa and HeLa S3) were seeded in 200 µl of serum reduced Opti-MEM medium. Per well, 0.75 µl Oligofectamine and 3 µl Opti-MEM were mixed and incubated for 5 min at RT. In a second reaction 2.5 µl of the respective silencer select siRNA (3 µM in concentration) was mixed with 22.5 µl of Opti-MEM. The Oligofectamine reaction was then transferred to the siRNA mix, and briefly vortexed. For complex formation the reaction was incubated at RT for 20 min and subsequently added drop wise onto the cells. After 16 h the medium was replaced with normal complete medium. 24 h after transfection each transfected 48-well was transferred after trypsin treatment to a 12-well. Cells were subjected to further analysis 48 h after transfection.

2.3.3 Generation of stable cell lines

2.3.3.1 Principle of retroviral transduction

For generation of stable cell lines a retroviral transduction system of Molony Murine Leukemia Virus was used to produce high titer of recombinant virus particles. Therefore, HEK293T cells were transfected with different vectors. The pVPack-GP vector encodes viral structural proteins gag and the reverse transcriptase plus integrase pol. The pVPack-Eco vectors express the viral envelope protein specific for the target cells to be transduced. The gene of interest is cloned into a pRevTre2 vector. It contains a Tet-response element (TRE), composed of the tetO operator sequence. Furthermore, pRevTre2 contains 5' and 3' long terminal repeats (LTRs) that promote integration into the host cell genome and the minimal immediate early promoter of cytomegalovirus (CMV). The cotransfection of these vectors into HEK293T cells ensures the production of infectious replication-defective virus particles carrying the viral RNA coding for the gene of interest. HeLa wild type cells constitutively expressing the mouse cationic amino acid transporter (MCAT) (MCAT) retroviral receptor of the envelope protein and the Tet-On transactivator reverse tetracycline-responsive transcriptional activator (rtTA) were used as target cell line. These cells, $HeLa_{MCAT\text{-}TAM}$, were generated in this lab and previously termed $HeLa_{MT}$ (Engling et al., 2002), which can be used for virus transduction (Urlinger et al., 2000). After infection, the viral RNA genome is copied into DNA and eventually integrated into the host genome. Transcription of the gene of interest can be regulated by the addition of doxycycline (dox), a derivative of tetracycline. In the Tet-On gene expression system we used here, rtTA binds in the presence of dox to TRE and therefore activates the transcription of the gene under the control of the CMV promoter.

2.3.3.2 Experimental procedure

For generation of stable cell lines, the pVPack manual was followed according to manufacturer's instructions, which included the MBS mammalian transfection kit for host cell transfection (both from Stratagene). The following procedure was performed in a period of five days. On the first day, HEK293T cells were seeded onto 6-well plates. An amount of 9 µg of each DNA vector (pVPack-GP, pVPack-Eco and pRevTre2) were mixed with the gene of interest and subjected to sodium acetate precipitation. The DNA pellets were stored at 4°C with residual amounts of 70% ethanol. On the second day, HEK293T cells were transfected with the DNA for viral production. The DNA pellets were dried under a laminar flow hood and resuspended in 450 µl sterile deionized water, mixed with 50 µl of Solution I and 500 µl of Solution II followed by an incubation period of 10 min at RT. The mixture was added drop wise to the cells that were cultured in 2 ml MBS-containing medium 30 min prior to virus transduction. After 3 h, complete medium was replaced by complete medium

supplemented with 25 µM chloroquine. After 6 h, the medium was again replaced by fresh complete medium. On the fifth day, the virus particles were collected from the supernatant and filtered through a 0.45 µm filter membrane to retain the virus. A volume of 1.5 ml of the sterile viral supernatant plus DEAE-dextrane (dilution of 1:100) was added onto $HeLa_{MT}$ target cells, which were cultured in a 6-well plate format. Three days of viral transduction the efficiency was checked by FACS analysis.

2.3.3.3 Cell sorting

In order to isolate positive clones stably expressing the gene of interest in a doxycycline-dependent manner the cell lines were subjected to FACS sorting using a BD FACSAria cell sorter. Screening of successfully transduced cells was possible due to generation of fusion constructs to green fluorescence protein (GFP). $HeLa_{MT}$ cells were used to subtract GFP background signal derived autofluorescence of cells. The first round was an "on" sorting of cells, which were 24 h prior to sorting induced with 2 µg/ml of doxycycline and cells were collected according to their green fluorescence. After a period of seven days cells were collected that did not show green fluorescence, which were sorted in the absence of doxycycline. This ensures that fusion proteins are expressed in a doxycycline-dependent manner. The third round (after 7 days) was again an "on" sorting with doxycycline. Here, single cells were transferred to a 96-well plate. The single clones were expanded, again tested for their ability to respond to doxycycline to choose the cell clone that is used for following studies.

2.3.4 Fluorescence-activated cell sorting (FACS) analysis

For FACS analysis the FACSCalibur machine was used. With this method, single particles or cells can be measured when they pass the intersection of a laser beam. The signals give information about the relative size (forward light scatter, FSC), the relative complexity or granularity (side light scatter, SSC) as well as the fluorescence of a particle. The instrument is equipped with a laser that emits light at 488 nm to measure GFP fluorescence. A second laser diode emits light at 653 nm to measure allophycocyanin (APC), which is obtained from a fluorescently labeled antibody.

Immunolabeling of cells for FACS measurement (FACS assay)

After 48 h of siRNA knockdown, cells were induced for 16 h with doxycycline to induce expression of the reporter construct. Following this, cells were subjected to cell surface staining by immunolabeling with a primary and a secondary fluorescent labeled antibody.

Cells were cultivated in a 12-well format. Growth medium was aspirated and the cells were washed 1x with PBS. 300 µl of plain DMEM medium was added containing the first antibody (rabbit anti-GFP 1:500; rabbit anti-FGF2 1:200). The plates were gently shaken on ice for 1 h. Again, the antibody solution was aspirated, 1x washed with PBS and replaced by 300 µl of secondary antibody (goat anti-rabbit APC 1:500) followed by a 30 min incubation on ice. After an additional washing step with PBS, cells were detached with 50 µl of Cell Dissociation Buffer (Gibco) while incubating for 10 min at 37°C. The cells were transferred in a 1.5 ml test tube that contained 200 µl of plain DMEM medium. After labeling, cells were immediately subjected to FACS measurement and gently mixed prior to each measurement.

2.3.5 Immunofluorescence assay

Cells were grown in small optical glass dishes to a confluency of about 70%. Medium was removed and cells were washed with 2 ml of PBS. 1 ml of ice-cold acetone was added and incubated for 6 min at -20°C followed by three washing steps of PBS. Cells were blocked with 1% BSA for 10 min at RT. The primary antibodies were diluted in 350 µl of 1% BSA and incubated for 1 h at RT (mouse anti-ATP1A1 1:100; mouse anti-cadherin 1:100; rabbit anti-FGF2 1:100 (RG Nickel); mouse anti-FLAG 1:500; mouse anti-GM130 1:1,000; mouse anti-HA 1:500; mouse anti-transferrin receptor 1:500). After three washing steps with PBS, cells were again blocked and incubated for 30 min at RT with 350 µl of secondary fluorescently labeled antibody solution (Alexa Fluor 488, 546 or 633 1:500, respectively). The secondary antibodies were diluted in 1% BSA and incubated in the dark. To visualize the nuclei, SYTOX green (Life Technologies) was added at a dilution of 1:100,000 to the secondary antibody incubation. After labeling cells were washed three times and subjected to imaging on the confocal microscope LSM 510 (Zeiss) with remaining PBS on top.

2.3.6 Life-cell fluorescence microscopy

In case cells expressed a fluorescently-tagged proteins such as FGF-GFP or GFP-CD4, cells were grown on optical class dishes and the medium was replaced by PBS prior to imaging at the confocal microscope LSM 510 (Zeiss).

2.3.7 Duolink assay

Duolink® is an *in situ* proximity ligation assay (PLA) with the aim to detect interactions of endogenous proteins in single cells. In this technique cells were grown on glass bottom culture dishes (MatTek 10 mm microwell) fixed and stained as described in section 2.3.5 with two primary antibodies targeting two different proteins. Importantly, the two primary

antibodies should originate from different species, in this case from mouse and rabbit. The secondary antibodies are derived from the Duolink kit (Olink Bioscience) and are either specific to the primary mouse (PLA anti-mouse MINUS) or rabbit (PLA anti-rabbit PLUS) antibody (Figure 7b). Each of them is linked to a unique synthetic oligonucleotide that after coming into close proximity (<40 nm) can bind to each other. With the help of a DNA ligase, both oligonucleotides will be connected to each other forming a circularized DNA strand (Figure 7c). In a second step, a polymerase will amplify the DNA incorporating fluorescent probes. Therefore, upon antibody binding to adjacent proteins a highly fluorescent amplification product will be generated resulting in one red spot that corresponds to one interaction site (Figure 7e) (Söderberg et al., 2006). The sites of interaction can be quantified with a Duolink® ImageTool software that recognizes the interaction spots after assigning all the nuclei to the cells (Figure 7f). Staining with the secondary PLA antibodies, ligation, amplification as well as quantification were performed according to manufacturer's manual from Olink Bioscience. Images were acquired with the confocal microscope LSM 510 (Zeiss).

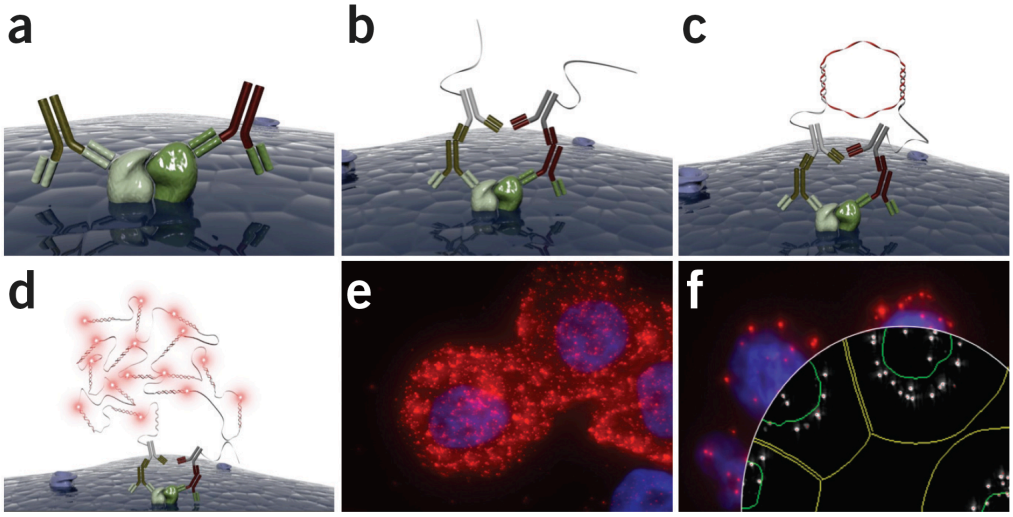

Figure 7: Principal of the Duolink assay. Image source: GEN Genetic Engeneering & Biotechnology News (Fredriksson et al., 2009)

2.4 Biochemical methods

2.4.1 Preparation of cell lysates from mammalian cells

Cells were washed with 1x PBS to remove residual medium. A volume of 100-200 µl of RIPA-buffer was added to a 12- to 6-well format of cell culture dishes and cells were scraped off with a cell scraper. For lysis, the suspension was transferred to a 1.5 ml test tube and incubate for 15 min on ice while vortexing every 5 min. As an alternative, he suspension can be passed through a needle. The samples were spun down tat 14,000 g for 10 min to separate the total protein from the cellular debris. The supernatant was transferred to a new tube and the protein concentration analyzed by bicinchoninic acid (BCA) assay (section 2.4.2). In general, 40-50 µg of total protein of the lysates were loaded onto a SDS-PAGE and subjected to further Western blot analysis.

RIPA buffer:	150 mM	NaCl
	1% (v/v)	NP-40
	0.5% (w/v)	Deoxycholic acid
	0.1% (w/v)	SDS
	50 mM	Tris pH 8.0
	in deionized water	

2.4.2 Measurement of protein concentrations

Protein concentration of recombinant proteins

By NanoDrop

Protein concentrations can be measured photospectroscopically using a NanoDrop ND-1000 spectrophotometer. Due to the absorbance of tyrosine and tryptophan residues at 280 nm protein concentrations can be determined. The absorbance is corrected for the protein specific extinction coefficient (E) and the molecular weight, calculated with ExPASy ProtParam tool, according to the amino acid sequence of the protein. Absorbance is measured and the concentration calculated following the Lambert-Beer equation:

$$c = \frac{A}{E \times b}$$

c = protein concentration [mg ml^{-1}]
b = path length [cm]
A = absorbance (no units)
E = extinction coefficient [M^{-1} cm^{-1}]

By BCA assay

After knockdown, cell lysates were prepared (section 2.4.1) to load equal amounts of total protein on a polyacrylamide gel (section 2.4.3) to monitor the success of the knockdown. Protein concentration determination was performed using a BCA protein assay quantification system (Pierce). For this procedure, 2.5 µl of lysate (of a 1:4 dilution) were diluted with 47.5 µl of deionized water and 200 µl of the BCA reagent (solution A: solution B = 50:1) were added. The reaction was incubated for 30 min at 60°C. A volume of 150 µl of each reaction was transferred to a 96 well plate and the absorbance was measured at 562 nm on an Elisa reader (Rosys Anthos 2001 plate reader, Anthos labtech). To determine the protein concentration, a BSA standard curve from 2.5-10 µg/ml was also measured in parallel.

2.4.3 SDS-polyacrylamide gel electrophoresis (SDS-PAGE)

Proteins were separated according to their molecular mass using gel electrophoresis standard conditions of Laemmli (Laemmli, 1970). Samples were boiled with 1x SDS sample buffer for 7 min at 95°C and shortly centrifuged before loading onto NuPAGE 4-10% Bis-Tris Gel from Life Technologies. Importantly, due to the aggregation of the endogenous Na^+/K^+-ATPase cell lysates were only boiled for 7 min at 60°C. To estimate the size of proteins, a protein ladder was included on each gel (PageRuler, Fermentas). Separation was performed using 1x MOPS running buffer (Life Technologies) with 500 µl of NuPAGE Antioxidant (Life Technologies) at 200 V for 50 min. Smaller proteins were separated using 1x MES buffer at 200 V and 35 min.

4x SDS sample buffer:	24 ml	Tris-HCl pH 6.8 (0.5 M)
	4 g	SDS
	12.5 ml	Glycerol
	2.5 ml	β-Mercaptoethanol
	2 ml	Bromphenol blue (1% (w/v))
	ad 50 ml	deionized water
1x MES running:	50 mM	MES, pH 7.3
	50 mM	Tris Base
	0.1% (w/v)	SDS
	1 mM	EDTA
1x MOPS running buffer:	50 mM	MOPS, pH 7.37
	50 mM	Tris
	0.1% (w/v)	SDS
	1 mM	EDTA

2.4.4 Protein detection in SDS-PAGE

To visualize protein bands after separation on SDS-PAGE, the gel was stained for 1-12 h with 20 ml InstantBlue (Expedeon) a Coomassie based staining solution. To obtain optimal staining the gel was washed in deionized water for at least 1 h.

2.4.5 Western blot analysis

Transfer of proteins to a membrane

After SDS-PAGE (section 2.4.3) the proteins were transferred to a methanol-activated polyvinylidene fluoride (PVDF) membrane (Immobilon-FL, Millipore) using a wet blotting apparatus (MiniPreotean Trans Blot, BioRad). To set up the Western blot all components were soaked in blotting buffer and assembled according to the following orientation: anode – Sponge – 2x Whatman paper – PVDF membrane – SDS-PAGE – 2x Whatman paper – Sponge – cathode . An ice block and a magnetic stir bar were placed in the blotting chamber, which was then filled up with blotting buffer. Protein transfer was performed on a magnetic stirrer at 100 V for 60 min.

Blotting buffer:	40 mM Glycine
	25 mM Tris base pH 8.8
	20% (v/v) Methanol
	in deionized water

Immunodetection of proteins

After transfer of the proteins the membrane was blocked 1 hour with 3% BSA at RT, followed by incubation with the primary antibody (see also section 2.1.5) for 1 h at RT (mouse anti-ATP1A1 1:200; mouse anti-ATP1B1 1:250; rabbit anti-FGF2 1:200 (RG Nickel); mouse anti-FLAG 1:300; mouse anti-GAPDH 1:20,000; rabbit anti-GFP 1:500; rabbit anti-tubulin 1:1,000). The membrane was washed 3x with PBS-Tween for 5 min. The secondary antibody was incubated at RT for 30 min (Alexa Fluor 680 goat anti-rabbit 1:10,000 and IRDye 800 CW goat anti-mouse 1:10,000). After 3x of 5 min washing with PBS-Tween, the membrane was stored in PBS in the dark. Visualization was performed using the LI-COR Odyssey imaging system. All primary and secondary antibodies were diluted in 3% BSA and stored at 4°C with 0.02% (w/v) sodium azide.

PBS (1x):	136.9 mM NaCl	8 g
	2.7 mM KCl	0.20 g
	1.7 mM KH_2PO_4	0.24 g
	80 mM Na_2HPO_4 2x H_2O	1.44 g
	ad 1 l	deionized water adjust to pH 7.4

PBS-Tween:	0.05% (w/v)	Tween 20
	1x	PBS

2.4.6 Protein expression in bacteria

An over night culture of 100 ml LB-Medium was inoculated with a glycerol stock and *E. coli* cells (section 2.1.10) were grown at 37°C with antibiotics. In the morning, the overnight culture was diluted 1:20 to inoculate a pre-culture that is grown for an additional 4-5 hours at 37°C. Finally, this pre-culture is again diluted 1:25 to inoculate 2 liters of 2YT-Medium. Most constructs were purified from 6-12 liters of medium. Protein expression was induced at OD_{600} 1.3-1.8 with 0.5 mM IPTG and the cells were incubated at 25°C o/n.

2.4.7 Affinity purification of proteins

The bacteria pellets were resuspended in lysis buffer using 20 ml of buffer per 2 liter of culture. The suspension was applied to a high-pressure homogenizer (Avestin) for 6 cycles to disrupt the cells. To clear the cell lysate, centrifugation for 1 hour, 33,000 rpm, 4°C using an ultracentrifuge (Beckman Coulter) with a 50.2Ti rotor was performed. All purifications were conducted on a Äkta purifier (GE Healthcare).

Lysis buffer:	1x	PBS
	1 tablet	Protease inhibitor per 100 ml of buffer
	1 mM	Benzamidine
	1 mM	PMSF
	1 mM	DTT
	2%	Glycerol
	0.1%	Trition X-100
	in deionized water	

As a general procedure the affinity columns (Nickel, Heparin or GSH) were first equilibrated with the appropriated wash buffer using 10 column volumes (CV) of buffer followed by loading of the cell lysate with a speed of 0.5 ml/min. The columns were washed with 10 CV of wash buffer. The proteins were eluted with a continuous gradient with the corresponding elution buffer over a time of 30 min with 0.5 ml/min. Protein elution was monitored on the Äkta system by measuring the absorption at 280 nm. The eluted protein fractions were analyzed on a SDS-PAGE and stained with InstantBlue to determine their quality. Finally, fractions were measured with NanoDrop using the specific extinction coefficient for the protein that was purified. In most cases buffer exchange was performed on PD-10 columns (GE Healthcare) or proteins were applied to size exclusion chromatography (section 2.4.8). If necessary, proteins were concentrated with Amicon Ultra-4 centrifugal filters (Millipore)

according to the manufacturer's manual. The samples were snap frozen and stored at -80°C.

Nickel (Ni) affinity purification

Ni-wash buffer:	25 mM	HEPES
	400 mM	NaCl
	40 mM	Imidazol
	2%	Glycerol
	in deionized water, adjust to pH 7.4	
Ni-elution buffer:	25 mM	HEPES
	500 mM	Nacl
	400 mM	Imidazol
	2%	Glycerol
	in deionized water, adjust to pH 7.4	

Glutathione (GSH) affinity purification:

GSH-wash buffer:	1x	PBS
	150 mM	NaCl
	2%	Glycerol
GSH-elution buffer:	1x	PBS
	20 mM	L-Glutathione
	2%	Glycerol, adjust to pH 8.0

Heparin affinity purification:

Heparin-wash buffer:	1x	PBS
	350 mM	NaCl
	2%	Glycerol
Heparin-elution buffer:	1x	PBS
	2 M	NaCl
	2%	Glycerol

2.4.7.1 Protein cleavage with thrombin

The glutathione-s-transferase (GST) moiety of the recombinant proteins GST-FGF2 and GST-CD1-3 was cleaved off by the serine protease thrombin that cuts at a specific recognition site, which was introduced before. Protein lysates were loaded on a GSH column as described above. After washing, 15 ml PBS containing 500 u of thrombin (GE Healthcare) were circulated for 2 h with a flow of 0.5 ml/min at RT over the column. The flow through of

GST-FGF2 was applied to a heparin column (section 2.4.7) for further purification. The flow through of GST-CD1-3 was again applied to a GSH column to remove residual GST followed by size exclusion chromatography (section 2.4.8.).

2.4.8 Size exclusion chromatography

This method is used to separate residual impurities after a first affinity purification step. A Superdex^{TM} 200 (GE Healthcare) column was used and equilibrated with one CV of 1x PBS. The protein samples were loaded with a 5 ml loop using an Äkta purifier. Migration of proteins were monitored by measuring absorption at 280 nm. Peak fractions were analyzed on a SDS-PAGE and stained with InstantBlue. Pooled fractions were snap frozen and stored at -80°C.

2.4.9 Pull-down assay

Performing pull-down assays means the immobilization of a protein to an affinity resin for capturing. In a second step a potential binding partner will be incubated together with the immobilized protein. Protein-protein interactions will be detected on a SDS-PAGE followed by staining with InstantBlue. In this experiment untagged FGF2, GST-CD1-3 and his-CD1-3 were covalently coupled to epoxy-activated sepharose 6B (GE Healthcare). GST-FGF2 and GST-CD1-3 were immobilized on GSH sepharose 4B (GE Healthcare) according to the manufacturer's instructions. After blocking with 3% of BSA the coupled resin was covered with 10 volumes of 1x PBS including 1 mM of benzamidine and 0.02% sodium azide for storage. For pull-downs, 100 µl of the epoxy and 10 µl of the GSH coupled suspension were used. The beads were washed once with 1 ml of 1x PBS and were incubated with the binding partner (25 – 50 µg) in 200 µl of pull-down buffer for 2 h at RT. After this incubation time, the unbound fraction (UB) was collected. Here, 50 µl of the supernatant were collected and 25 µl of 4x sample buffer were added. The resin was washed twice with 1 ml of pull-down buffer and once with 1 ml 1x PBS. The bound fraction (B) was eluted by adding 30 µl of 2x sample buffer. B and UB fractions were boiled for 7 min at 95°C. A SDS-PAGE was loaded with 2.5-5% of the volume of the UB fraction and 50% of the volume of the bound fraction. B and UB bands were quantified on the Odysee infrared imaging system. The ratio of UB to B was calculated and normalized to wild type protein to compare the binding capacity of various mutant proteins.

Pull-down buffer:	1x PBS
	0.05% (w/v) Tween 20
	1 mM Benzamidine

2.4.10 Hydrogen deuterium exchange experiments (HDX)

A stock solution containing 50 pmol of untagged FGF2 and 280 pmol hisCD1-3 was prepared in PBS buffer (pH 7.2) and diluted with 15-fold of the corresponding D_2O buffer (pD 7.2) to start the deuterium exchange labeling reaction. FGF2 was analyzed alone or together with hisCD1-3 after an incubation of 1 h at RT, respectively. A time course was performed taking an aliquot of the exchange reaction after 10 s, 1 min, 10 min, 1h and 4h. The labeling reaction was quenched with an equal amount of pre-chilled quench buffer and immediately frozen on dry ice. Samples were stored at -80°C prior to pepsin digestion and mass spectrometry analysis (see work flow Figure 8).

Quench buffer:	0.8 M	guanidine hydrochloride
	0.8%	formic acid

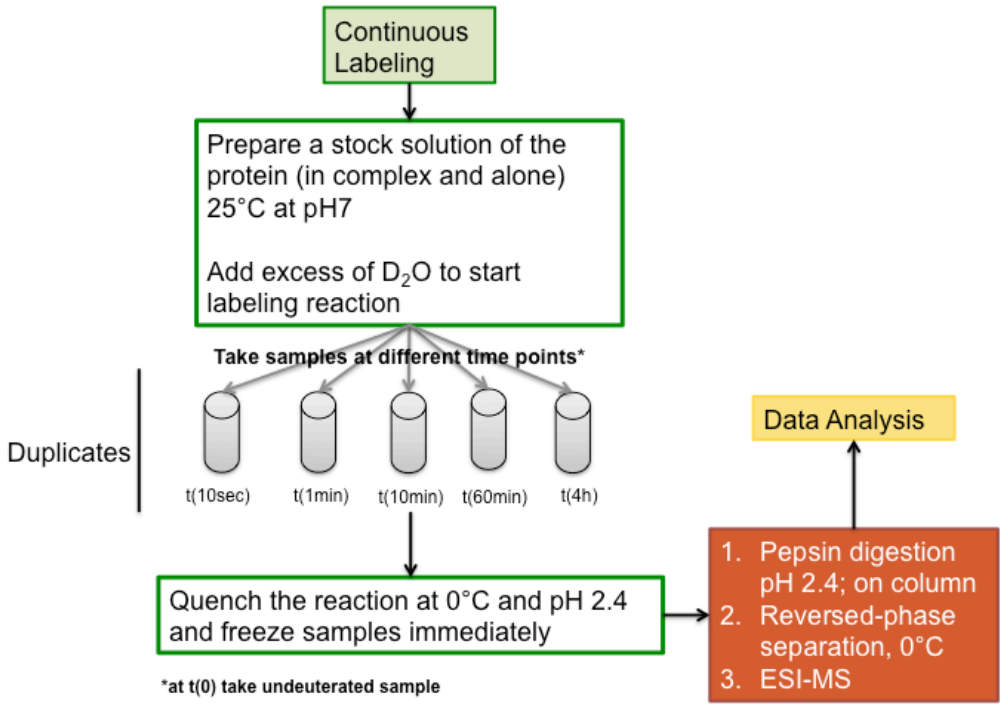

Figure 8: Sequential workflow of a HDX experiment.

2.4.11 Chromatography and mass spectrometry

Each frozen sample was thawed rapidly and injected into a custom Waters nanoACQUITY UPLC HDX ManagerTM and analyzed. The protein samples were digested using a Poroszyme immobilized pepsin cartridge (Applied Biosystems), which was accommodated within the UPLC system. The cooling chamber of the UPLC system, which housed all the chromatographic elements, was held at 0.1°C for the entire time of the measurements. The injected peptides were trapped and desalted for 3 min at 100 µl/min and then separated in

8 min by an 8–40% acetonitrile:water gradient at 60 µl/min. The separation column was a 1.0×50.0 mm ACQUITY UPLC C18 BEH (Waters Corporation) containing 1.7 µm particles and the back pressure averaged 8800 psi at 0.1°C. All experiments were performed in duplicates. Mass spectra were obtained with a Waters XEVO G2 TOF equipped with standard ESI source (Waters Corporation). The instrument configuration was the following: capillary was 3.2 kV, trap collision energy at 6 V, sampling cone at 35 V, source temperature of 80°C and desolvation temperature of 175°C. Mass spectra were acquired over an m/z range of 100 to 2,000. Mass accuracy was ensured by calibration with 500 fmol/µl GFP, and was less than 10 ppm throughout all experiments. The mass spectra were processed with the software Protein Lynx Global Server 2.5 and DynamX^{TM} (Waters Corporation) by centroiding an isotopic distribution corresponding to the +2, +3, or +4 charge state of each peptide. Deuteration levels were calculated by subtracting the centroid of the isotopic distribution for peptide ions of undeuterated protein from the centroid of the isotopic distribution for peptide ions from the deuterium labeled sample. The resulting relative deuterium levels were automatically plotted versus the exchange time.

2.4.12 Amplified luminescence proximity homogenous (AlphaScreen) assay

This assay was used to perform an AlphaScreen® that allowed for the identification of small molecules that interfere with the protein-protein interaction of CD1-3 and FGF2. This assay is based on two different types of coated beads. In this particular case Glutathione coated Donor Beads and Nickel Chelate Acceptor Beads were used that allowed for the recruitment of affinity-tagged proteins such as GST-CD1-3 and hisFGF2. Donor beads were excited at 680 nm which concomitant results in the production of singlet oxygen. These oxygen species can diffuse within a radius of 200 nm. If an Acceptor Bead is within this proximity the energy of the oxygen will be transferred and light produced that can be detected at 520-620 nm (see Figure 9).

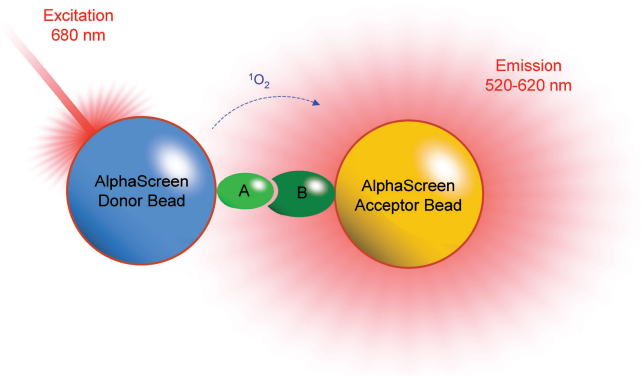

Figure 9: Schematic illustration of the AlphScreen principle Image Source: PerkinElmer Life and Analytical Sciences

2.4.12.1 AlphaScreen: pilot screen

The AlphaScreen was carried out in collaboration with the Chemical Biology Core Facility at The European Molecular Biology Laboratory (EMBL) of Dr. Joe Lewis in Heidelberg. For the pilot screen a total of 4080 compounds were tested for their ability to compete for the binding of GST-CD1-3 and hisFGF2 that were previously immobilized onto Donor and Acceptor Beads at a final concentration of 30 nM and 60 nM, respectively (this was also true for the cross-titration experiment). The compounds were based on three commercial available libraries from AMRI, Enamine and Cambridge. Compounds were solved in 0.4% DMSO and transferred to 384-well ProxiPlate (PerkinElmer) at a final concentration of 40 µM. The protein partner GST-CD1-3 and hisFGF2 were added and incubated at RT for 1 h. AlphaScreen® Glutathione Donor Beads (Perkin Elmer) and Nickel Chelate Acceptor Beads (from the AlphaScree® Histidine Detection Kit, PerkinElmer), both at a final concentration of 7.5 µg/ml, were transferred to this reaction and subsequently incubated for another 2 h until the plates were measured on an EnVision Plate Reader (PerkinElmer). As a buffer 0.1% (w/v) BSA and 0.05% (w/v) Tween 20 was used in 1x PBS. Beads were excited at 680 nm and the emission was measured within a range of 520 – 620 nm. The screen was carried out in duplicates and the percentages of derived from the compounds were calculated from a reaction without inhibitor. As a measurement for the quality of the assay for each plate the Z'-value was calculated taking into account the variation of the positive (reaction without inhibitor) and negative controls (without protein) applied on each plate.

$$Z' \text{value} = 1 - \frac{3(\sigma_{pos} + \sigma_{neg})}{|\mu_{pos} - \mu_{neg}|}$$ σ = standard deviation; µ = mean

AlphaScreen cross titration assay

2.4.12.2 AlphaScreen competition assay

For competition the following proteins were used: untagged versions of CD1-3, FGF2 and Δ25 FGF2. All of them were stored in 1x PBS with 50 % glycerol. To start with, stock solutions of all proteins were generated and adjusted to a final concentration of 14.28% glycerol in assay buffer. Stocks (3x assay concentration): 90 µM CD1-3; 27 µM FGF2; 27 µM Δ25 FGF2. A 1:2 serial dilution was performed in 96-well storage plate with assay buffer containing 14.28% of glycerol (14 dilutions). In the meantime, the affinity-tagged binding partners were mixed in assay buffer without glycerol.

Binding partners stock (3x assay concentration):

GST-Tec 93.75 nM and his-FGF2 187.5 nM
GST-CD1-3 93.75 nM and his-FGF2 187.5 nM
GST-Titin 60 nM and His-MBP-CARP 60 nM

A volume of 5 µl of the protein binding pairs and 5 µl of the serial dilution of the competitor proteins were combined in a 384-well ProxiPlate (PerkinElmer) and incubated at RT for 70 min. Acceptor and Donor Beads (see section above) were prepared in assay buffer at a concentration of 0.0225 mg/ml (3x assay concentration). Again, 5 µl of the bead suspension were added to the 348-well plate. After an additional incubation time of 105 min at RT the plate was analyzed on an EnVision Plate Reader (PerkinElmer). The median of three replicates was calculated and each protein pair was plotted against the final concentration of the competitor protein. The value half maximum of competition (IC_{50}) can be determined with a non-liner regression one site IC_{50} fit with GraphPad 5.0c. Based on the equation from Cheng and Prusoff (Cheng and Prusoff, 1973) it is assumed that the determined IC_{50} value corresponds to the K_d value. This happens when the tracer (L) molecule in this case hisFGF2 has a 10x lower concentration then the binding partner GST-CD1-3 or GST-Tec, both immobilized on beads. Furthermore, the protein concentration of both immobilized proteins has to be at least 10x less than the expected K_d value. With this assumption L/Kd_{LT} equals zero and leads to $K_d = IC_{50}$ (see Figure 10).

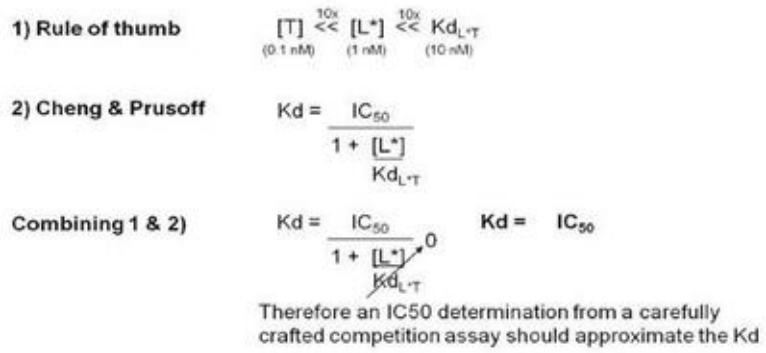

Figure 10: Calculation of the Kd value by the AlphaScreen competition assay. (http://www.perkinelmer.com/resources/technicalresources/applicationsupportknowledgebase/alphalisa-alphascreen-no-washassays/determiningkd.xhtml#DeterminingKdwithanAlphaassay-CompetitionbindingassaysfordeterminationofKd) Adapted from PerkinElmer Inc. Copyright 1998-2013.

Assay buffer:	1x PBS
	0.1% (w/v) BSA
	0.05 % (w/v) Tween 20

The proteins GST-Titin and His-MBP-CARP were provided by Peter Sehr (EMBL). GST-Tec from Giuseppe LaVenuta (BHZ) and Δ25 FGF2 from Julia Steringer (BZH).

3 Results

Previous experiments revealed that FGF2 binds PI(4,5)P_2 at the inner leaflet of the plasma membrane (Temmerman et al., 2008). Only phosphorylated FGF2 can be secreted from cells and only in a fully folded state directly across the plasma membrane. Subsequently, it is immobilized on the cell surface via HSPGs (Torrado et al., 2009; Zehe et al., 2006). Our laboratory conducted a genome-wide RNAi screen where core components of FGF2 secretion have been identified (Ebert et al., 2010). Ebert and co-workers revealed that Tec kinase, which is a direct interaction partner of FGF2. Phosphorylation of FGF2 at tyrosine 82 was found to regulate FGF2 secretion in cells (Ebert et al., 2010).

The aim of this work was to identify additional components of the FGF2 secretion machinery derived from the genome-wide RNAi screen, with the final goal to functionally characterize their role in FGF2 secretion on a molecular level.

3.1 Identification of the screening hit ATP1A1 from the genome-wide RNAi screen

In the genome-wide RNAi screen a total of 9102 human genes were screened (doctoral thesis, Antje Ebert 2009). Each gene product was targeted with three independent siRNAs. As a readout, the secretion of a doxycycline-inducible reporter FGF2-GFP was monitored and quantified by using the On-Cell-Western assay after siRNA mediated knockdown (Ebert et al., 2010). Each well of a 384-well plate was spotted with one gene-specific siRNA using the solid phase reverse-transfection method (Figure 11).

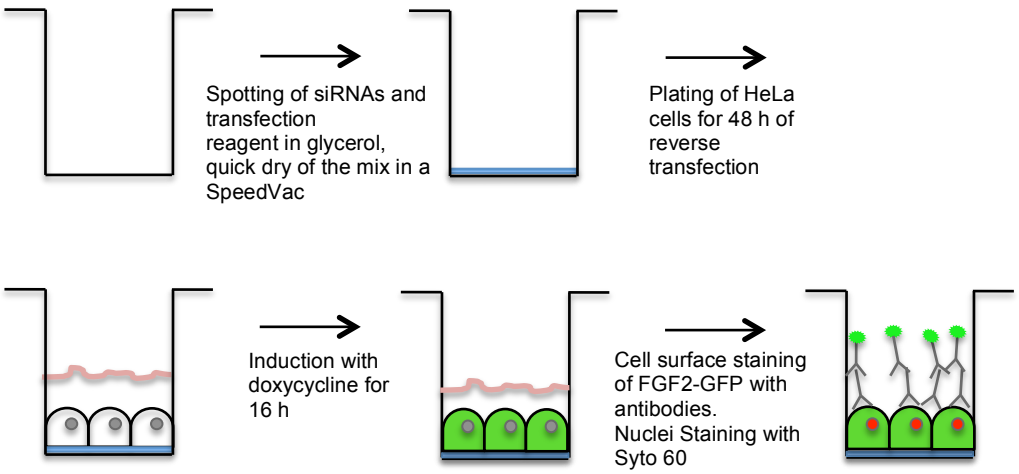

Figure 11: Workflow of solid phase reverse-transfection with siRNAs in a 384 multi-well format. The illustration represents a single well of a 384 plate, each spotted with one specific siRNA.

A mix of siRNA, transfection reagent and glycerol was added to each well and dried in a SpeedVac to preserve the coated siRNAs. This was performed in collaboration with the RNAi screening facility at the BioQuant. A selection of siRNAs termed “druggable genome” (targeting 9102 human genes) from Ambion was spotted on 384-well plates in four replicates. For the screening procedure HeLa FGF2-GFP cells were plated and allowed to attach on this pre-coated wells for siRNA uptake. After a knockdown period of 48 h cells were induced for 16 h to initiate the expression of the reporter gene. Afterwards, an antibody staining against GFP and a secondary fluorescently labeled antibody was applied to detect and quantify surface-associated FGF2-GFP using a LI-COR infrared imaging system.

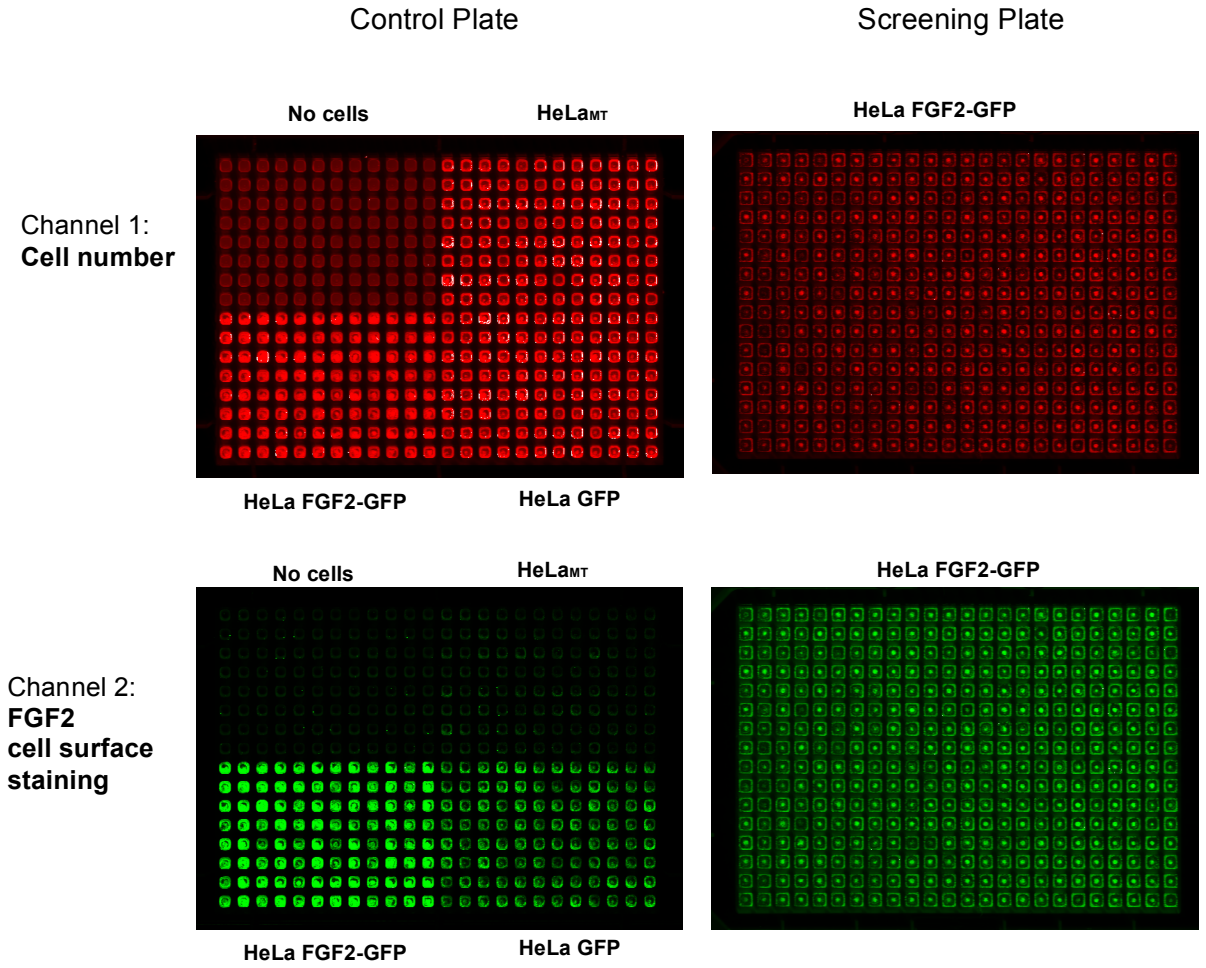

Figure 12: Representation of 384-well screening plate analyzed with a LI-COR infrared imaging system. In channel 1 (red) signals are obtained from nuclei staining reflecting the total cell number. In channel 2 (green) signals correspond to cells surface associated FGF2-GFP obtained through antibody staining. The left panel represents controls to demonstrate the principle of this assay. Considering the cell surface signal (green), no signals were obtained when the plate is empty or with HeLaMT cells not expressing any construct. A strong surface signal was obtained with FGF2-GFP expressing HeLaMT cells. Only a minor background signal was observed when cells expressed GFP alone due to a small portion of unspecific cell lysis. In contrast each cell line can be detected in the red channel for the nuclei staining with Syto 60. The panel represents a typical screening plate showing both channels.

Cell surface signals were corrected for the amount of cells, which were visualized with a fluorescent dye (Syto60) that stained the nuclei. The right panel of Figure 12 represents a typical screening plate from the genome wide RNAi screen.

Mean scores of the hits were calculated and classified according to criteria's published by Ebert at al., 2010. Shortly, for a positive regulator, a hit had to meet the following criteria: if one siRNA out of three was functional the mean score should be smaller than -3. If at least two siRNAs were functional the mean score should be -1.5 or lower. In both cases a p-value lower than 0.05 was required to reach sufficient significance. From this screen a list of 113 gene products could be generated representing the most potent genes affecting FGF2 secretion in a positive or negative way (doctoral thesis, Antje Ebert 2009), unpublished. In this study we focused on the identification of positive regulators of FGF2 secretion. Among those, the gene product ATP1A1, α-subunit isoform 1 (α1-subunit) of the Na^+/K^+-ATPase was found as a putative positive regulator of FGF2 secretion.

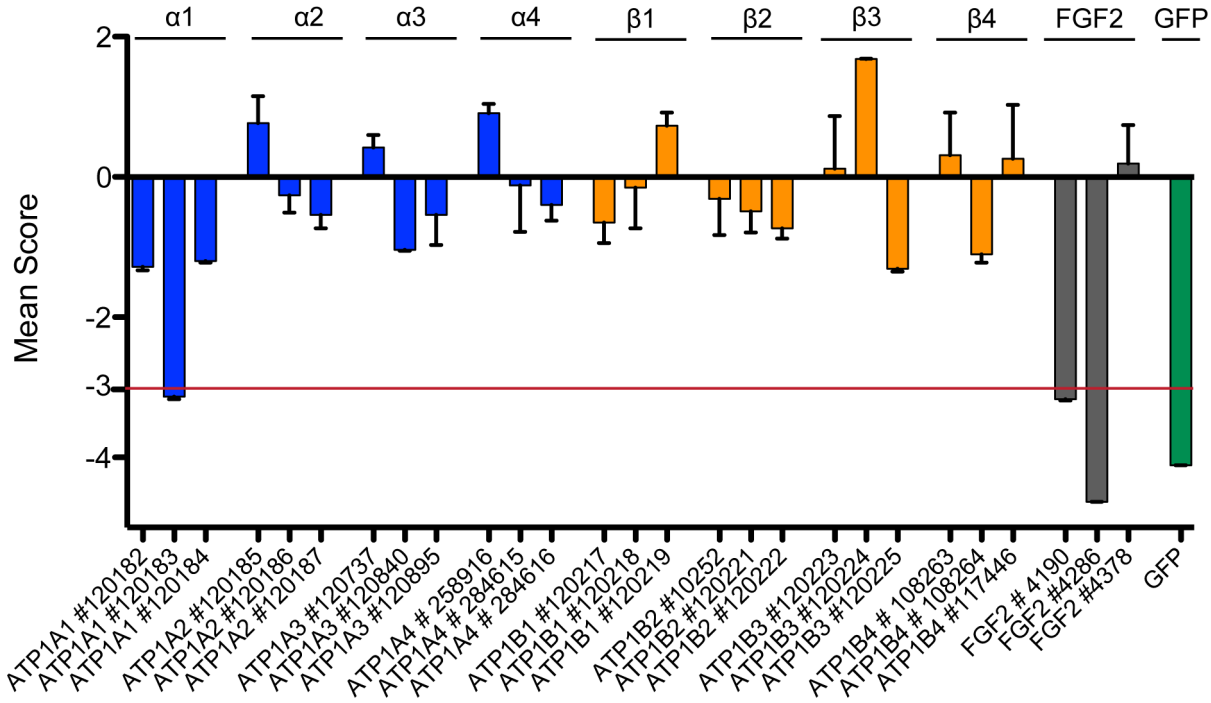

Figure 13: Primary screening hits of the Na^+/K^+-ATPase knockdown obtained from the genome-wide RNAi screen. Initial screening data of isoforms α1-4, β1-4 and of control siRNAs FGF2 and GFP. The numbering corresponds to the siRNA ID of Ambion, GFP siRNA was custom designed. Values represent the average of four separate experiments. Errors show the standard deviation of the mean. A positive regulator of secretion was defined as a hit when one siRNA out of three had a score smaller than -3. When at least two siRNAs out of three were functional, the threshold was lower than -1.5. In both cases p-values were <0.05.

In general, the Na^+/K^+-ATPase consists of two subunits the α- and β-subunit. For the active transport of ions across the plasma membrane it is known that both subunits have to be assembled in a 1:1 stoichiometry (Scheiner-Bobis and Farley, 1994). In mammalian cells the existence of four different isoforms have been shown for the α- and β-subunit, respectively that are termed ATP1A1 (α1), ATP1A2 (α2), ATP1A3 (α3) and ATP1A4 (α4). This is also true for the β-subunit ATP1B1 (β1), ATP1B2 (β2), ATP1B3 (β3) and ATP1B4 (β4). As a result, only the knockdown of the α1 isoform showed a reduction in FGF2 secretion for one siRNA with a mean score of -3.1 and a p-value of 0.04 (Figure 13) (doctoral thesis, Antje Ebert 2009). In contrast, none of the β-isoforms were found to have any significant impact on FGF2 secretion after siRNA-mediated knockdown. Furthermore, control siRNAs are depicted in Figure 13 targeting the reporter gene. Two siRNAs against *FGF2* were found to be functional with a score of -3.1 and -4.6 and the siRNA against GFP with a score of -4.1, all of them with high significance (p-value <0.05).

3.2 Analysis of Na^+/K^+-ATPase isoforms in HeLa cells using RT-PCR

The main finding of the screen was that exclusively the siRNA targeting the α1-subunit resulted in a significant down regulation of FGF2 secretion. To investigate this in more detail, HeLa cells were analyzed for the expression of different isoforms of the α- and β-subunits. For this purpose, cDNA was prepared (section 2.2.4) from HeLa and HeLa S3 cells and isoform specific primers were used according to the study of Yoshimura et al., 2008. In agreement with this publication we found the isoforms α1, β1 and β3 in $HeLa_{MT}$ and $HeLa_{MT}$ S3 laboratory cell lines (Yoshimura et al., 2008). The origin of these cell lines are described in section 2.3.3. In short, they are carrying the doxycycline trans-activator as well as the receptor, for viral transduction a prerequisite for the generation of stable cell lines. Following these findings all further analyses will focus on the isoforms present in these HeLa cell lines.

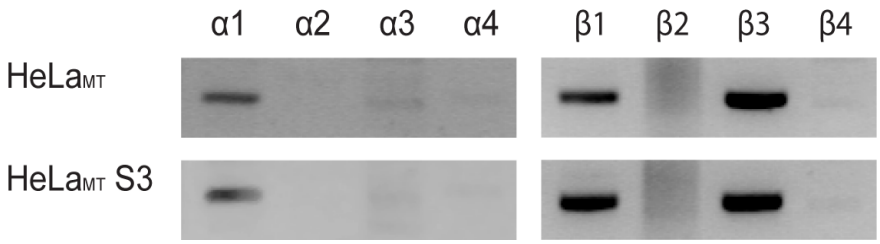

Figure 14: α- and β-isoforms of the Na^+/K^+-ATPase present in HeLa and HeLa S3 cells. Total RNA was isolated from $HeLa_{MT}$ and $HeLa_{MT}$ S3 cells and the mRNA was translated into cDNA. Isoform specific primers were used to check with PCR for the presence of mRNA isoforms of the α- and β-subunits.

3.3 Validation of the Na^+/K^+-ATPase phenotype in FGF2 secretion by FACS analysis

In addition to the On-Cell-Western assay (see section 3.1) the validation of α1, β1, and β3 was performed to obtain a second independent readout to monitor FGF2 secretion. The siRNAs, which were chosen in the validation procedure, differ in sequence from the siRNAs that have been used during the primary screen. Concomitantly with this, optimized silencer select siRNAs were received from Ambion, which allowed for the reduction of siRNA amounts and transfection reagent. This minimizes additional stress and toxicity for the cells. As described in detail in section 2.3.4, the flow cytometry (FACS) assay was used as a readout to detect secreted FGF2 after siRNA knockdown of the Na^+/K^+-ATPase subunits.

3.3.1 Characterization of the HeLa FGF2 cell line for FACS validation

To carry out the FACS assay $HeLa_{MT}$ S3 cells were generated as cells expressing untagged FGF2 additional to GFP from an internal ribosomal entry site (IRES) construct in a doxycycline-dependent manner (HeLa $S3_{FGF2\_IRES\_GFP}$, Figure 15). After virus transduction, cells bearing the reporter construct stably integrated in their genome were enriched by sorting, according to their GFP fluorescence (section 2.3.3.3). Cell surface associated FGF2 could be detected with antibody staining and quantified by flow cytometry (Figure 15). For this experimental setup HeLa $_{FGF2\_IRES\_GFP}$ S3 cells were grown as adherent cells. The advantage of having the S3 derivate of HeLa cells is that they can be tightly regulated with doxycycline.

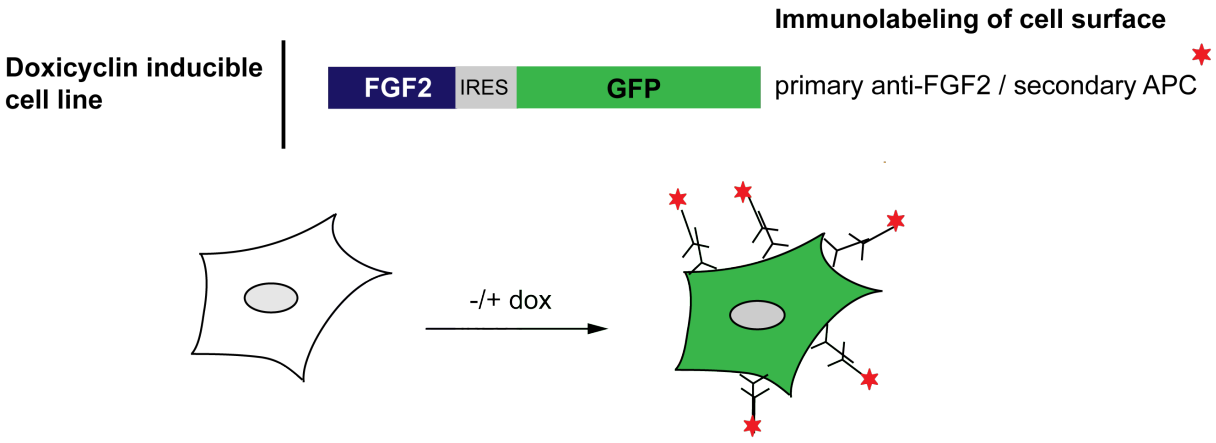

Figure 15: Principle of a doxycycline-inducible cell line. After 48 h of knockdown cells were stained with a primary anti-FGF2 antibody and a secondary fluorescently labeled antibody (APC) to quantify the cell surface signals by flow cytometry.

In general, the expression level of GFP was very low as there is only a moderate change observed by FACS after the addition of doxycycline. In contrast, cell surface staining of FGF2 is considerably increased after expression of FGF2 (Figure 16). Showing a broad dynamic range of this assay that allows for the detection of secreted FGF2 after siRNA-mediated knockdown. Moreover, this cell line mimics the natural secretion mechanism by having FGF2 expressed as an untagged version.

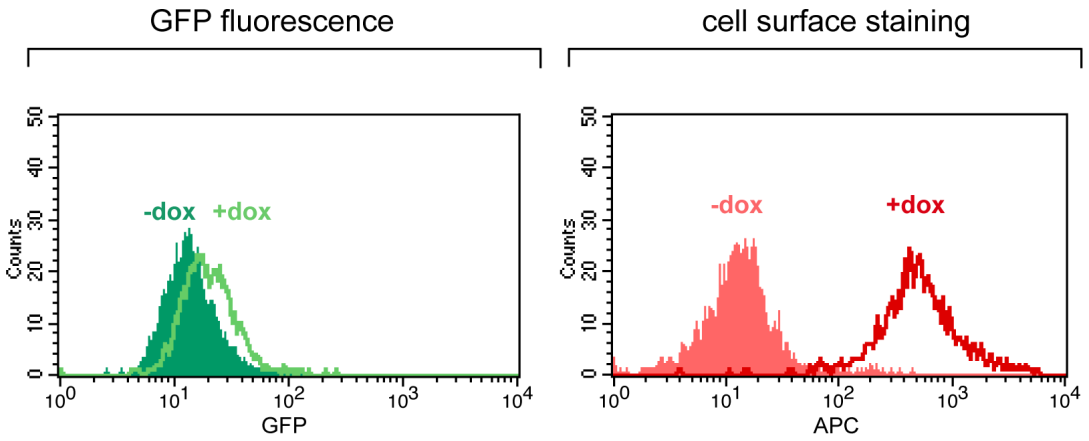

Figure 16: Flow cytometry analysis of HeLa$_{MT}$ S3 cells stably expressing FGF2 from an IRES construct (HeLa S3$_{FGF2_IRES_GFP}$). In the left panel GFP expression is depicted and the right panel shows the population of FGF2 that is found on the cell surface, both in absence and presence of doxycycline (dox). Cell surface attached FGF2 could be quantified by antibody staining against FGF2 with a primary antibody and a second fluorescently labeled antibody for visualization in flow cytometry.

3.3.2 RNAi-mediated down regulation of the α- and β-subunits of the Na^+/K^+-ATPase analyzed by FACS

In order to perform the knockdown experiments, HeLa S3$_{FGF2_IRES_GFP}$ cells were seeded on the first day and subjected to siRNA transfection on the next day for a period of 48 h. Subsequently, doxycycline was added for 16 h to induce expression of the reporter construct. Secreted FGF2 was quantified by flow cytometry (section 2.3.4). Using a siRNA against *GAPDH* served as a negative control whereas a siRNA against *FGF2* was used as a positive control to monitor the functionality of this assay by directly down regulating the *FGF2* reporter gene. Three independent siRNAs were used to target the α1-subunit #1 (ID: s1718), #2 (ID: s1719) and #3 (ID: s1720), respectively. Figure 17A shows that knockdown of the α1subunit indeed leads to decreased FGF2 secretion. This was true for all three siRNAs used and was also the case when *FGF2* was directly down regulated. No effect was observed with a siRNA targeting *GAPDH*. To monitor the knockdown efficiencies cell lysates of the various knockdowns were prepared and subjected to Western Blot analysis. As depicted in Figure 17B, the three different siRNAs against the α1-subunit substantially

decreased the amount of protein expressed in the cells after 48 h of knockdown time. This was also the case for protein levels of GAPDH and FGF2 after knockdown of the corresponding gene. Antibody staining of tubulin was introduced to show as loading control. FGF2 expression was not affected by knockdown of the Na^+/K^+-ATPase α1-subunits.

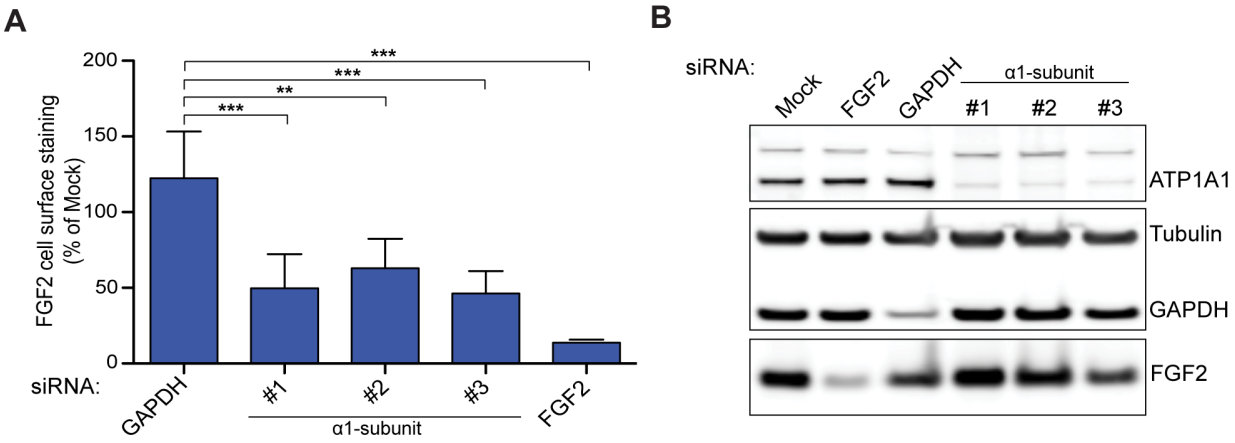

Figure 17: RNAi based validation of the α1-subunit as a factor involved in FGF2 secretion. Stable HeLa S3 cell lines expressing FGF2 in a doxycycline-dependent manner were subjected to 48 h of siRNA knockdown followed by quantification of cell surface located FGF2. **A)** Knockdown of the α1-subunit was performed using thee independent siRNAs (#1, #2, #3). *GAPDH* and *FGF2* siRNAs served as controls. FGF2 on the cell surface was quantified with flow cytometry assay and mean values were plotted from five separate experiments. Results were expressed as a percentage of mock treated cells. Error bars show the standard deviation of the mean and asterisks indicate the level of statistical significance calculated with GraphPad Prism 5.0c (unpaired two-tailed t-test; ns = not significant; * = p-value ≤ 0.05; ** = p-value ≤ 0.01; *** = p-value ≤ 0.001). **B)** After knockdown cell lysates were subjected to Western blot analysis. The membrane was decorated with antibodies against α1 (ATP1A1), GAPDH and FGF2 to show knockdown efficiencies. Staining with an anti-β-tubulin antibody was used as loading control.

In order to address whether knockdowns of the two isoforms of the β-subunit (β1 and β3) in HeLa S3 cells can confirm the data obtained from the On-Cell-Western screening assay, the β1 (ID: s1734) and β3 siRNAs (ID: s1741) were used separately as well as in combination. The controls, GAPDH and FGF2 were kept the same. In this case, no significant difference between the GAPDH control and the knockdowns of the β-subunits were observed. However, the β3-subunit seemed to be slightly up regulated (Figure 18A). Due to the lack of isoform specific antibodies, quantitative real-time PCR (qRT-PCR) was performed showing sustainable knockdown efficiencies of the mRNA levels of β1 and β3 (Figure 18B).

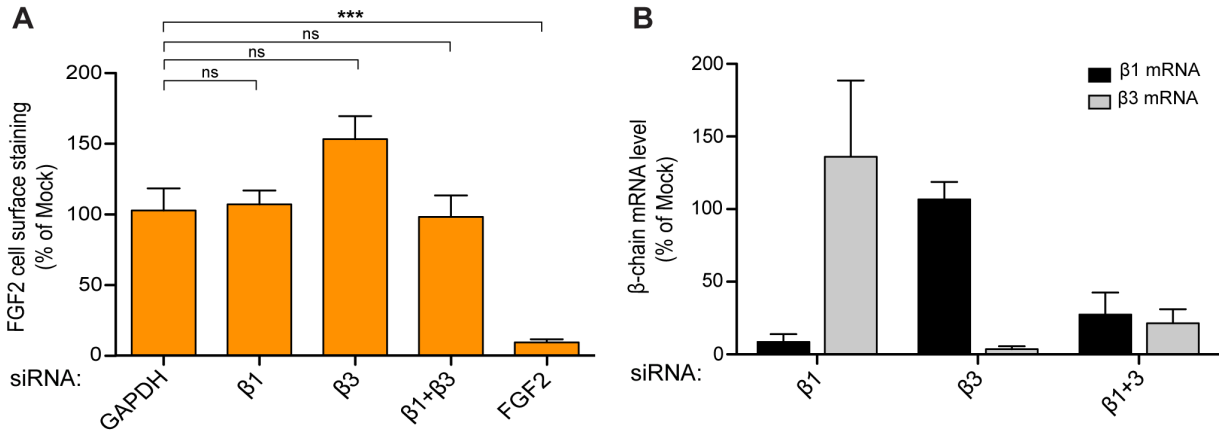

Figure 18: RNAi based validation of the β-subunit as a factor involved in FGF2 secretion. Stable HeLa S3 cell lines expressing FGF2 in a doxycycline-dependent manner were subjected to 48 h of siRNA knockdown followed by quantification of cell surface located FGF2. **A)** Flow cytometry was used to quantify FGF2 secretion after knockdown of the β1 and β3-subunit as well as in a double knockdown. *GAPDH* and *FGF2* were used as control siRNAs. Mean values were calculated from n = 5 experiments. Error bars show the standard deviation of the mean and asterisks indicate the level of statistic significance calculated with GraphPad Prism 5.0c (unpaired two-tailed t-test; ns = not significant; * = p-value ≤ 0.05; ** = p-value ≤ 0.01; *** = p-value ≤ 0.001). **B)** To analyze knockdown efficiencies the mRNA of β1 and β3 was detected and quantified by performing qRT-PCR. Mean values represent three independent experiments. Error bars show the standard deviation of the mean.

In summary, we could confirm with a different secretion assay (FACS assay) and by distinctive siRNAs targeting the α1-subunit of the Na^+/K^+-ATPase that secretion of FGF2 was significantly reduced (to almost 50% of mock treated cells). On the other hand, secretion of FGF2 was not impaired when neither the β1 nor the β3-subunit was subjected to siRNA knockdown. In both cases kbyenockdown efficiencies were proven either on the protein by Western Blot analysis or mRNA levels by qRT-PCR. These results point to the likelihood that only the α-subunit and not the β-subunit plays a role in FGF2 secretion.

3.4 Establishment of a cellular system to monitor pleiotropic effects after RNAi knockdown

To ensure that siRNA-mediated knockdown of the α1-subunit has a specific impact on FGF2 secretion, a cellular model system was established. In this system, secretion of a protein that passes through the classical secretory pathway was monitored. This assay was used to determine whether pleiotropic effects that could be triggered by RNAi treatment occur. Such pleiotropic effects could compromise cellular function and thus, have an impact on protein secretion.

3.4.1 Characterization of GFP-CD4 cell line for FACS analysis

For this reason a GFP-CD4 tagged stable $HeLa_{MT}$ doxycycline-inducible cell line was generated ($HeLa_{GFP-CD4}$). For the establishment of this cell line the extracellular portion of the CD4 receptor was replaced by GFP. A signal peptide was fused N-terminally for delivery of GFP-CD4 to the plasma membrane throughout the classical secretory pathway (see Figure 19A).

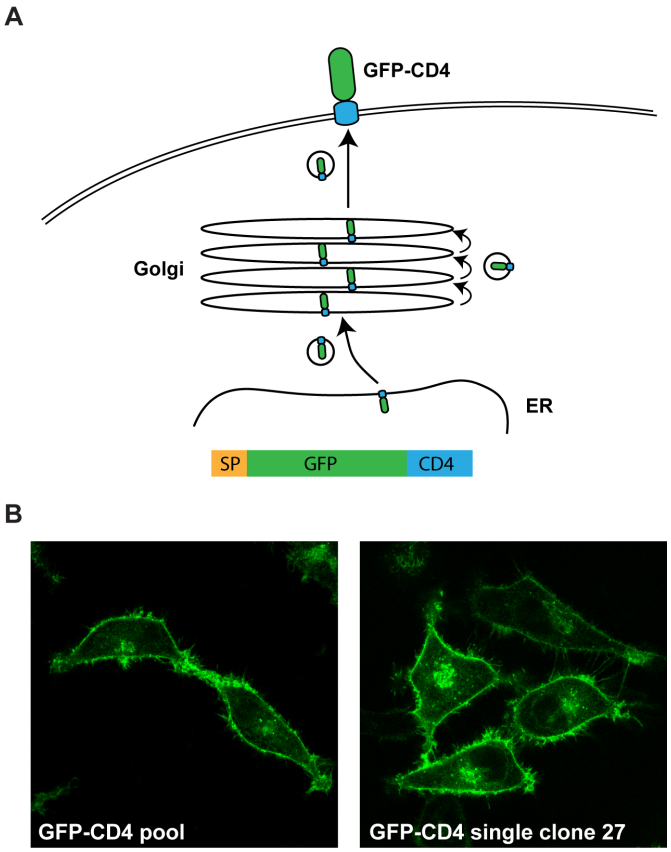

Figure 19: Illustration (A) and live cell images (B) of the $HeLa_{MT}$ GFP-CD4 cell line. In **(A)** the secretion pathway of the GFP-CD4 construct is depicted. In panel **(B)** images of GFP-CD4 expressing cells show that the construct localizes to the plasma membrane.

The generation of stable cell lines is described in detail in materials and methods (section 2.3.3.3). Cells having the GFP-CD4 DNA successfully integrated into their genome were enriched by three sorting steps, according to their fluorescence (“bright”, “dark” and “bright” sorting). From this pool of cells single clones were generated and analyzed for their ability to be regulated with doxycycline. As depicted in Figure 19B, both the GFP-CD4 cell pool and the single clone 27 showed identical localization within $HeLa_{MT}$ cells. The protein GFP-CD4 localizes mostly at the plasma membrane but is also found at perinuclear regions where it is stuck in the secretory pathway. However, from FACS analysis it was evident that the GFP-CD4 single clone could be more tightly regulated with doxycycline than the pool. This is

depicted in Figure 20, which shows that the cell population of the single clone is well separated after induction with doxycycline, which is not the case for the pool. This can be observed for the expression level (green) and the population, which is detected on the cell surface (red). Therefore, the single clone was chosen to perform further FACS analysis for siRNA-mediated knockdowns.

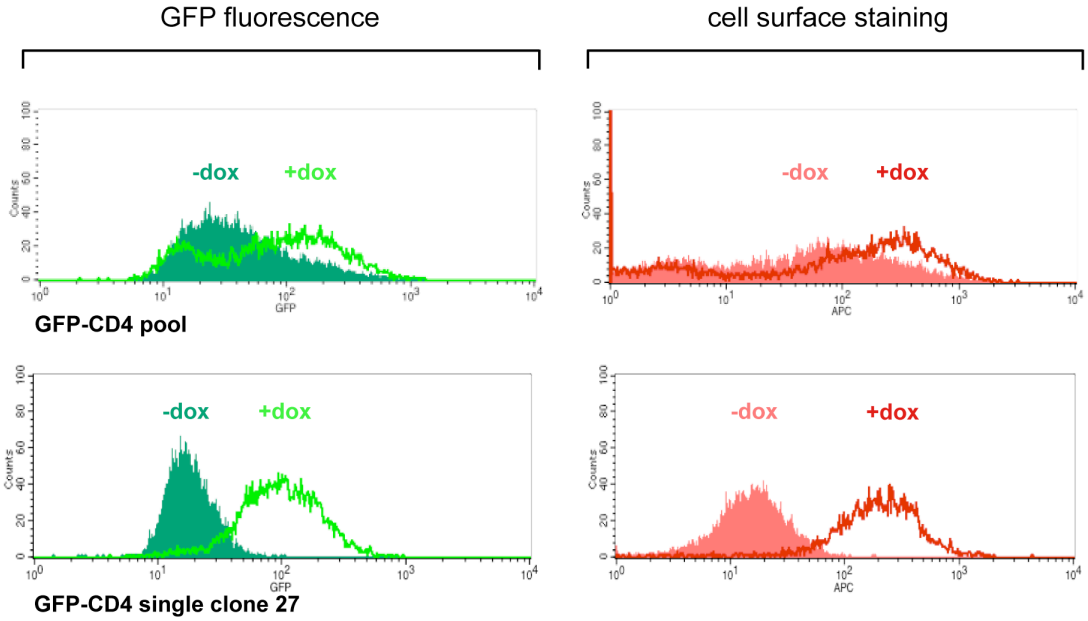

Figure 20: Flow cytometry analysis of HeLa$_{MT}$ cells stably expressing GFP-CD4. In the left panel GFP expression is depicted (green) and the right panel (red) shows the population of GFP-CD4 that is found on the cell surface, both in absence and presence of doxycycline (dox). This can be detected by antibody staining against GFP and a second fluorescently labeled antibody.

3.5 RNAi-mediated down regulation of the α1-subunit in the GFP-CD4 HeLa cell line using FACS analysis

In order to investigate whether pleiotropic effects occur the described HeLa$_{GFP-CD4}$ cell line was used to perform knock down experiments. Since GFP-CD4 is a protein secreted via the classical ER/Golgi-dependent pathway it was not expected that secretion would be affected after α1-subunit knockdown. The procedure was the same as described in section 3.3.2 and also equal amounts of siRNAs were used targeting the α1-subunit. As a control a siRNA against GFP was introduced which down regulates the reporter construct. Furthermore, also a siRNA against β-COP was included. β-COP belongs to the protein complex coatomer, a structural component of COPI vesicles that mediate retrograde transport from the Golgi to the ER and also in the Golgi apparatus between Golgi cisternae (Rothman and Wieland,

1996). Thus, β-COP knockdown blocks transport through the classical secretory pathway. As represented in Figure 21, none of the siRNAs targeting the α1-subunit had an impact on GFP-CD4 secretion (red bars) as well as on the total GFP-CD4 expression level (green bars). There were also no general effects observed that had an influence on, for example, cell viability.

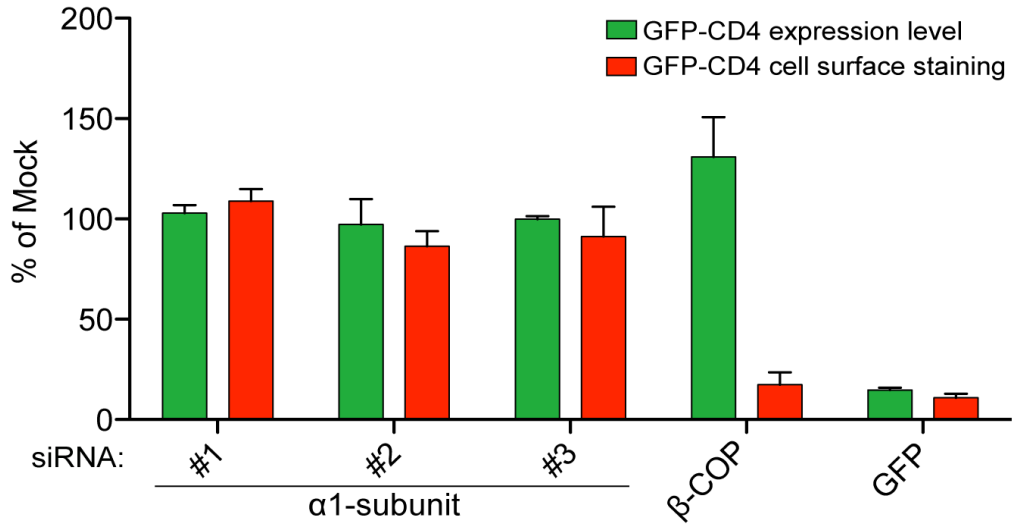

Figure 21: Investigation of pleiotropic effects after RNAi-mediated down regulation of the α1-subunit in HeLa$_{GFP-CD4}$ cell line. Stable HeLa$_{MT}$ cells expressing GFP-CD4 in a doxycycline-dependent manner were subjected to 48 h of siRNA knockdown followed by quantification of cell surface located GFP-CD4. **A)** Knockdown of the α-subunit was performed using thee independent siRNAs (#1, #2, #3), β-COP and GFP siRNAs served as controls. GFP-CD4 on the cell surface was quantified by flow cytometry assay where the green bars represent the total expression levels of GFP-CD4 and the red bars the GFP-CD4 population that can be detected on the cell surface after antibody staining. Mean values were plotted from three separate experiments where error bars were calculated according to the standard deviation. Results were expressed as a percentage of mock treated cells.

Only the control siRNAs showed decreased GFP-CD4 secretion. As expected, the GFP siRNA reduced both the expression level and the GFP-CD4 population that can be detected on the cell surface, whereas the β-COP knockdown only reduces the secreted population detected on the cell surface. Knockdown efficiencies were controlled by Western blot analysis. Equal amounts of lysates were loaded and visualized by GAPDH signals as loading control. As it is shown in Figure 22, all siRNAs directed against the α1-subunit (*ATP1A1*), *GFP* and *β-COP* were functional as they show reduced levels of the corresponding proteins.

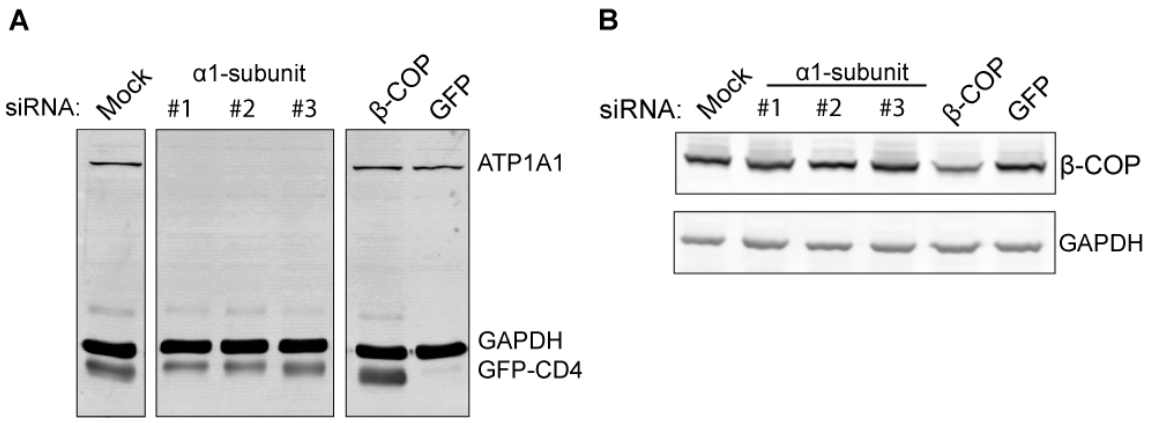

Figure 22: Western blot analysis of HeLaGFP-CD4 cell line after RNAi-mediated knockdown. After knockdown cell lysates were subjected to Western blot analysis. The membrane was decorated with antibodies against α1 (ATP1A1) and GFP **(A)**. On the right panel **(B)** knockdown efficiency of β-COP was monitored. In both cases staining against GAPDH served as a loading control. Showing that siRNAs directed against the various genes specifically reduce the protein levels of the respective targets.

3.6 Co-localization of endogenous α1-subunit and FGF2 in HeLa cells by conventional immunofluorescence staining

For the next step in this study it was of great interest to analyze the localization of endogenous α1-subunit of the Na^+/K^+-ATPase and FGF2. For this purpose $HeLa_{MT}$ cells were fixed and co-immunostained with an anti-FGF2 antibody and an anti-α1 (ATP1A1) antibody. A secondary fluorescently labeled antibody was directed against the primary antibody and images were taken with the confocal microscope (section 2.3.5.). The results show that both proteins are located on the plasma membrane. This could be an indication that the α1-subunit interacts with FGF2 on the plasma membrane to facilitate FGF2 secretion.

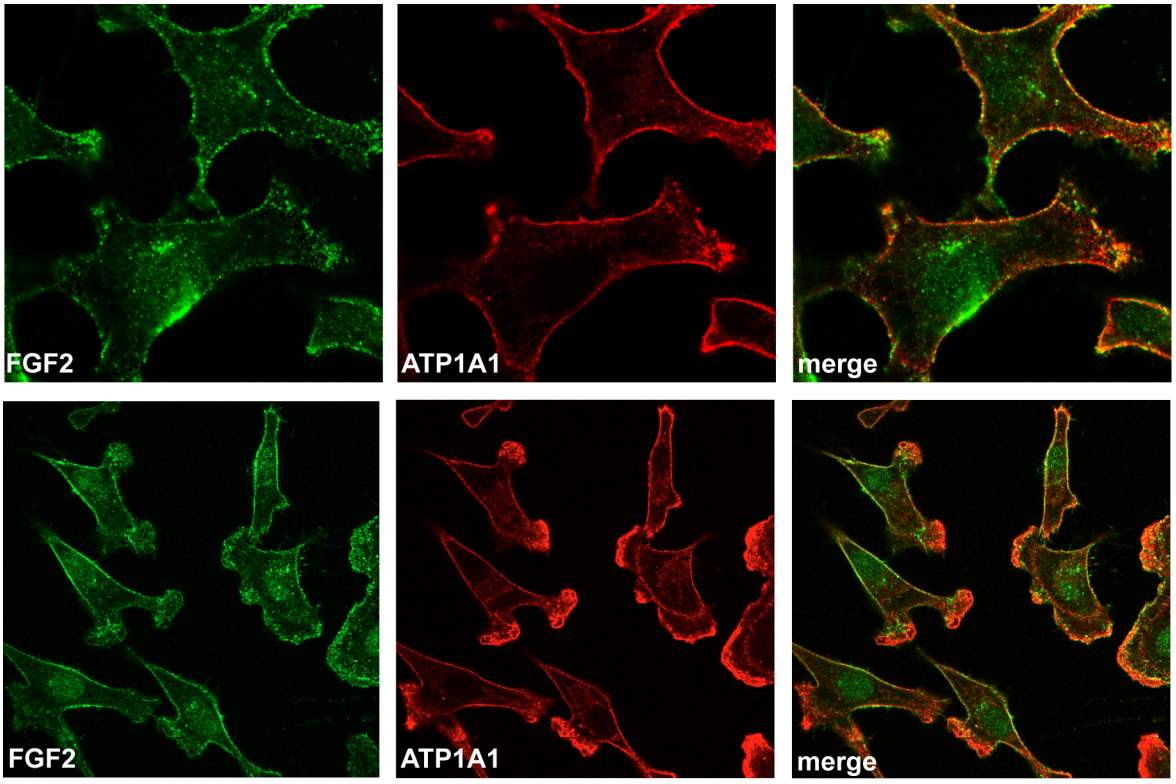

Figure 23: Co-localization of FGF2 and α1-subunit (ATP1A1) on the plasma membrane of HeLa cells. FGF2 (green) and α1 (ATP1A1) (red) of the Na^+/K^+-ATPase were antibody/immunostained in $HeLa_{MT}$ cells. Pictures were taken with the confocal microscope with 60x (upper panel) and 40x (lower panel) of magnification. Both channels were merged and yellow regions indicate co-localization of both proteins on the plasma membrane.

3.7 Co-localization of endogenous α1-subunit and FGF2 in HeLa cells using an *in situ* Duolink detection method

As described in section 2.3.7 the Duolink assay was applied to detect and quantify close interactions of proteins less than 40 nm apart from each other. Another advantage of this method is that also endogenous and transient interactions can be visualized due to the amplification step of the secondary antibodies. The aim of this assay was to quantify the interaction between FGF2 and ATP1A1 (α1-subunit). First, normal immunofluorescence stainings were performed to optimize fixation conditions and dilutions of the antibodies.

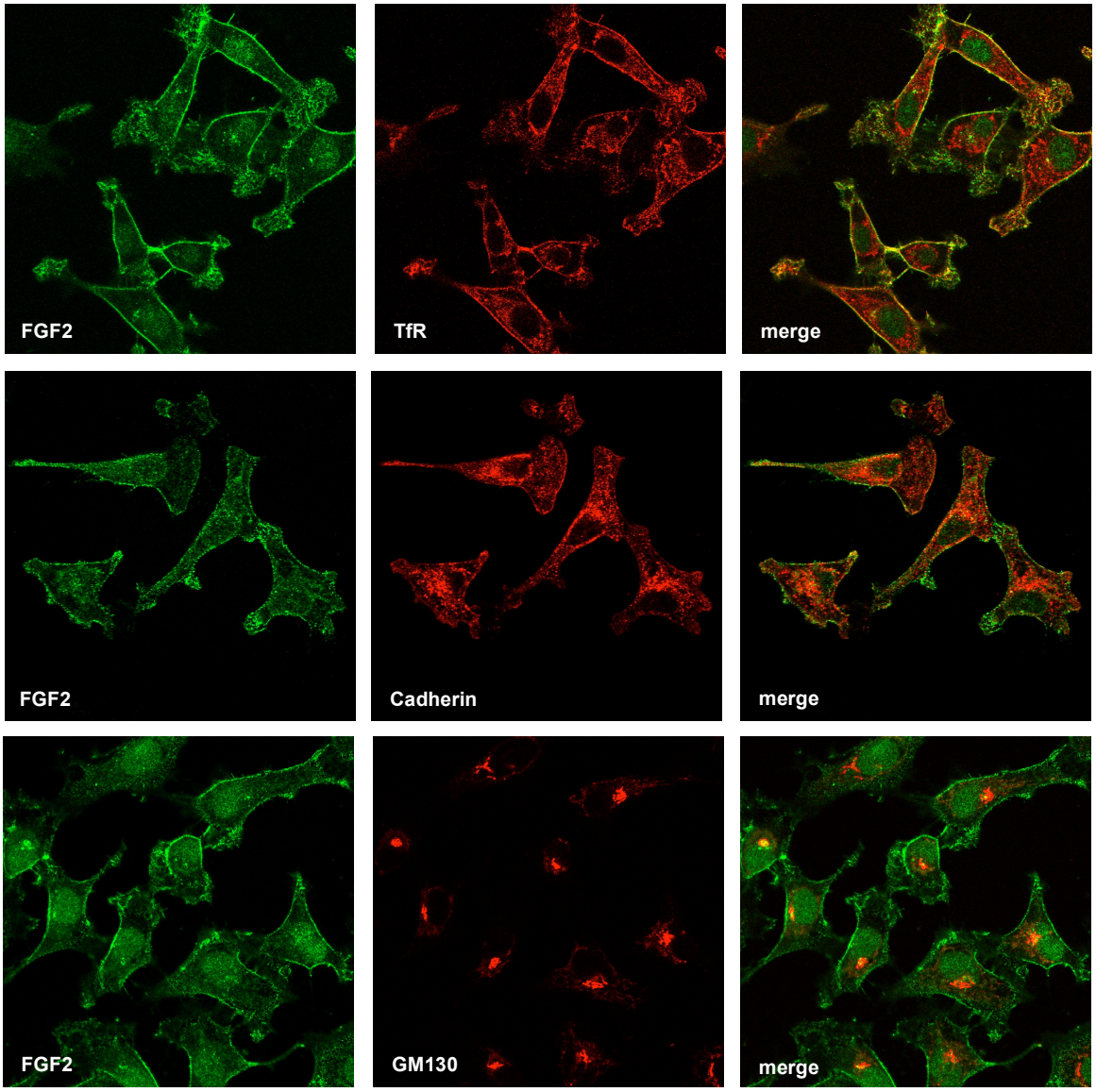

Figure 24: Co-localization of FGF2 and the marker proteins on the plasma membrane and Golgi. HeLa$_{MT}$ cells were stained with antibodies against FGF2 (green) and plasma membrane markers such as the transferrin receptor (TfR) and cadherin in red, respectively. The *cis*-Golgi marker is visualized in the lower panel (red). Pictures were taken on the confocal microscope with a 40x magnification. Both channels were merged and yellow regions indicate co-localization of both proteins on the plasma membrane.

Besides the co-staining of ATP1A1 and FGF2 (Figure 23) control antibodies were used that target either the plasma membrane or the Golgi apparatus. Consequently, the membrane markers cadherin and the transferrin receptor (TfR) were chosen. The Golgi was stained with an antibody targeting the *cis*-Golgi matrix protein GM130. As seen in Figure 24, FGF2 is mainly found in the nucleus and on the plasma membrane (green). The latter is also the case for TfR and cadherin (red). GM130 shows a typical Golgi staining (red). Following this procedure, the primary antibody pairs were used for immunofluorescence staining after fixation of the cells. Secondary antibodies from the Duolink assay were used, which carry a small DNA linker that can be ligated upon interaction and subsequently be amplified (section 2.3.7). Thus, red spots correspond to the amplified signal and represent one protein-protein interaction within 40 nm. As depicted in Figure 25, signals were observed when the cells were co-stained with an antibody against the α1-subunit (ATP1A1) and FGF2. This was also the case for the TfR and FGF2 as well as with cadherin and FGF2. Only minor background staining was observed with GM130 and FGF2 or when the FGF2 and ATP1A1 antibodies were applied alone.

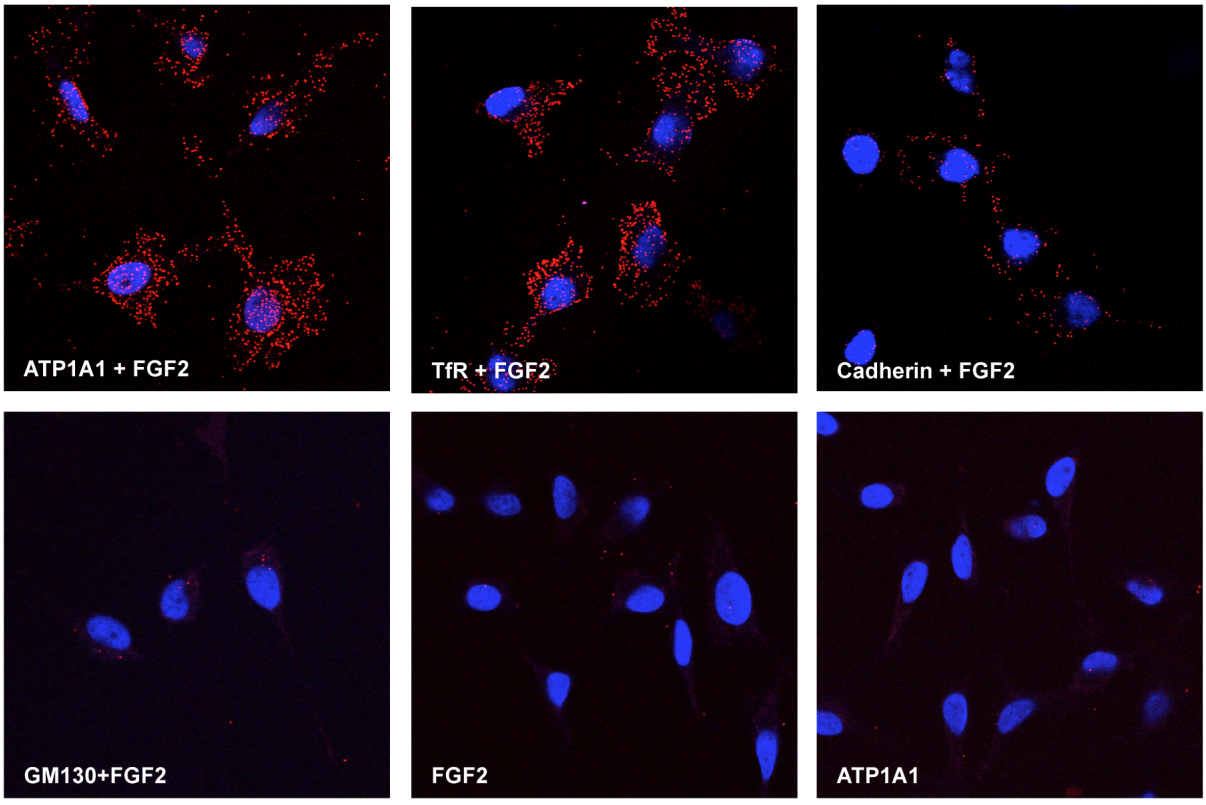

Figure 25: *In situ* Duolink proximity assay. Cells were co-stained with the antibodies ATP1A1 (the α1-subunit), transferrin receptor (TfR), cadherin and GM130 in combination with FGF2. To visualize background staining FGF2 and ATP1A1 antibodies were used separately. Red spots represent an interaction, which is observed when the protein pairs are in close proximity (≤40 nm). Nuclei are depicted in blue (Sytox green).

A Duolink software tool was used, which can automatically identify the cells by the nuclei staining and quantifies the sites of interaction. The quantification is plotted in Figure 26, which represents an average of absolute counts of interaction sites (red spots) per cell. As a result, most of the interactions sites are found between the α1-subunit and FGF2 but no significant difference was observed to another plasma membrane resident protein, namely TfR. Applying single antibody staining against ATP1A1 shows the background of this assay, which was in the range of the co-staining with the Golgi protein GM130 as well as for the membrane protein cadherin and FGF2.

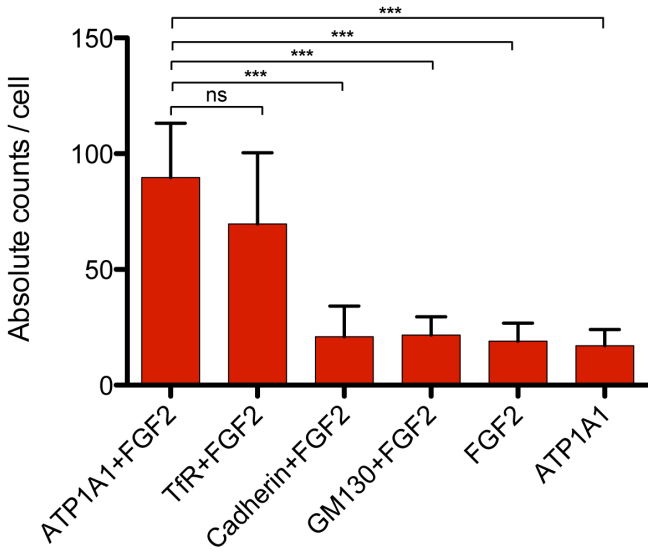

Figure 26: Quantification of the *in situ* Duolink proximity assay. The absolute interaction sites were counted per cell using the Duolink software tool and a mean was calculated from n = 4 experiments. In each experiment about 30 – 50 cells were analyzed. Error bars represent the standard deviation of the mean and asterisks indicate the level of statistical significance calculated with GraphPad Prism 5.0c (unpaired two-tailed t-test; ns = not significant; * = p-value ≤ 0.05; ** = p-value ≤ 0.01; *** = p-value ≤ 0.001).

This data implies that the α1-subunit (ATP1A1) is indeed found in close proximity to FGF2 on the plasma membrane. However, also the TfR in combination with FGF2 result in similar signal intensity.

3.8 Interaction studies of subdomains of the α1-subunit with FGF2

In order to investigate whether there is a direct interaction between the α1-subunit of the Na^+/K^+-ATPase and FGF2, recombinant proteins of the α1-subunit cytoplasmic domains were expressed and their binding to FGF2 was tested in conventional pull-down assays as well as in the AlphaScreen assay (section 2.4.12). The α1-subunit of the heterodimeric

complex of the Na^+/K^+-ATPase is a transmembrane protein with 10 membrane-spanning α-helices. As visualized in the illustration of the Na^+/K^+-ATPase (Figure 27) the α1-subunit contains three prominent cytoplasmic domains that are mainly involved in ion transport across the plasma membrane to maintain the electrochemical gradient of the cell (Kaplan, 2002). One hypothesis is that a potential interaction of FGF2 with the α1-subunit might occur in the cytoplasm, prior to FGF2 export. Therefore, only the cytoplasmic domains were expressed in *E. coli* and analyzed for their capability to bind FGF2.

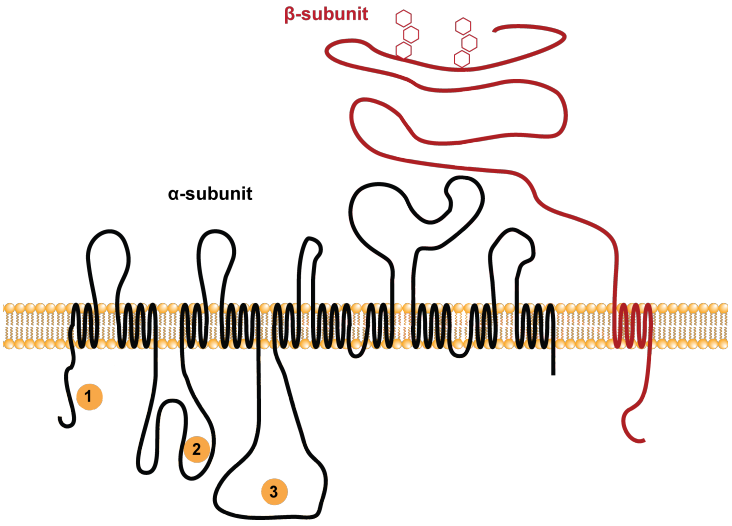

Figure 27: Illustration of the Na^+/K^+-ATPase representing the α- and β-subunit. The regions 1, 2, and 3 are indicating the three cytoplasmic domains (CD), which were expressed in *E. coli*.

For this reason, the cytoplasmic domains (CD), termed CD1, CD2 and CD3, were expressed separately as well as fused together. Fusion constructs of the domains were connected with a small linker region. An overview of the proteins that were expressed is depicted in Figure 28. In further experiment the cytoplasmic domains were mainly expressed as N-terminal GST fusion constructs.

Figure 28: Overview of the fusion constructs obtained from the cytoplasmic domains (CD) of the Na^+/K^+-ATPase. Image source: Dr. Hans-Michael Müller, BZH Heidelberg

3.8.1 Pull-down experiments of the cytoplasmic domains of the α1-subunit and FGF2

The pull-down experiments were performed with untagged FGF2 that was coupled to epoxy beads. The coupled beads were incubated with different N-terminal GST fusion constructs of the cytoplasmic domains that consist of the three major loops of the α-subunit of the Na^+/K^+-ATPase. After subsequent washing steps the input (I), unbound (UB) and bound (B) fractions were loaded on a gel, subjected to Coomassie staining and analyzed for their capability to bind to FGF2 (section 2.4.9).

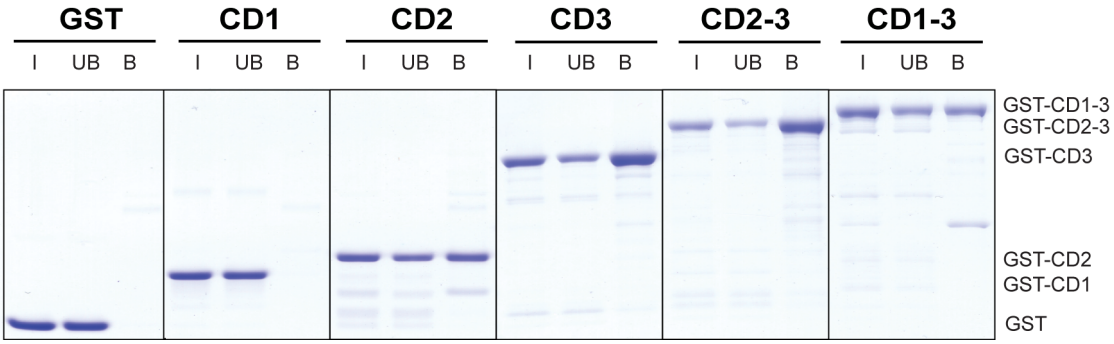

Figure 29: Pull-downs of the cytoplasmic domains of the Na^+/K^+-ATPase with FGF2. N-terminal GST fusion constructs of the cytoplasmic domains (CD) of the Na^+/K^+-ATPase were incubated with FGF2, which was immobilized on epoxy beads. 2.5% of the input (I) and unbound (UB) fractions and 50% of the bound (B) were loaded on the gel for subsequent Coomassie staining.

As a result the cytoplasmic domains CD2 and CD3 were found in the bound fraction (Figure 29). This implicates that both domains are capable to bind to FGF2. Consequently, also CD1-3 as well as CD2-3 was bound to FGF2.

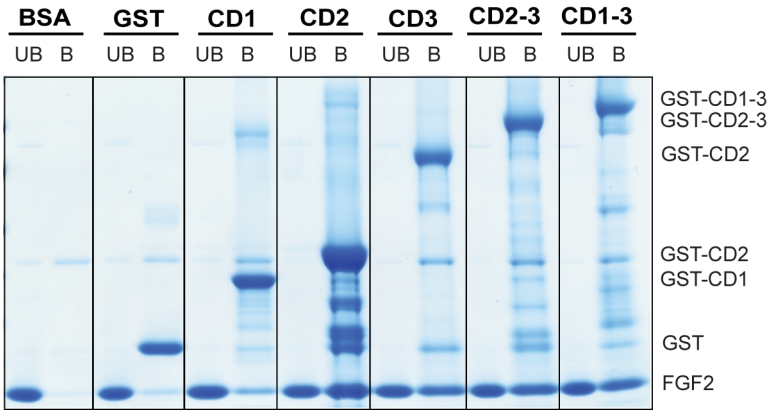

Figure 30: Pull-downs of FGF2 with GST-tagged cytoplasmic domains of the Na^+/K^+-ATPase. Untagged FGF2 was incubated with the cytoplasmic domains (CD) of the Na^+/K^+-ATPase that were immobilized on GSH-beads. 2.5% of the input (I) and 50% of the bound (B) were loaded on the gel and subjected for subsequent Coomassie staining.

In contrast, the cytoplasmic domain 1 (CD1) as well as the GST control do not bind to FGF2. To prove the results obtained from the epoxy pull-down experiments in a second approach, the GST fusion variants of the cytoplasmic domains were immobilized on GSH-beads. The coupled beads were incubated with untagged FGF2 and unbound (UB) and bound (B) fractions were loaded on a gel, which was stained with Coomassie. Figure 30 shows that also here FGF2 can bind to the cytoplasmic domains CD2 and CD3 of the Na^+/K^+-ATPase but not to CD1 and GST. Unspecific binding of FGF2 to empty BSA coated GSH-beads was not observed.

To summarize this section: when having the three major cytoplasmic domains or loops expressed alone (CD1, CD2 and CD3) it is clearly indicated, that the domains CD2 and CD3 have the capability to bind to FGF2. This can be also observed when fusion constructs such as CD2-3 and CD1-3 were used in the pull-down experiments. This indicates, that there is a direct interaction between FGF2 and the cytoplasmic domains of the Na^+/K^+-ATPase.

3.8.2 Establishment of an AlphaScreen® assay to detect protein interactions between the cytoplasmic domains of the α1-subunit and FGF2

In order to have another readout to determine protein-protein interactions, the AlphaScreen assay was applied and established with the help of the Chemical Biology Core Facility at the European Molecular Biology Laboratory (EMBL) in Heidelberg. A detailed description of the method is found in section 3.8.2. Instead of using single cytoplasmic domains, CD1-3 will be used in this assay to investigate the binding constants of FGF2 to the cytoplasmic domains (Figure 28). The CD1-3 construct was chosen because it is well expressed and remains sta9ble during purification. To perform this assay GST-CD1-3 was immobilized on Glutathione coated Donor Beads and hisFGF2 was immobilized on Nickel Chelate Acceptor Beads as depicted in Figure 31.

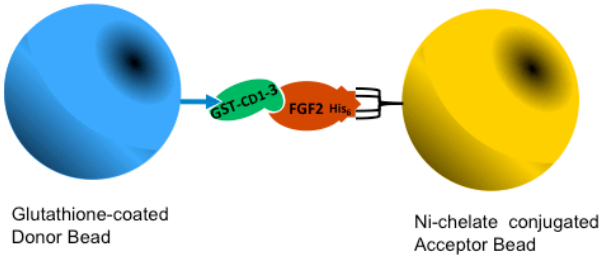

Figure 31: Illustration of the AlphaScreen setup. To perform the AlphaScreen assay GST-CD1-3 was immobilized on Glutathione-coated Donor Beads and hisFGF2 on Ni-chelate conjugated Acceptor Beads. Only upon protein-protein interaction of GST-CD1-3 and hisFGF2 beads come in close contact and excited Donor Beads (680 nm) can transfer their energy to Acceptor Beads, which emit light at 520-620 nm that can be detected and quantified.

If the Donor Beads are excited they produce singlet oxygen that can diffuse within a radius of 200 nm. If an Acceptor Bead is within this range, due to protein-protein interaction, energy will be transferred and the emitted light can be measured (for more details see section 2.3.7.). Establishing this method requires optimization of protein as well as bead concentration. Hence, a cross titration experiment was performed where the concentration of hisFGF2 and GST-CD1-3 were varied while the concentrations of Donor and Acceptor Beads were kept constant.

		GST-CD1-3 (nM)							
		1000.0	500.0	250.0	125.0	62.5	31.3	15.6	0.0
His-FGF2 (nM)	2000.0	16123	19574	19459	19845	17062	16240	12199	1396
	1000.0	12974	19537	21804	22217	19714	16142	12013	806
	500.0	7055	12567	18848	18763	17122	15196	11698	791
	250.0	5726	7152	10713	12635	14080	13302	11140	1124
	125.0	3432	4807	7713	9892	11704	11938	10509	1651
	62.5	3530	3779	5982	7674	9977	10328	10158	2341
	31.3	2787	3062	4617	5720	7751	9142	8913	2733
	0.0	2774	2379	1408	1058	755	421	425	449

Figure 32: Cross-titration experiment for optimization of the AlphaScreen assay conditions. As indicated above, varying amounts of GST-CD1-3 and hisFGF2 were added to the reaction plate and incubated for 1 h at RT. Donor and Acceptor beads were transferred to each reaction on the plate at a final concentration of 30 nM and 60 nM, respectively. After an additional incubation time of 2 h at RT the plate was applied for measurement.

With this experiment a reasonable signal to noise ratio was determined. In Figure 32 the result of a cross-titration experiment is depicted. It can be observed that with increasing amounts of proteins also the total signal increases. However, this occurs only to a certain extent due to the 'hooking effect'. This effect is generated because of reached saturation of the beads, which in turn leads to an inhibitory effect of free binding partners. The following experimental setup was used for all further AlphaScreen tests. AlphaScreen assays were performed in this thesis with protein concentrations of 30 nM for GST-CD1-3 and 60 nM for hisFGF2. In cross-titration experiments (Figure 32), by using these conditions, a signal of 10328 arbitrary units was reached that was still 23 times elevated over the background signal of 449 arbitrary units, having no proteins bound to the beads. This resulted in an optimal signal to noise ratio of the assay with a moderate concentration of proteins.

3.8.3 Determination of binding constants of the interaction between the cytoplasmic domains of the α1-subunit and FGF2 using an AlphaScreen competition assay

To obtain binding constants of the interaction between, GST-CD1-3 and hisFGF2, a competition assay was performed based on the AlphaScreen principle. In this case protein-binding pairs after conjugation with the corresponding beads, were pre-incubated with increasing amounts of either untagged CD1-3 or untagged FGF2 that act as free soluble competitors of the interaction. For a detailed description of this method see section 2.4.12.2. Untagged CD1-3 and untagged FGF2 were derived from cleavage of N-terminal GST fusion constructs. In addition, a Δ25 FGF2 construct lacking the first 25 N-terminal amino acids that was expressed and purified without any affinity tag from *E. coli* was included as competitor. This could be obtained by using a heparin affinity column, as FGF2 has high affinity to heparin. Beside competition for the interaction between GST-CD1-3 and hisFGF2 the protein pairs GST-Tec/hisFGF2 and GST-Titin/hisCARP were used as a control. Tec kinase is a well-characterized binding partner of FGF2 with a determined K_d value of ~0.5 µM (unpublished data, Giuseppe La Venuta, BZH Heidelberg). Titin is a structural component of the sarcomere, which is the basic contractile unit of muscles. Titin is known to interact with the cardiac ankyrin repeat protein (CARP) in the heart sarcomere (Miller Bang Labeit 2003). This protein-protein interaction was used as a control to rule out unspecific binding effects that could occur when CD1-3 or FGF2 were applied as competitors.

Figure 33 represents a summary of the results obtained from the competition experiments, which shows that CD1-3 as well as FGF2 and Δ25 FGF2 can compete for the interaction of GST-CD1-3 and hisFGF2. The concentrations for the half maximum of inhibition (IC_{50}) were determined and the following values were obtained: IC_{50} of 141.1 nM for the competition with CD1-3; 967.5 nM for the competition with FGF2; and 657.1 nM for the competition with Δ25 FGF2. Furthermore, also the interaction between GST-Tec and hisFGF2 could be outcompeted by CD1-3 or both FGF2 variants. The median IC_{50} value obtained was 551.4 nM, which was similar to the K_d value experimentally tested by Giuseppe La Venuta. If we apply the approximation introduced by the method of Cheng and Prusoff we can assume that the determined IC_{50} values corresponds to K_d values (for detailed explanation see section 2.4.12.2).

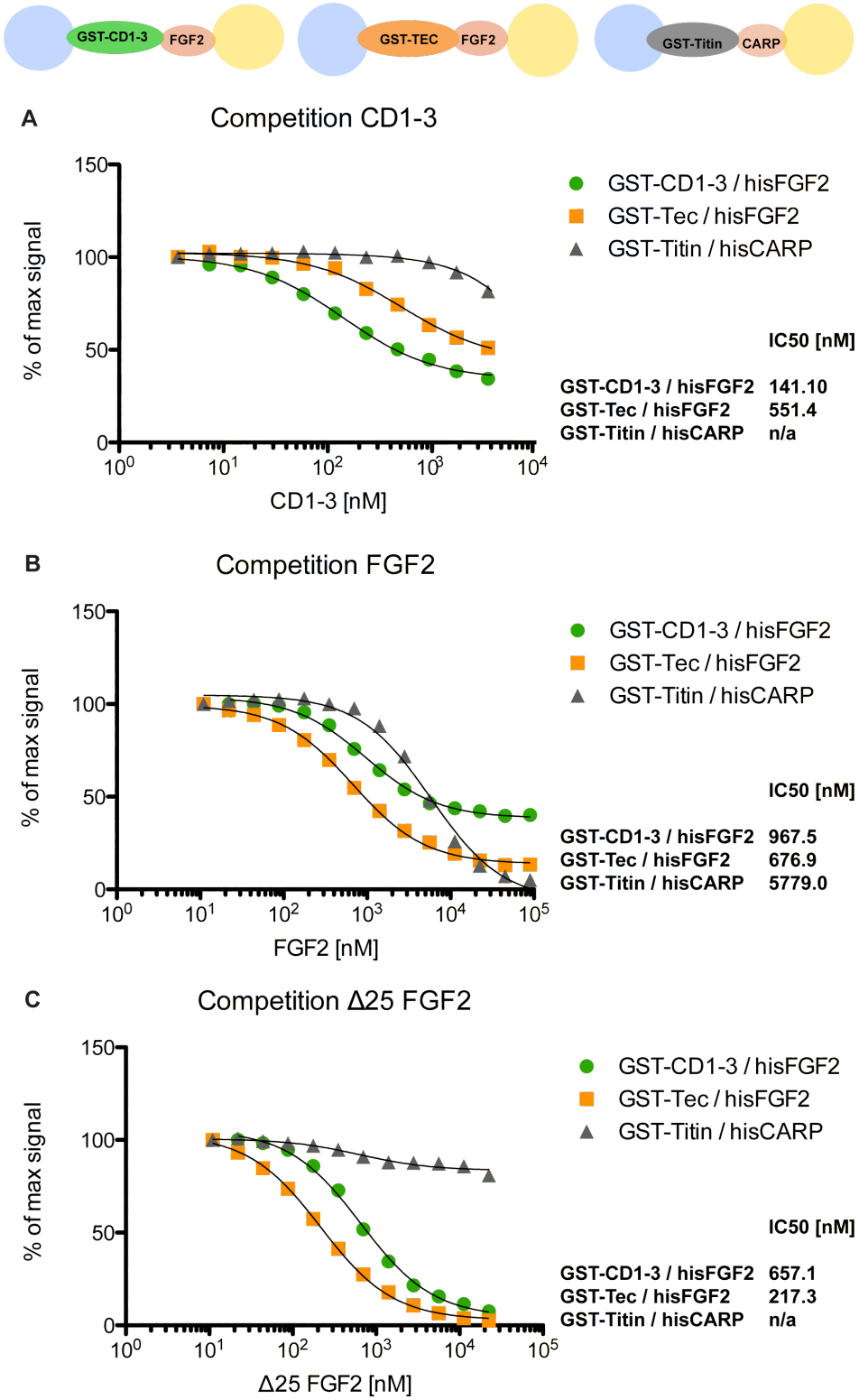

Figure 33: AlphaScreen competition experiments. The protein pairs GST-CD1-3/hisFGF2; GST-Tec/hisFGF2 and GST-Titin/hisCARP were immobilized on either Glutathione Donor Beads or Nickel Chelate Acceptor Beads. Increasing amounts of untagged CD1-3 and FGF2 as well as Δ25 FGF2 were titrated into the binding experiment. As readout the AlphaScreen setup was used. The median of three replicates was calculated and each protein pair was plotted against the concentration of the competitor protein. IC50 values were calculated with GraphPad Prism 5.0c (non-linear regression analysis, one site fit IC50; n/a = not available)

When considering the control proteins GST-Titin and hisCARP, there was a minor background observed when high concentrations of the competitor proteins were used. This was only the case when CD1-3 or FGF2 were used as competitors because both proteins were derived from N-terminal GST fusion constructs. We assume that residual impurities of GST after cleavage can at high concentrations compete for the binding of GST-Titin to the Glutathione Donor Beads. In contrast, this was not the case when Δ25 FGF2 was used as a competitor, which was not purified from a GST-tag. These data conclude that GST-CD1-3 and hisFGF2 are interacting with a K_d value of 657.1 nM when Δ25 FGF2 was used as a competitor.

3.8.4 Development of a small compound screen using an AlphaScreen based detection method

With having the AlphaScreen assay in hand it was possible to screen for a subset of small molecules or chemical compounds that could block the protein-protein interaction of GST-CD1-3 and hisFGF2. This small molecule-screening library contained a total of 4,080 compounds, which were composed of three commercially available libraries. The ultimate goal of such a screening procedure would be to identify initial leading compounds, which can be further developed and finally applied as a drug that potentially can inhibit FGF2 secretion. A drug that could block FGF2 secretion is of particular interest to be applied in cancer because FGF2 has been shown to be a crucial factor involved in tumor-induced angiogenesis (Seghezzi et al., 1998). With the AlphaScreen setup, both proteins were pre-incubated with inhibitors before the Donor and Acceptor Beads were added to the reaction plate for conjugation. After measuring the AlphaScreen signal the percentage of inhibition was calculated from each inhibitor. To make a statement about the assay quality, the Z'-value was calculated for each screening plate (13 in total). With this formula (see section 3.8.4) four different parameters were taken into account that are the mean and standard deviation calculated from both, the positive and negative controls found on each screening plate, representing the upper and lower limit of the assay. A good Z'-value is only obtained when the mean of both controls are strongly different to each other and the standard deviation of both are as small as possible. An excellent assay quality is reached when the Z'-value is close to 1 to have a good dynamic range of the assay.

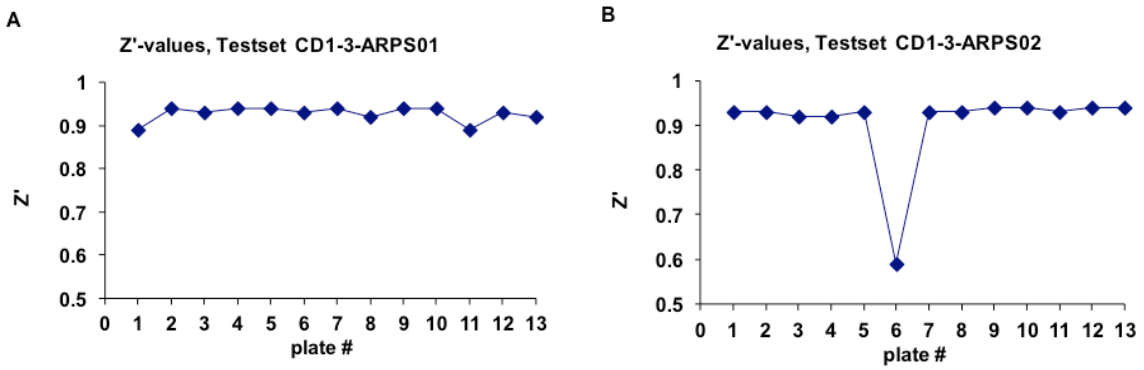

Figure 34: Z'-values of the pilot screen calculated for each screening plate. Calculation of the Z'-values (section 3.8.4) was performed from each screening plate taking into account the mean and standard deviation of the positive and negative control on each plate. A Z'-value between 0.5 and 1 shows an excellent assay quality. **(A)** and **(B)** representing replicates of the screening procedure.

In Figure 34 the Z'-values of each screening is depicted. The pilot screen was carried out in duplicates. Apart from the outlier of the replication plate 6 almost all Z'-values were between 0.9 and 1 showing an excellent assay quality. In addition, when the percentages of inhibition were plotted against each other it was shown that there was a high reproducibility between the two runs with a correlation coefficient (R^2) close to 1.

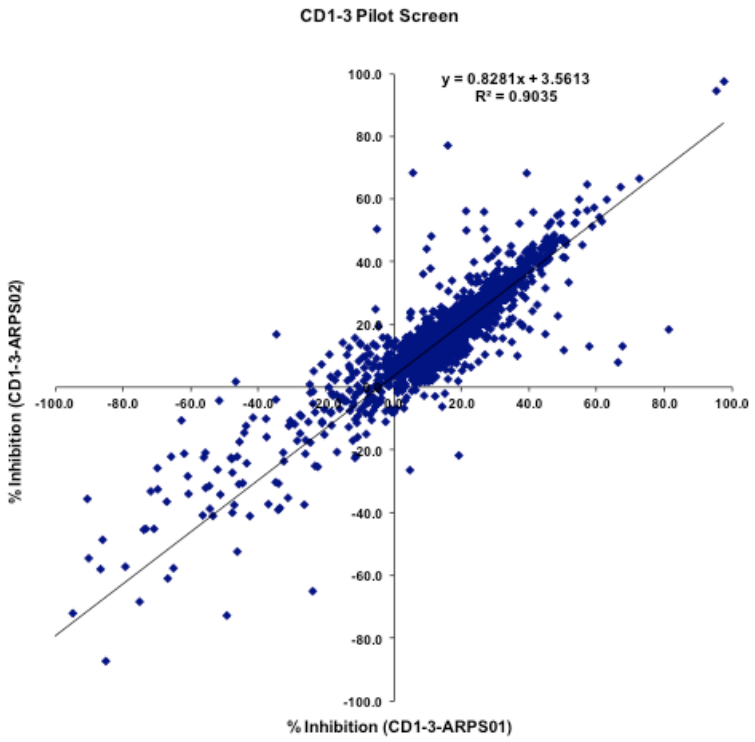

Figure 35: Determination of the correlation coefficient of the pilot screen. The values for the percentage of inhibition of two independent runs were plotted against each other and the R^2 was calculated.

From this pilot screen 5 compounds could be extracted showing an inhibitory effect of the interaction between GST-CD1-3 and his FGF2 that was in the range of 35.5 – 53.5% (Table 3). In general, these compounds were not found to be positive in other AlphaScreens (indicated by the corresponding small median) giving some evidence that these hits are no false positive candidates. In the future, these compounds will be tested in a secretion assay to assess whether they can block FGF2 export from cells.

Table 3: Hits derived from the pilot screen

Compound #	Supplier	% of Inhibition (Average of duplicates)	Median of AlphaScreens
#1	ChemBridge	53.8	6.5
#2	AMRI	46.0	3.5
#3	ChemBridge	53.8	9.9
#4	AMRI	37.0	3.8
#5	ChemBridge	35.5	1.9

In summary, it was possible to establish an AlphaScreen assay that was used to determine a binding constant between GST-CD1-3 and hisFGF2, which was determined with a K_d of 657 nM. Furthermore, with this setup it was possible to screen an initial compound library that allowed for the identification of 5 drug-like components that could inhibit the interaction of GST-CD1-3 and hisFGF2 to a certain extend (35.5 - 53.5% of inhibition).

3.9 Hydrogen Deuterium Exchange (HDX) experiments

The aim of this method is to determine the binding region between CD1-3 and FGF2. This technique was carried out in collaboration with the John Engen Laboratory in Boston. A detailed workflow of this method is described in materials and methods (section 2.4.10). The principle of this reaction is based on the rapid exchange of amide hydrogens in the peptide bonds of proteins that are exposed to a solvent. If the solvent is changed from water (H_2O) to deuterated water (D_2O), deuterons will be incorporated into the solvent-exposed regions of the protein of interest and the increase of mass can be followed after peptic digestion with pepsin and subsequent mass analysis with a mass spectrometer. If proteins interact with each other there will be protected regions that are less accessible to the solvent and consequently, to deuterium exchange. Hence, there is less incorporation of deuterium in the protected binding region. Peptides that are engaged in the interaction with the binding

partner result in lower masses respect to the same peptides of the protein incubated in absence of binding partner (see illustration Figure 36). In order to investigate the binding regions between FGF2 and the cytoplasmic domains of the Na^+/K^+-ATPase the CD1-3 construct was used. In this case, a histidine-tagged version of CD1-3 (hisCD1-3) was used as binding partner in combination with untagged FGF2 that was generated after cleavage of the N-terminal GST moiety. For this purpose FGF2 was first applied alone and subjected to pepsin digestion to obtain peptides that were evaluated for their relative deuterium uptake.

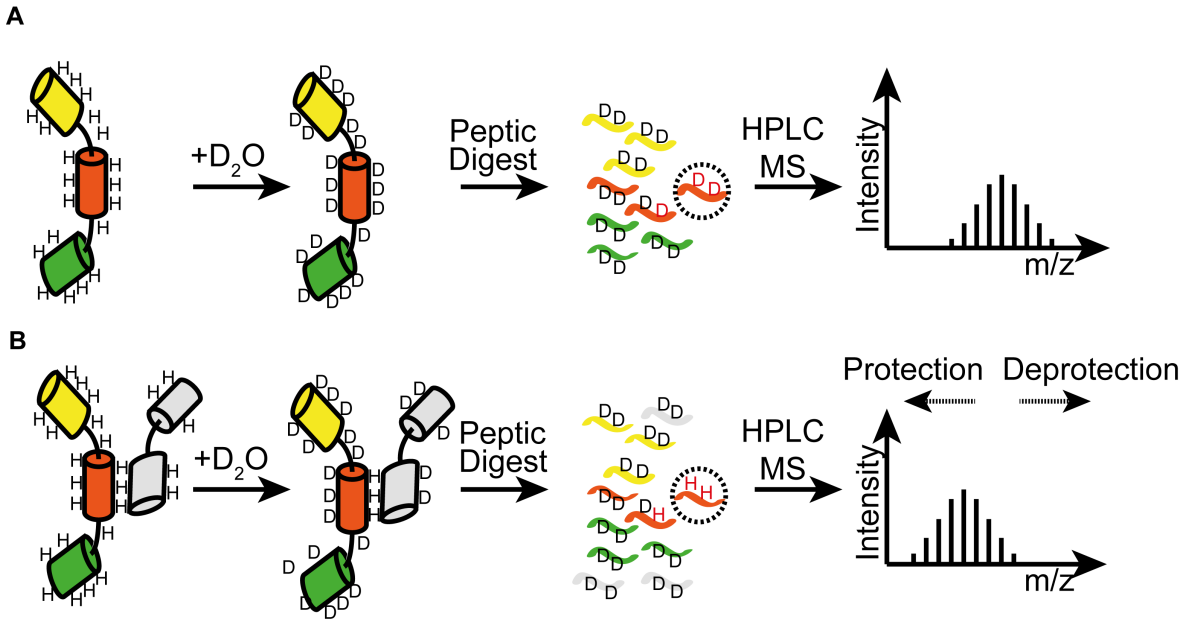

Figure 36: Principle of a HDX experiment to investigating the interface of protein-protein interactions. Image source: Hentze N., Mayer MP., ahead of print in Journal of Visulized Experiments (JoVE).

As depicted in Figure 37 there are regions of FGF2, especially on the N- and C-terminus (red and orange), showing high exchange rates with deuterium. This can happen to exposed surfaces and/or very flexible regions. On the other hand there are other parts such as the black beta sheet that is buried inside the molecule, which shows only moderate exchange rates.

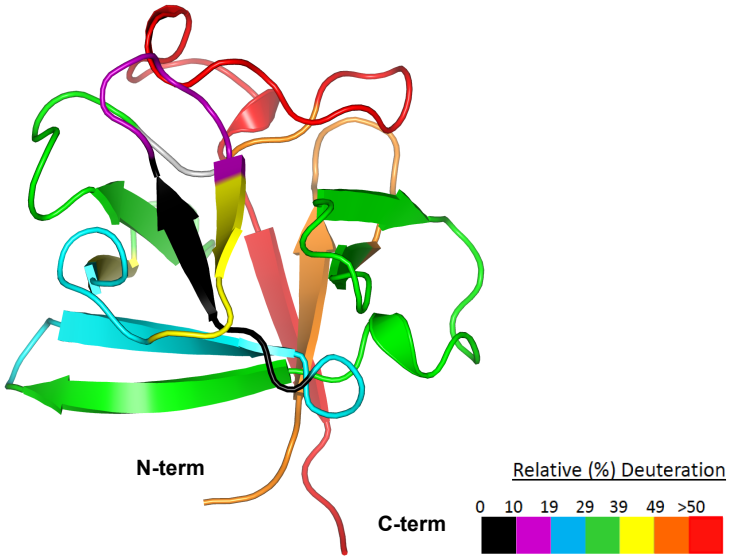

Figure 37: Relative deuterium uptake of FGF2. Untagged FGF2 was incubated for 4 h with deuterated buffer and subsequently subjected to a pepsin digestion. The peptides were separated and analyzed with a mass spectrometer. The relative deuterium uptake was calculated from each peptide and was assigned to the FGF2 molecule. Color code visualizes deuterium uptake.

3.9.1 HDX experiment of FGF2 in complex with the cytoplasmic domains of the α1-subunit

The final goal of this experiment was to investigate the binding region on the side of the FGF2 molecule when in a complex with hisCD1-3. For this reason FGF2 in absence of the binding partner was continuously labeled with deuterium, the reaction was stopped and the protein was subjected to pepsin digestion to analyze the incorporation of deuterium into FGF2 peptides. This was compared to a reaction were FGF2 was pre-incubated with hisCD1-3 at conditions were both proteins form a complex. Subsequently, deuterium uptake of FGF2 peptides alone and in a complex with hisCD1-3 was compared. These results are summarized in Figure 38 representing parts of the peptides of FGF2 (the full analysis is depicted in the appendix). The red line represents peptides that were generated from FGF2 alone and the blue line corresponds to FGF2 peptides obtained after 1 h of incubation with hisCD1-3. The regions where differences in deuterium uptake was observed are shown in red, yellow, green, and blue (Figure 38). Almost all peptides obtained from the complex have less deuterium incorporated. This effect was pronounced in the very N-terminal part of the molecule (red) in regard to other regions were only less than 1 Da of mass change was observed. Drawing the conclusion that hisCD1-3 might protect the N-terminus of FGF2 from hydrogen deuterium exchange, possibly by binding to this specific region of the FGF2 molecule.

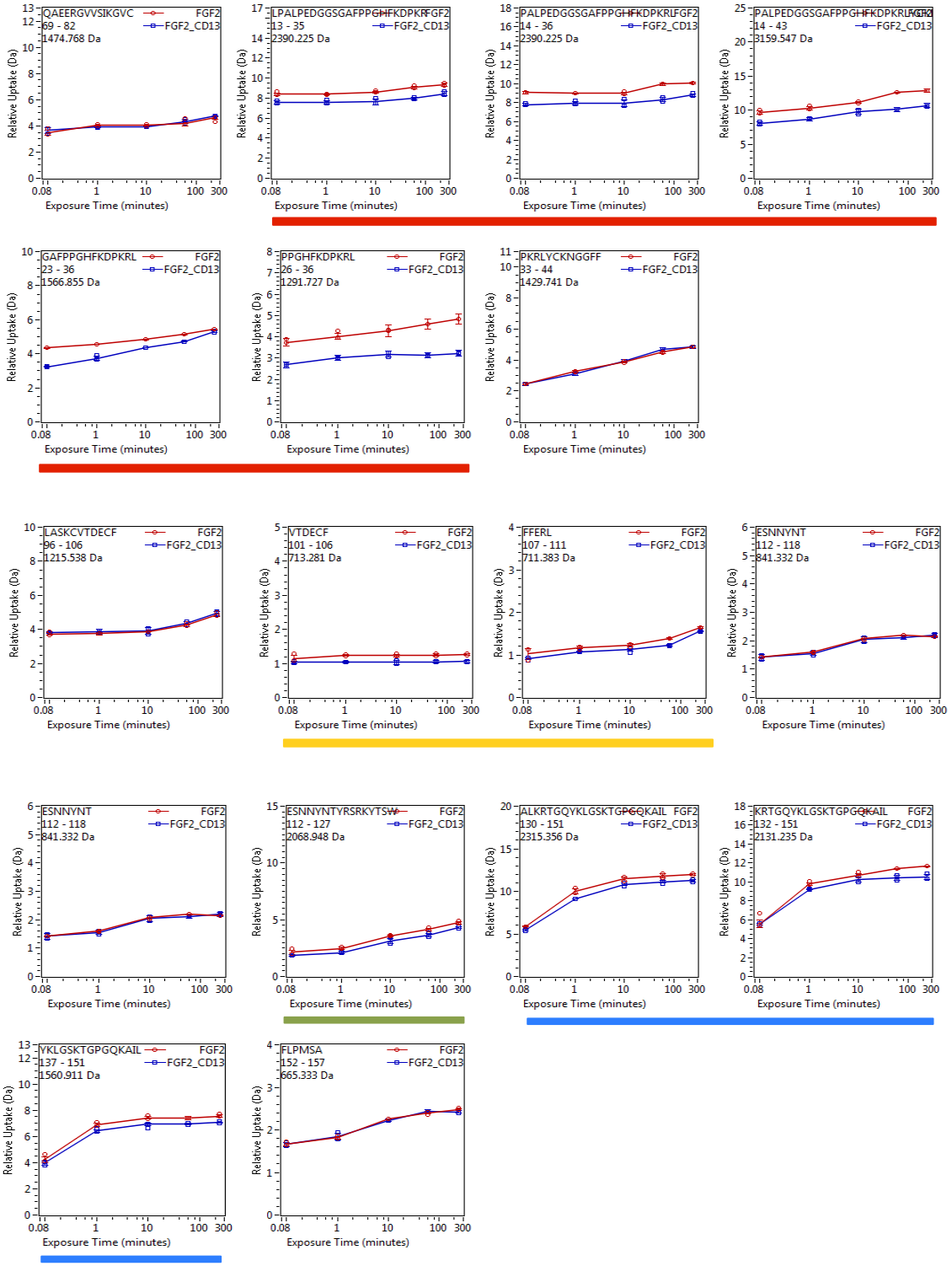

Figure 38: HDX experiment of FGF2 without and in complex with hisCD1-3. FGF2 was analyzed either separately or in complex with hisCD1-3 subjected to HDX. Parts of the peptides covering FGF2 are depicted above where FGF2 was analyzed alone (red) or in complex with hisCD1-3 (blue). For both reactions proteins were incubated for 1 h at RT before the continuous labeling with D_2O was initiated. Samples were taken at the following time points: 10 s, 1 min, 10 min, 1 h and 4 h and immediately afterwards subjected to pepsin digestion, peptide separation and mass spectrometry. The colored regions show peptides that have incorporated less deuterium because FGF2 was incubated together with hisCD1-3.

3.10 Verification of the HDX experiments by mutational analysis of FGF2

FGF2 mutants were generated according to the data obtained from the HDX experiments. As described in section 3.9.1 there were four regions in FGF2 observed showing a protection respect to the deuterium incorporation after pre-incubation with hisCD1-3. As depicted in Figure 39 these regions were assigned to the FGF2 crystal structure and charge reverse mutations were generated on amino acids that were exposed on the surface of these parts of the molecule. In total four mutants were cloned and purified from *E. coli*: hisFGF2 K27E/D28K; hisFGF2 D99R; hisFGF2 T121R and hisFGF2 K138E.

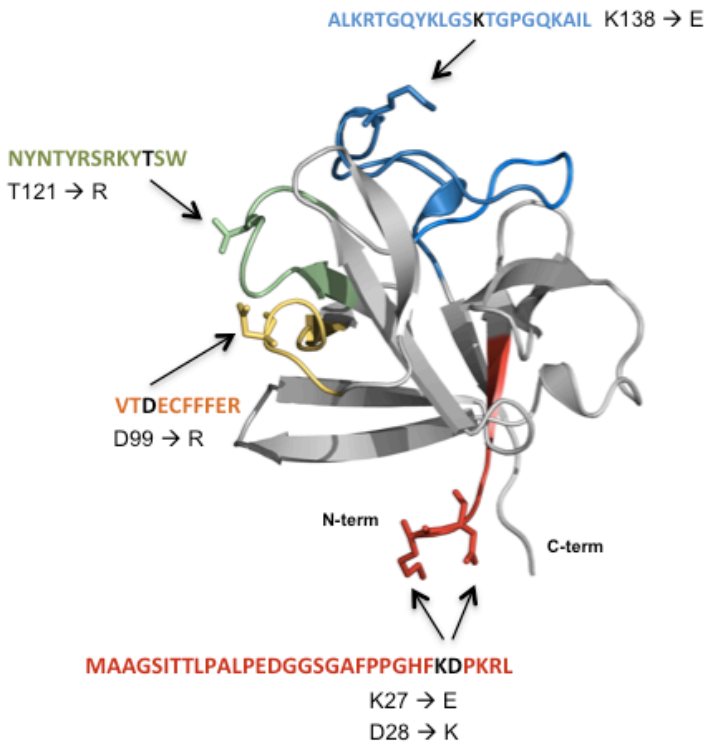

Figure 39: Overview of the reverse charge FGF2 mutants cloned after the HDX analysis.

3.10.1 Pull-down experiments of the FGF2 mutants

In order to verify the ability of the FGF2 mutants to bind to CD1-3, pull-down experiments were carried out. In addition to the point mutations described above, further mutants were included in this analysis. This was a truncation mutant where 25 amino acids were removed from the N-terminus of FGF2 (Δ25 FGF2). This mutant was expressed without affinity tag and was purified with a heparin column from cell lysates (kindly provided from Dr. Julia Steringer, BZH Heidelberg). Beside the 25 amino acid deletion construct of FGF2 a second N-terminal deletion construct was generated lacking the first 28 amino acids. In this case, it was expressed as an N-terminal fusion to GST.

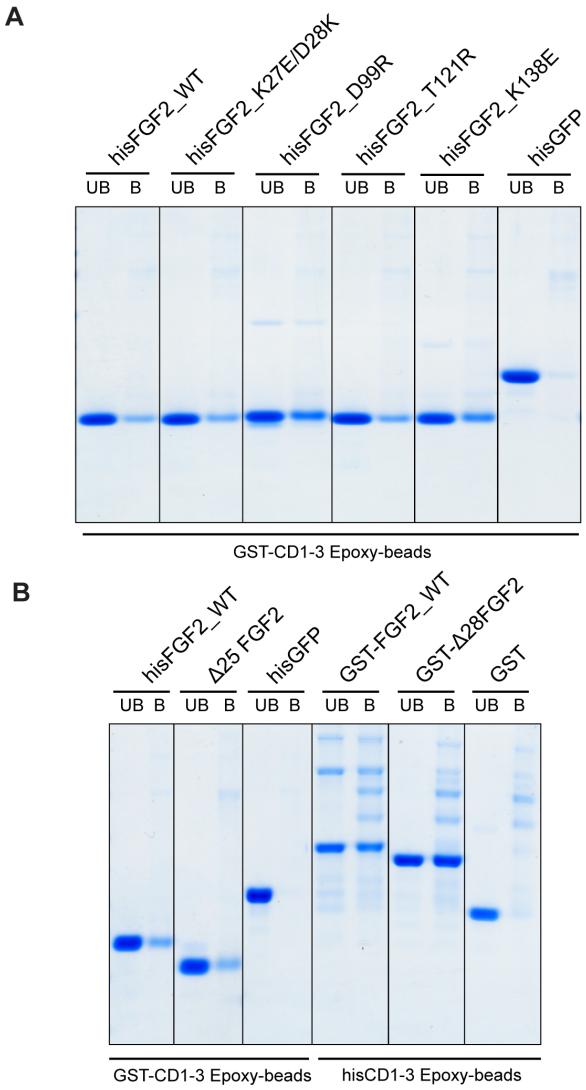

Figure 40: Pull-down experiments of FGF2 mutants with CD1-3 coupled Epoxy-beads. 100 µl of slurry Epoxy-beads coupled to either GST-CD1-3 or hisCD1-3 (~100 µg) were incubated for 1 h at RT with 50 µg of FGF2 variants and control proteins such as GST and hisGFP. 5% of the unbound (UB) and 50% of the bound (B) fraction was loaded on a SDS-PAGE and subjected to Coomassie staining.

Pull-downs of histidine-tagged FGF2 mutants as well as Δ25 FGF2 were tested for their ability to bind to GST-CD1-3 immobilized on epoxy beads. In case, GST-FGF2 proteins were applied in the pull-down experiments, hisCD1-3 coupled epoxy beads served as a potential binding partner. As a control the proteins hisGFP and GST were used. Bound (B) and unbound fractions (UB) fractions were loaded on a gel, which was subsequently subjected to Coomassie staining. B and UB bands were quantified using a LI-COR infrared imaging system (section 2.4.9). A ratio was calculated between B/UB to compare the binding ability of mutant FGF2 to that of FGF2 wild type (FGF2_WT) protein. For this reason his-tagged mutants were compared to hisFGF2wt wild type protein and GST-FGF2 mutants to GST-FGF2 wild type (GST-FGF2_WT).

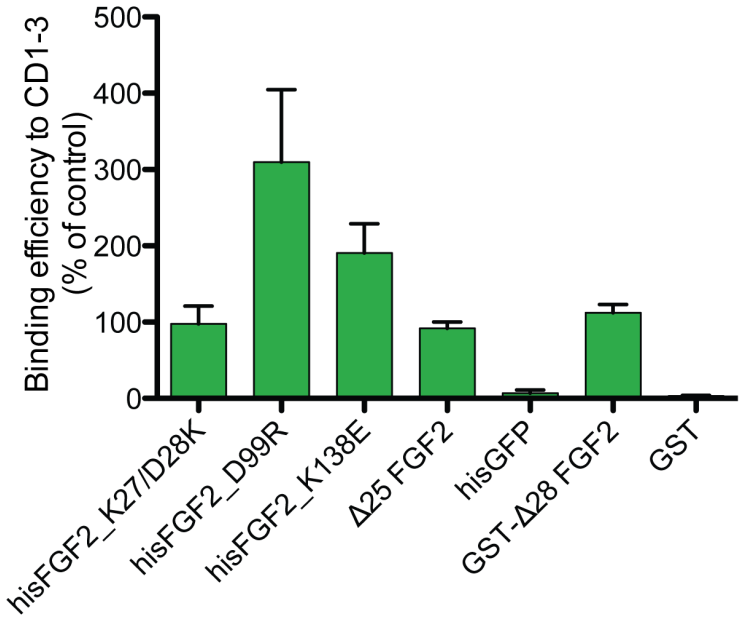

Figure 41: Quantification of pull-down experiments of FGF2 mutants with CD1-3 coupled Epoxy-Beads. Bands were quantified using the LI-COR infrared imaging platform. A ratio of B/UB was calculated and the signals were expressed as a percentage of hisFGFwt (for his constructs) or GST-FGF2wt (for GST constructs). Error bars show the standard deviation of the mean of five independent experiments.

The results obtained from this binding experiment of the various FGF2 mutants did not reflect the initial HDX experiments, which suggested a strong protection at the N-terminal region of FGF2. Neither the 25 nor the 28 amino acid deletion construct had an influence on binding to CD1-3 when compared to the binding affinity of wild type FGF2 to CD1-3 (see quantification in Figure 41). Also no difference was observed for the hisFGF2_K27E/D28K mutant. Interestingly, the mutants of hisFGF2_D99R, hisFGF2_T121R and hisFGF2_K138E had even an increased binding affinity to bind to hisCD1-3 when compared to wild type FGF2. To this extent, no FGF2 mutants could be identified that had a reduced binding affinity to CD1-3.

4 Discussion

Most secretory proteins are transported in vesicular intermediates along the classical secretory pathway to reach their final destination. Typically, these proteins carry a hydrophobic signal sequence that allows them to be targeted to the ER/Golgi-dependent export route followed by vesicular fusion with the plasma membrane to be released into the extracellular medium (Nickel and Wieland, 1998).

More than 20 years ago a different export pathway has been described and was later termed as “unconventional protein secretion”. This class of proteins are characterized by the absence of a signal sequence, they do not reside within the ER or Golgi compartment, and thus lack ER/Golgi specific modifications (Muesch et al., 1990; Nickel and Rabouille, 2009). A couple of unconventional routes for protein secretion have been described so far ranging from vesicular intermediates such as lysosomes, autophagosomes, or multivesicular bodies to release by membrane shedding or direct translocation across the plasma membrane (Nickel, 2005). Recently, a class of membrane proteins have been identified that bypass the Golgi apparatus to reach the plasma membrane even though being targeted to the ER (Grieve and Rabouille, 2011; Rabouille et al., 2012).

One of the best-characterized examples of unconventionally secreted proteins is fibroblast growth factor (FGF2), which is a strong mitogen involved in tumor-induced angiogenesis. Moreover, this protein is important for the maintenance of cellular processes such as cell proliferation and differentiation (Bikfalvi et al., 1997). Its secretion is mediated by direct translocation across the plasma membrane through the formation of a transient lipidic pore (Steringer et al., 2012; Torrado et al., 2009). Hallmarks of FGF2 secretion are the phosphoinositide $PI(4,5)P_2$ at the inner leaflet of the plasma membrane for recruitment and HSPGs at the extracellular side for directional export and immobilization of FGF2 molecules on the cell surface (Temmerman et al., 2008; Zehe et al., 2006). In addition, phosphorylation of FGF2 by Tec kinase regulates FGF2 secretion, which might be du to the stabilization of the hydrophilic pore consisting of molecules in the plasma membrane (Ebert et al., 2010).

This study aimed at the characterization of further proteinaceous factors involved as either core components or regulatory factors of FGF2 secretion. Following a genome-wide RNAi screen, which is documented in the doctoral thesis of Antje Ebert (this department), a subset of such components was found. Among those the α1-subunit of the Na^+/K^+-ATPase was identified. In order to determine a possible role of this protein in FGF2 secretion, the data presented in this study focus on the molecular characterization of the α1-subunit.

4.1 Characterizing the role of the Na^+/K^+-ATPase in FGF2 secretion

In the genome-wide RNAi screen the α1-subunit was revealed as a potential positive regulator of FGF2 secretion. The α1-subunit is part of the Na^+/K^+-ATPase, being closely associated with the β-subunit to build up the functional heterodimeric complex, which acts in ion transport. The energy required for the transport of three sodium ions out of the cell for every two potassium ions pumped in, is provided by hydrolysis of ATP. Simultaneously, the Na^+/K^+-ATPase maintains the electrochemical gradient across the cell membrane. Prior work has documented that ouabain, a specific inhibitor of the Na^+/K^+-ATPase, leads to reduced FGF2 secretion (Dahl et al., 2000; Florkiewicz et al., 1998). Ouabain belongs to the group of cardiotonic steroid and is a well-known inhibitor of the Na^+/K^+-ATPase. It exerts its function while binding to the extracellular portion of the α-subunit und thus interferes with the ion transport function of the sodium pump (Palasis et al., 1996; Schoner and Scheiner-Bobis, 2007).

The studies of Dahl and Florkiewicz revealed the Na^+/K^+-ATPase as a factor involved in FGF2 secretion. However, prior results were mainly based on pharmacological evidence. When they applied ouabain to different cell lines including human embryonic kidney cells (HEK293T) and two monkey kidney cell lines (CV-1 and COS-1) FGF2 secretion was reduced in comparison to untreated cells (Dahl et al., 2000; Florkiewicz et al., 1998). In these studies the high concentration of ouabain (100 µM) was controversial exceeding many folds the half maximum inhibitory concentration (IC_{50}) to block the pumping function of the Na^+/K^+-ATPase. In literature for example, IC_{50} values for HEK293T and CV-1 cells were found to be in a sub-micromolar range of 0.3 and 11 µM, respectively (Kockskämper et al., 1997; Schulz and Cantley, 1988). It remains questionable, whether the decrease in FGF2 secretion was due to the specific inhibition of the Na^+/K^+-ATPase or to possible side effects that could occur as a result of the high concentrations of ouabain. Interestingly, it has been reported that ouabain can induce endocytosis of the Na^+/K^+-ATPase (Cook et al., 1982; Liu and Shapiro, 2007; Núñez-Durán et al., 1988). If this would have been the case in these studies, it might be possible that internalization of the Na^+/K^+-ATPase leads to a reduction of the α-subunit at the plasma membrane where it is hypothesized to support FGF2 secretion. On the other hand Dahl and colleagues obtained remarkable data, which showed that ouabain resistant α-subunits from rat could rescue the secretion defect of FGF2 from CV-1 and HEK293T cells (Dahl et al., 2000).

In order to carry out the validation procedure of the Na^+/K^+-ATPase from the genome-wide siRNA screen, it had to be determined, which isoforms of each subunit are expressed in HeLa cells. It was demonstrated that among the four possible isoforms of the α-subunit

(α1, α2, α3, α4) and β-subunit (β1, β2, β3, β4), respectively, only α1, β1- and β3 subunits are expressed in these cells. This was important to know because early data demonstrated, that in a monkey kidney cell line not only the α1-subunit but also the α2- and α3-subunits from rat were capable to rescue FGF2 secretion (Dahl et al., 2000). For this reason, both isoforms of the β-subunits were taken under consideration in the validation procedure.

To address the role of the α1-, β1- and β3-subunits in FGF2 secretion, *in vivo* secretion analyses were performed using HeLa cells stably expressing FGF2. In this case, siRNAs were chosen, which differed in sequence from those used during the genome-wide RNAi screen. After RNAi-mediated knockdown of the encountered isoforms of the α- and β-subunits, FGF2 secretion was quantified and compared to the secretion efficiency of control cells. This approach confirmed the initial screening data. Knockdown of the α1-subunit, which was targeted by three independent siRNAs showed a reduction of FGF2 secretion up to 50% compared to control cells. In order to exclude pleiotropic effects, knockdowns of the α-subunit were repeated in a stable HeLa cell line. As an additional control, export of GFP-CD4, a protein that passes the classical secretory pathway, was monitored showing no impaired secretion. This result indicates that down regulation of the α1-subunit has a specific effect on FGF2 and does not compromise any other cellular function such as protein transport or cell viability.

For the β-subunit down regulation neither of the β1- nor the β3-isoform had an effect on FGF2 secretion. In contrast, when the β3-subunit was depleted from HeLa cells, a slight up-regulation of FGF2 secretion was observed. In most tissues the Na^+/K^+-ATPase is predominantly expressed and assembled in a α1β1 isoform complex. Down regulation of the β3-isoform might favor the assembly of the α1-subunit with the β1-subunit and hence increase the number of α1-subunits being delivered to the plasma membrane and thus triggering FGF2 secretion. Noteworthy to mention, that Na^+/K^+-ATPase only assembled as a heterodimeric complex can leave the ER. Studies in MDCK canine kidney cells for example showed, that the α1-subunit predominantly assembles with higher affinity to the β1-subunit than to the β2-subunit (Tokhtaeva et al., 2012).

Effects of ouabain on FGF2 secretion could not be tested in HeLa cells due to toxic consequences after addition of the Na^+/K^+-ATPase inhibitor. Supplementation of ouabain at nanomolar concentrations induced cell detachment and morphological changes in HeLa cells (data not shown). This happened already a few hours after the addition of ouabain, which was not compatible with the FACS secretion assay to measure FGF2 export. It was shown that treatment of HeLa cells with rather low concentrations (70 - 100 nM) of ouabain induced morphological changes and apoptotic cell death, which might be due to the very low IC_{50} value of 18 nM determined for these cells (Ramirez-Ortega et al., 2006).

In summary, the results obtained from the siRNA-mediated knockdowns of the α- and β-subunits are in agreement with pharmacological studies where the Na^+/K^+-ATPase was inhibited by ouabain. However, the data of this study provides clear evidence that only the α-subunit not the β-subunit is involved in FGF2 secretion.

4.2 Co-localization of the α1-subunit and FGF2 in HeLa cells

Data obtained from the siRNA-mediated knockdowns of the validation procedure provided strong evidence for a role of the α1-subunit of the Na^+/K^+-ATPase in FGF2 secretion. Therefore, it was of particular interest to localize both proteins in HeLa cells to investigate whether there is a potential cellular compartment for the interaction of FGF2 and the α1-subunit.

Immunofluorescence analysis of endogenous protein levels of the α1-subunit and FGF2 could clearly demonstrate that both proteins are localized at the plasma membrane of HeLa cells. Moreover, co-staining of cells with antibodies directed against both epitopes of FGF2 and α1-subunit, gave raise to a co-localization signal at the plasma membrane.

In order to investigate whether the plasma membrane could be the compartment of a potential direct interaction between these two proteins, a novel protein interaction assay was carried out. This so-called Duolink assay is an *in situ* proximity ligation assay that should resolve subcellular protein interactions at a distance of 0 - 40 nm. Therefore, protein-protein interactions of FGF2 and the α1-subunit were analyzed. As controls, other plasma membrane resident proteins, which are known not to interact with FGF2, were chosen and examined including transferrin receptor and cadherin. Since FGF2 is absent from the Golgi compartment the Golgi protein GM130 was additionally tested.

Quantification analyses showed that there were almost as much interaction sites observed for FGF2 and the α1-subunit as for FGF2 and the transferrin receptor. Interaction sites of the protein pairs FGF2/Cadherin and FGF2/GM130 caused only minor signals that were in the range of background. The background of the assay was defined by signals that were obtained when only one antibody either against FGF2 or ATP1A1 (α1-subunit) was used. Although there is no known evidence for an interaction of FGF2 with transferrin receptor there were similar amounts of interaction spots detected for transferrin receptor as for the α1-subunit of the Na^+/K^+-ATPase. It seems likely that there is a certain limitation of the assay. This implies that also proteins that are in close proximity (in a range of 0 - 40 nm), which reside for example in the same sub-domains at the plasma membrane, can give a signal even if there is no direct interaction.

From these data, also including the conventional immunofluorescence assay we can conclude that both proteins are in close proximity at the plasma membrane. Although a direct interaction between the α1-subunit and FGF2 cannot be postulated it can be hypothesized that a potential role for the α1-subunit to act in FGF2 secretion might be carried out at the plasma membrane.

4.3 Interaction studies of the cytoplasmic domains of the α1-subunit and FGF2

Subcellular co-localization experiments showed that the α1-subunit and FGF2 are both enriched at the plasma membrane in HeLa cells. In addition, Dahl and co-workers performed co-immunoprecipitation experiments and were capable to either co-purify FGF2 or the α1-subunit from cell lysates of CV-1 cells. However, at these conditions both proteins were over expressed in cells. These experiments provide only qualitative data on the protein interaction of the α1-subunit and FGF2, which binding capacities were not further quantified. In addition, co-immunoprecipitation experiments cannot rule out that the nature of this interaction is indirectly mediated through an additional binding partner.

According to the data obtained from the immunofluorescence assay we hypothesize a potential interaction site for FGF2 at the cytoplasmic regions of the Na^+/K^+-ATPase. In order to investigate whether there is a direct interaction between the α1-subunit and FGF2 we expressed and purified the cytoplasmic domains from the human α1-subunit in *E. coli*. This approach was chosen, because the α1-subunit naturally consists of 10 transmembrane domains, which represents a major obstacle for protein purification. In particular the first three cytoplasmic domains (CD1, CD2, and CD3) that are involved in ion transport and ATP hydrolysis of the Na^+/K^+-ATPase were further analyzed. The domains were either separately expressed (CD1, CD2, CD3) or as fusion constructs (CD2-3, CD1-3) with a short linker region between the domains. Pull-down experiments were performed where either the various cytoplasmic domains or FGF2 were immobilized on beads acting as a binding partner for the other protein. Both experiments lead to the same conclusion: FGF2 directly interacts with the cytoplasmic domains CD2 and CD3 as well as to the CD2-3 and CD1-3 fusion constructs of the α1-subunit. In conclusion, it is highly probable that a direct interaction of FGF2 and the α1-subunit occurs at the cytoplasmic site and presumable at the plasma membrane of a cell.

Analyses of the binding interface between FGF2 and cytoplasmic domain of the α1-subunit

In order to investigate the interaction interface of FGF2 and CD1-3 hydrogen deuterium exchange (HDX) experiments were performed. Regions that take part in the binding reaction are less accessible to incorporation of deuterium at their amide hydrogens in the peptide bond.

When FGF2 was applied for HDX experiments the relative deuterium uptake of the molecule was analyzed over time. In particular, the N- and C- terminal parts of FGF2 showed up to 50% of deuterium incorporation, which demonstrates that these regions are very flexible. In addition, FGF2 was analyzed after pre-incubation with CD1-3 to shift most of the free FGF2 molecules to form a complex with CD1-3. This experiments revealed that when FGF2 is in a complex with CD1-3, an increased protection of the N-terminus of FGF2 can be observed, which was pronounced for the first 28 amino acids of FGF2. Three other parts of the molecule showed only subtle changes in deuterium uptake after binding to CD1-3. The findings indicate that after binding of FGF2 to CD1-3 the N-terminal flexible region of FGF2 becomes stabilized, thus being involved in binding to CD1-3.

To test this hypothesis, FGF2 deletion mutants were generated lacking either the first 25 or 28 amino acids. In addition, further charge reverse mutants were designed comprising all regions that showed protection from deuterium uptake. For this reason surface exposed amino acids of this areas were chosen and replaced by amino acids with opposite charge states. The following mutants were generated (hisFGF2 K27E/D28K; hisFGF2 D99R; hisFGF2 T121R and hisFGF2 K138E) also including Δ25 FGF2 and analyzed by pull-down experiments for their ability to bind to GST-CD1-3.

None of the tested mutants showed impaired binding efficiency to GST-CD1-3 when compared to hisFGF2 wild type protein. Even the N-terminal truncation mutant of FGF2 (Δ25 FGF2) as well as the mutant that carried two point mutations at the N-terminus (hisFGF2 K27E/D28K) did not show any difference in binding to GST-CD1-3. Since not only the 25 amino acids were suggested to be involved in binding but rather the first 28 amino acids, an additional mutant was created lacking the fist 28 (GST-Δ28) amino acids of the N-terminus of FGF2. Because this mutant could not be purified as an untagged version such as Δ25 FGF2 it was N-terminally fused to GST. Subsequently, binding of this mutant was tested to hisCD1-3. The binding efficiency of GST-Δ28 was compared to GST-FGF2 wild type protein again, showing no difference.

Taken together, mutational analysis could not confirm the obtained data from HDX experiments, which predicted the N-terminus of FGF2 as the most probable region for

binding to CD1-3. Since in pull-down experiments reduced binding affinities could not be demonstrated for the truncation mutants, the N-terminal part of FGF2 is not considered to be directly involved in binding to CD1-3. Moreover, no other region determined in HDX experiments could be confirmed with charge reverse mutants of FGF2.

These experiments could be extended to create not only charge reverse mutants but also mutations to neutral amino acids such as alanine. In addition, also more quantitative methods to measure protein-protein interactions such as fluorescence polarization experiments or the AlphaScreen assay could be applied. This would allow detecting also subtle changes in binding affinities, which might be incapable of measurement by conventional pull-down experiments. Furthermore, it would be of great importance to repeat the HDX experiments not only looking into the interaction interface of the FGF2 molecule but also into the one of CD1-3. With this approach the binding region between CD1-3 and FGF2 could be investigated and verified by a mutational analysis.

Binding affinities of the cytoplasmic domains of the α1-subunit to FGF2

The AlphaScreen assay was applied in order to obtain binding constants for the interaction between hisFGF2 and the cytoplasmic domains (GST-CD1-3). Different proteins were used as competitors: untagged CD1-3, untagged full-length FGF2, and untagged Δ25 FGF2. To compete for the binding of GST-CD1-3/hisFGF2 the following IC_{50} values were determined: For untagged CD1-3 it was 141.1 nM, for untagged FGF2 967.5 nM and 657.1 nM were obtained for untagged Δ25 FGF2.

As a control an unrelated protein binding pair GST-Titin/hisCARP was used to monitor unspecific binding effects. The binding of GST-Titin/hisCARP was affected at very high concentrations of the competitor proteins CD1-3 and FGF2, respectively, which was not observed for Δ25 FGF2. An obvious explanation for these observations are the origins of FGF2 and CD1-3. Both constructs were derived from N-terminal fusions to GST, which were cleaved after purification. Following cleavage there was still a faint band of residual GST visible on a Coomassie gel. For this reason, free GST could compete at high concentrations of both FGF2 as well as CD1-3 for the binding to the Glutathione Acceptor Beads, thus leading to elution of the immobilized GST binding partner. This small impureness would explain the sensitivity towards the control proteins GST-Titin/hisCARP. Notably, this was not observed for the Δ25 FGF2 construct, which was not purified starting from a GST fusion protein but by affinity chromatography using immobilized heparin.

From these results we can conclude a specific competition for full-length FGF2 and CD1-3 proteins, because the control proteins GST-Titin/hisCARP were only affected at higher

concentrations. Moreover the observed behavior occurred at concentrations where the competition curve of GST-CD1-3/hisFGF2 almost reached a plateau. However, due to this issue the IC_{50} values might be not fully reliable. Since the control was not affected by Δ25 FGF2 as a competitor, we assume a K_d value of 657.1 nM for the interaction between hisFGF2 and the cytoplasmic domain GST-CD1-3. In this experimental setup the determined IC_{50} value (657.1 nM) corresponds to the K_d value (for detailed explanation see section 2.4.12.2). As shown by previous pull-down experiments, binding of Δ25 FGF2 to CD1-3 is comparable to wild type FGF2, thus concluding that the absence of the N-terminal amino acids should not cause any artifacts in this competition assay.

Furthermore, a binding constant of GST-Tec and hisFGF2 was also determined with a K_d value of 217.3 nM, which is in good agreement with the K_d value of 500 nM observed in previous studies (personal communication, Giuseppe La Venuta). Interestingly, not only FGF2 but also CD1-3 was able to compete for the interaction of GST-Tec and hisFGF2. This observation suggests that Tec kinase and CD1-3 might share the same binding region of the FGF2 molecule, which may prove to be relevant for mechanistic details of the overall process of FGF2 secretion.

4.4 Small compound screen to identify inhibitors of the interaction between the cytoplasmic domains of the α1-subunit and FGF2

The AlphaScreen assay, which was used in this thesis to determine binding affinities between the cytoplasmic domain CD1-3 of the α-subunit and FGF2 was further employed to screen for small compounds able to interfere with this interaction. The rational of this approach was to identify lead compounds serving as the starting point for the development of inhibitors blocking the FGF2 secretion. The long-term aim of this approach is to achieve pharmacological tools able to act against the pro-angiogenic effects of FGF2. In addition, FGF2 is an important target since it was recently demonstrated to have an anti-apoptotic effect, which leads to resistance of tumor cells towards chemotherapeutic drugs (Salm et al., 2013). However, such a drug-developmental process involves many steps. If a compound can be identified from such a screening procedure it first has to be optimized in order to improve its potency. Furthermore, cytotoxicity tests have to be performed as well as pharmacokinetic studies and toxicological investigations, which eventually lead to a potential drug candidate. In this study the experimental basis for a large-scale small molecule screen was established and a “lead screen” was performed.

The initial pilot screen included a total of 4,080 compounds that were tested for their ability to compete for the binding of GST-CD1-3 and hisFGF2. These compounds covered 13

screening plates. Statistical parameters were calculated for each plate. Z'-values close to the theoretical optimum of 1 for almost every plate proved the excellent quality of the assay. In addition, the screen was performed in duplicates showing a very good reproducibility with a correlation coefficient that was likewise close to 1.

From this pilot screen 5 compounds could be identified that were able to inhibit the interaction between GST-CD1-3 and hisFGF2 from 35.5% to up to 53.8%. In the meanwhile also the lead screen was carried out, which covered 75,000 compounds and also showed an excellent assay quality represented by the Z'-values close to 1. In summary, 161 hits were identified as capable of inhibiting the interaction of GST-CD1-3 and FGF2 with more than 35%. Among those 13 compounds showed an inhibitory effect of more than 70%. In addition, it was possible to cluster these hits into 7 different compound classes according to their chemical structures. The fact that the hits are not randomly distributed among the screening library but rather cluster into several chemical subgroups indicates high significance of the obtained screening hits. Beyond these observations, the 5 hits from the pilot screen could be reconfirmed. This comprehensive analysis provides the possibility to test the hits of the lead screen in a cell based secretion assay to assess the ability of these inhibitors to block FGF2 secretion.

4.5 Model of the α1-subunit as a part of the FGF2 secretion mechanism

In the current study, RNAi-mediated down-regulation demonstrated that the α-subunit independent of the β-subunit of the Na^+/K^+-ATPase might play a role in FGF2 secretion from cells. Interaction studies of the cytoplasmic domains of the α-subunit and FGF2 using an *in vitro* biochemical assay showed a direct interaction between these two molecules, which interaction can be specifically blocked by small compound inhibitors. In addition, both proteins co-localize in cells at the plasma membrane. For this reason, it is most likely that a direct interaction of FGF2 and the α1-subunit occurs at the cytoplasmic site close to the plasma membrane to drive export of FGF2 *in vivo*.

Based on this study it could be clearly demonstrated that FGF2 secretion (as far it concerns the contribution of the Na^+/K^+-ATPase) is only dependent on the α-subunit. Since exclusively the heterodimeric complex of the Na^+/K^+-ATPase, composed of both the α-subunit and the β-subunit, can act in ion transport functions we conclude that the enzyme activity is not important for FGF2 secretion. This is in line with previous studies, which showed that compounds perturbing the ion gradient without inhibiting the Na^+/K^+-ATPase, have no influence on FGF2 secretion (Florkiewicz et al., 1998). Furthermore, it was demonstrated that

FGF2 could traverse the membrane of inside-out vesicles derived from plasma membrane in the absence of ATP (Schäfer et al., 2004).

A recent study presented remarkable data in HeLa cells where a pool of unassembled α1-subunits was detected in the plasma membrane of these cells (Yoshimura et al., 2008). This is of particular interest because the Na^+/K^+-ATPase leaves the ER assembled in a 1:1 stoichiometry complex consisting of the α- and β-subunit *en route* to the plasma membrane. It was shown that the β1 and β3-subunits have a much faster turnover than the α1-subunit, which can remain in the plasma membrane. Since the function of such a pool of unassembled α1-subunits still remains elusive, one possibility could be that they act in FGF2 secretion. It is commonly accepted that the Na^+/K^+-ATPase plays a role in other cellular processes besides carrying out ion transport functions to maintain the electrochemical gradient of a cell. For example, it is well-established that a subset of Na^+/K^+-ATPases which reside in caveolae do not take part in ion pumping but rather act as signal transducers after binding of cardiotonic steroids (Liang et al., 2007; Xie and Cai, 2003).

So far, it remains unclear how the α-subunit participates in FGF2 secretion. One possibility could be that the α1-subunit is involved in the recruitment of FGF2 molecules to the plasma membrane prior to $PI(4,5)P_2$ binding. Due to the interaction between FGF2 and the cytoplasmic domains 2 and 3 of the α1-subunit, it is conceivable that one or even two FGF2 molecules could simultaneously bind to the α-subunit on the cytoplasmic site close to the plasma membrane. In a second step FGF2 might be transferred to $PI(4,5)P_2$, where it gets phosphorylated by Tec kinase following oligomerization that leads to the formation of a lipidic pore.

Another possible scenario is that the α1-subunit might stabilize and control the integrity of such a transient lipidic pore formed of FGF2 molecules in the plasma membrane. The α1-subunit with its 10 transmembrane segments might act as a scaffold stabilizing the pore and even contributing to a certain microenvironment of lipids enriched in $PI(4,5)P_2$ and cholesterol, which are essential for FGF2 secretion (Temmerman et al., 2008). In addition, the α1-subunit might be involved in regulation of pore formation processes preventing the uncontrolled passage of ions or small molecules that could penetrate the pore during FGF2 secretion. This would point to the direction that the α1-subunit can open and close such a lipidic FGF2 pore to control the entry and release of FGF2 molecules that continuously traverse the lipid bilayer prior to extraction by membrane proximal HSPGs and immobilization in the extracellular space.

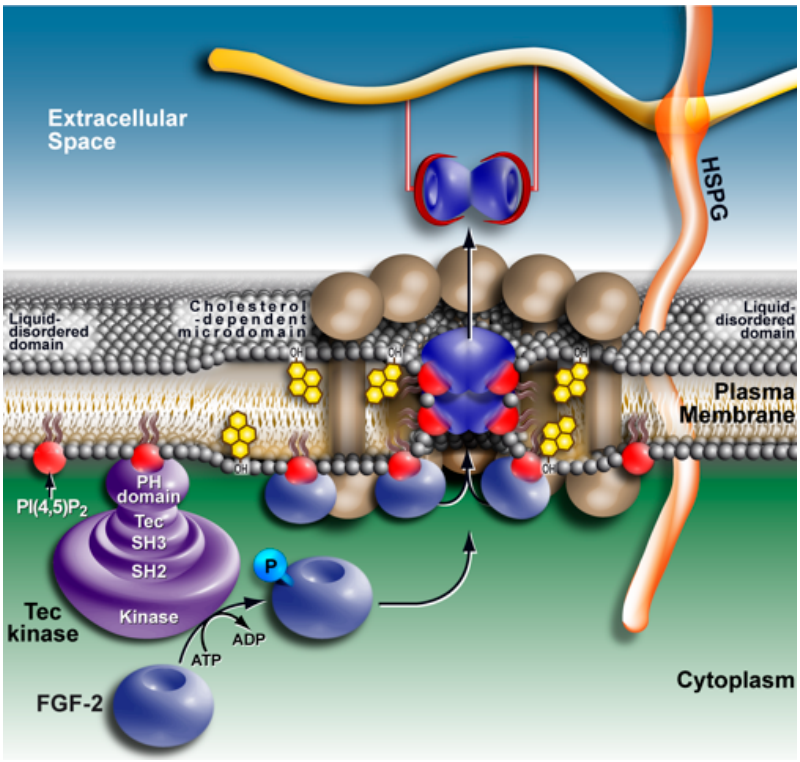

Figure 42: Model of FGF2 membrane translocation. FGF2 is secreted by direct translocation across the plasma membrane. FGF2 is recruited to the inner leaflet of the plasma membrane where the α-subunit might function as a docking platform followed to binding to $PI(4,5)P_2$. Subsequently, FGF2 gets phosphorylated at tyrosine 82 by Tec kinase, which leads to the stabilization of $PI(4,5)P_2$ induced oligomers forming a toroidal lipidic membrane pore through which the molecules can traverse the plasma membrane. HSPGs in the extracellular space extract FGF2 molecules from the plasma membrane due to much higher affinity and immobilize them on the cell surface. Moreover, the α1-subunit might act as a scaffold by stabilizing such a transient lipidic pore, or even control the opening and closing of such a pore. Adapted from Nickel 2010. Current Opinion in Biotechnology 2010, 21:621-626

4.6 Future perspectives

In this study the involvement of the α1-subunit in FGF2 secretion has been shown by *in vivo* and *in vitro* experiments. However, the exact mechanism by which the α1-subunit facilitates FGF2 secretion remains to be ascertained.

In vitro reconstitution experiments could be a way to address the question whether the α1-subunit is involved in either recruitment of FGF2 to the plasma membrane to function as a docking platform prior to $PI(4,5)P_2$ binding or whether it controls and stabilizes the pore. The generation of proteoliposomes in a plasma membrane-like lipid background containing the α1-subunit and $PI(4,5)P_2$ might answer these questions. In a different approach the cytoplasmic domains CD1-3 could be anchored to liposomes either through a lipidated version of the molecule or through recruitment of his-tagged CD1-3 by a Nickel-NTA lipid incorporated in the liposomes. In case that the α1-subunit is acting as a docking platform for

FGF2, recruitment and pore formation might be accelerated showing different kinetics that could be monitored by the leakage assay.

When hypothesized that the α1-subunit acts as a gate to control the opening and closing of such a pore, reconstitution of this protein might hamper the entry of small fluorescent tracer molecules into liposomes. The same experimental setup can be used as a negative control in absence of the α1-subunit. The incorporation of HSPGs inside the lumen of such proteoliposomes might even contribute to a process where FGF2 molecules completely traverse these artificial membranes (and end up inside their lumen). In addition, electrophysiology methods can be applied to measure the influx of divalent calcium ions into the cell by calcium imaging. This would allow comparing untreated cells with those subjected to siRNA-mediated knockdown of the α1-subunit. Such information might suggest whether cells are less susceptible to control the entry of small molecules or ions such as calcium in absence of the α1-subunit.

Another future aspect would be to investigate the distribution of FGF2 and the α-subunit in polarized cells. In polarized tissue the Na^+/K^+-ATPase localizes towards the basolateral membrane (Farr et al., 2009; Muth et al., 1997). Therefore, it is of particular interest to investigate whether FGF2 secretion also occurs at these sites of the cell and shows the same distribution pattern.

Furthermore, future work is planned to continue with the verification of the small compound screen, which aimed to identify inhibitors of the interaction between the cytoplasmic domains of the α1-subunit and FGF2. This will implicate to test the inhibitors in a FGF2 secretion assay to examine their functionality *in vivo*. Such an inhibitor could be a valuable tool in research to block FGF2 secretion in many cell types to investigate FGF2 specific effects as for example in cell development or angiogenesis. In addition, such an inhibitor might help to elucidate further details of the secretion mechanism of FGF2. In particular, it might be possible to study whether membrane binding to $PI(4,5)_2$ can still occur even when the interaction between the α1-subunit and FGF2 is interrupted. Finally, such an inhibitor would pave the way for the future development of a novel anti-angiogenic drug and could help to prevent resistance to chemotherapies where autocrine FGF2 signaling has been seen to inhibit apoptosis of tumor cells.

Finally, it would be of great interest to investigate whether the α1-subunit of the Na^+/K^+-ATPase is a common regulator in unconventional protein secretion. In this way other unconventional secreted proteins such as Tat, which seems to be secreted in a similar way than FGF2, can be tested for their dependence on the α1-subunit in secretion.

5 References

Abeywardena, M.Y., McMurchie, E.J., Russell, G.R., and Charnock, J.S. (1984). Species variation in the ouabain sensitivity of cardiac Na+/K+-ATPase. A possible role for membrane lipids. Biochem. Pharmacol. *33*, 3649–3654.

Abraham, J.A., Mergia, A., Whang, J.L., Tumolo, A., Friedman, J., Hjerrild, K.A., Gospodarowicz, D., and Fiddes, J.C. (1986). Nucleotide sequence of a bovine clone encoding the angiogenic protein, basic fibroblast growth factor. Science *233*, 545–548.

Ago, H., Kitagawa, Y., Fujishima, A., Matsuura, Y., and Katsube, Y. (1991). Crystal structure of basic fibroblast growth factor at 1.6 A resolution. J. Biochem. *110*, 360–363.

Axelsen, K.B., and Palmgren, M.G. (1998). Evolution of substrate specificities in the P-type ATPase superfamily. J. Mol. Evol. *46*, 84–101.

Backhaus, R., Zehe, C., Wegehingel, S., Kehlenbach, A., Schwappach, B., and Nickel, W. (2004). Unconventional protein secretion: membrane translocation of FGF-2 does not require protein unfolding. J. Cell. Sci *117*, 1727–1736.

Bagrov, A.Y., Shapiro, J.I., and Fedorova, O.V. (2009). Endogenous cardiotonic steroids: physiology, pharmacology, and novel therapeutic targets. Pharmacol. Rev *61*, 9–38.

Baldwin, T.A., and Ostergaard, H.L. (2001). Developmentally regulated changes in glucosidase II association with, and carbohydrate content of, the protein tyrosine phosphatase CD45. J. Immunol. *167*, 3829–3835.

Barrientos, S., Stojadinovic, O., Golinko, M.S., Brem, H., and Tomic-Canic, M. (2008). Growth factors and cytokines in wound healing. Wound Repair Regen *16*, 585–601.

Beggah, A.T., Jaunin, P., and Geering, K. (1997). Role of glycosylation and disulfide bond formation in the beta subunit in the folding and functional expression of Na,K-ATPase. J. Biol. Chem. *272*, 10318–10326.

Beggah, A.T., Béguin, P., Bamberg, K., Sachs, G., and Geering, K. (1999). beta-subunit assembly is essential for the correct packing and the stable membrane insertion of the H,K-ATPase alpha-subunit. J. Biol. Chem. *274*, 8217–8223.

Belz, G.G., Breithaupt-Grögler, K., and Osowski, U. (2001). Treatment of congestive heart failure--current status of use of digitoxin. Eur. J. Clin. Invest. *31 Suppl 2*, 10–17.

Bikfalvi, A., Klein, S., Pintucci, G., and Rifkin, D.B. (1997). Biological Roles of Fibroblast Growth Factor-2. Endocrine Reviews *18*, 26–45.

Blanco, G., and Mercer, R.W. (1998). Isozymes of the Na-K-ATPase: heterogeneity in structure, diversity in function. Am. J. Physiol *275*, F633–650.

Blanco, G., Sánchez, G., and Mercer, R.W. (1995a). Comparison of the enzymatic properties of the Na,K-ATPase alpha 3 beta 1 and alpha 3 beta 2 isozymes. Biochemistry *34*, 9897–9903.

Blanco, G., Koster, J.C., Sánchez, G., and Mercer, R.W. (1995b). Kinetic properties of the alpha 2 beta 1 and alpha 2 beta 2 isozymes of the Na,K-ATPase. Biochemistry *34*, 319–325.

Blobel, G., and Dobberstein, B. (1975). Transfer of proteins across membranes. I. Presence of proteolytically processed and unprocessed nascent immunoglobulin light chains on membrane-bound ribosomes of murine myeloma. J Cell Biol *67*, 835–851.

Bonaldi, T., Talamo, F., Scaffidi, P., Ferrera, D., Porto, A., Bachi, A., Rubartelli, A., Agresti, A., and Bianchi, M.E. (2003). Monocytic cells hyperacetylate chromatin protein HMGB1 to redirect it towards secretion. EMBO J. *22*, 5551–5560.

Bossard, C., Laurell, H., Van den Berghe, L., Meunier, S., Zanibellato, C., and Prats, H. (2003). Translokin is an intracellular mediator of FGF-2 trafficking. Nat. Cell Biol *5*, 433–439.

Brodie, C., Bak, A., Shainberg, A., and Sampson, S.R. (1987). Role of Na-K ATPase in regulation of resting membrane potential of cultured rat skeletal myotubes. J. Cell. Physiol. *130*, 191–198.

Bublitz, M., Poulsen, H., Morth, J.P., and Nissen, P. (2010). In and out of the cation pumps: P-Type ATPase structure revisited. Curr Opin Struct Biol.

Bukau, B., and Horwich, A.L. (1998). The Hsp70 and Hsp60 chaperone machines. Cell *92*, 351–366.

Cao, Y., and Pettersson, R.F. (1993). Release and subcellular localization of acidic fibroblast growth factor expressed to high levels in HeLa cells. Growth Factors *8*, 277–290.

Ceccarelli, S., Visco, V., Raffa, S., Wakisaka, N., Pagano, J.S., and Torrisi, M.R. (2007). Epstein-Barr virus latent membrane protein 1 promotes concentration in multivesicular bodies of fibroblast growth factor 2 and its release through exosomes. Int. J. Cancer *121*, 1494–1506.

Chang, H.C., Samaniego, F., Nair, B.C., Buonaguro, L., and Ensoli, B. (1997). HIV-1 Tat protein exits from cells via a leaderless secretory pathway and binds to extracellular matrix-associated heparan sulfate proteoglycans through its basic region. AIDS *11*, 1421–1431.

Chen, P.X., Mathews, P.M., Good, P.J., Rossier, B.C., and Geering, K. (1998). Unusual degradation of alpha-beta complexes in Xenopus oocytes by beta-subunits of Xenopus gastric H-K-ATPase. Am. J. Physiol. *275*, C139–145.

Cheng, Y., and Prusoff, W.H. (1973). Relationship between the inhibition constant (K1) and the concentration of inhibitor which causes 50 per cent inhibition (I50) of an enzymatic reaction. Biochem. Pharmacol. *22*, 3099–3108.

Chow, D.C., and Forte, J.G. (1995). Functional significance of the beta-subunit for heterodimeric P-type ATPases. J. Exp. Biol. *198*, 1–17.

Clausen, T. (2003). Na+-K+ pump regulation and skeletal muscle contractility. Physiol. Rev. *83*, 1269–1324.

Contreras, R.G., Flores-Beni Tez, D., Flores-Maldonado, C., Larre, I., Shoshani, L., and Cereijido, M. (2006). Na+,K+-ATPase and hormone ouabain:new roles for an old enzyme and an old inhibitor. Cell. Mol. Biol. (Noisy-Le-Grand) *52*, 31–40.

Cook, J.S., Tate, E.H., and Shaffer, C. (1982). Uptake of [3H]ouabain from the cell surface into the lysosomal compartment of HeLa cells. J. Cell. Physiol. *110*, 84–92.

Corsi, A.K., and Schekman, R. (1996). Mechanism of polypeptide translocation into the endoplasmic reticulum. J. Biol. Chem. *271*, 30299–30302.

Crambert, G., Hasler, U., Beggah, A.T., Yu, C., Modyanov, N.N., Horisberger, J.D., Lelièvre, L., and Geering, K. (2000). Transport and pharmacological properties of nine different human Na, K-ATPase isozymes. J. Biol. Chem. *275*, 1976–1986.

Crambert, G., Fuzesi, M., Garty, H., Karlish, S., and Geering, K. (2002). Phospholemman (FXYD1) associates with Na,K-ATPase and regulates its transport properties. Proc. Natl. Acad. Sci. U.S.A. *99*, 11476–11481.

Dahl, J.P., Binda, A., Canfield, V.A., and Levenson, R. (2000). Participation of Na,K-ATPase in FGF-2 secretion: rescue of ouabain-inhibitable FGF-2 secretion by ouabain-resistant Na,K-ATPase alpha subunits. Biochemistry *39*, 14877–14883.

Dalbey, R.E., and von Heijne, G. (1992). Signal peptidases in prokaryotes and eukaryotes - a new protease family. Trends in Biochemical Sciences *17*, 474–478.

Denny, P.W., Gokool, S., Russell, D.G., Field, M.C., and Smith, D.F. (2000). Acylation-dependent protein export in Leishmania. J. Biol. Chem. *275*, 11017–11025.

Deora, A.B., Kreitzer, G., Jacovina, A.T., and Hajjar, K.A. (2004). An annexin 2 phosphorylation switch mediates p11-dependent translocation of annexin 2 to the cell surface. J. Biol. Chem. *279*, 43411–43418.

DIEFENBACH, W.C., and MENEELY, J.K., Jr (1949). Digitoxin; a critical review. Yale J Biol Med *21*, 421–431.

Dupont, N., Jiang, S., Pilli, M., Ornatowski, W., Bhattacharya, D., and Deretic, V. (2011). Autophagy-based unconventional secretory pathway for extracellular delivery of IL-1β. EMBO J. *30*, 4701–4711.

Ebert, A.D., Laussmann, M., Wegehingel, S., Kaderali, L., Erfle, H., Reichert, J., Lechner, J., Beer, H.-D., Pepperkok, R., and Nickel, W. (2010). Tec-kinase-mediated phosphorylation of fibroblast growth factor 2 is essential for unconventional secretion. Traffic *11*, 813–826.

Ellgaard, L., and Helenius, A. (2001). ER quality control: towards an understanding at the molecular level. Curr. Opin. Cell Biol. *13*, 431–437.

Ellgaard, L., and Helenius, A. (2003). Quality control in the endoplasmic reticulum. Nat. Rev. Mol. Cell Biol. *4*, 181–191.

Engleka, K.A., and Maciag, T. (1992). Inactivation of human fibroblast growth factor-1 (FGF-1) activity by interaction with copper ions involves FGF-1 dimer formation induced by copper-catalyzed oxidation. J. Biol. Chem. *267*, 11307–11315.

Engling, A., Backhaus, R., Stegmayer, C., Zehe, C., Seelenmeyer, C., Kehlenbach, A., Schwappach, B., Wegehingel, S., and Nickel, W. (2002). Biosynthetic FGF-2 is targeted to non-lipid raft microdomains following translocation to the extracellular surface of CHO cells. J. Cell. Sci *115*, 3619–3631.

Ensoli, B., Barillari, G., Salahuddin, S.Z., Gallo, R.C., and Wong-Staal, F. (1990). Tat protein of HIV-1 stimulates growth of cells derived from Kaposi's sarcoma lesions of AIDS patients. Nature *345*, 84–86.

Eriksson, A.E., Cousens, L.S., Weaver, L.H., and Matthews, B.W. (1991). Three-dimensional structure of human basic fibroblast growth factor. Proc. Natl. Acad. Sci. U.S.A. *88*, 3441–3445.

Eriksson, A.E., Cousens, L.S., and Matthews, B.W. (1993). Refinement of the structure of human basic fibroblast growth factor at 1.6 A resolution and analysis of presumed heparin binding sites by selenate substitution. Protein Sci. *2*, 1274–1284.

Faham, S., Hileman, R.E., Fromm, J.R., Linhardt, R.J., and Rees, D.C. (1996). Heparin structure and interactions with basic fibroblast growth factor. Science *271*, 1116–1120.

Farr, G.A., Hull, M., Mellman, I., and Caplan, M.J. (2009). Membrane proteins follow multiple pathways to the basolateral cell surface in polarized epithelial cells. J. Cell Biol. *186*, 269–282.

Florkiewicz, R.Z., Majack, R.A., Buechler, R.D., and Florkiewicz, E. (1995a). Quantitative export of FGF-2 occurs through an alternative, energy-dependent, non-ER/Golgi pathway. J. Cell. Physiol *162*, 388–399.

Florkiewicz, R.Z., Majack, R.A., Buechler, R.D., and Florkiewicz, E. (1995b). Quantitative export of FGF-2 occurs through an alternative, energy-dependent, non-ER/Golgi pathway. J. Cell. Physiol *162*, 388–399.

Florkiewicz, R.Z., Anchin, J., and Baird, A. (1998). The inhibition of fibroblast growth factor-2 export by cardenolides implies a novel function for the catalytic subunit of Na+,K+-ATPase. J. Biol. Chem *273*, 544–551.

Freedman, R.B. (1995). The formation of protein disulphide bonds. Curr. Opin. Struct. Biol. *5*, 85–91.

Gardella, S., Andrei, C., Ferrera, D., Lotti, L.V., Torrisi, M.R., Bianchi, M.E., and Rubartelli, A. (2002). The nuclear protein HMGB1 is secreted by monocytes via a non-classical, vesicle-mediated secretory pathway. EMBO Rep. *3*, 995–1001.

Gee, H.Y., Noh, S.H., Tang, B.L., Kim, K.H., and Lee, M.G. (2011). Rescue of ΔF508-CFTR trafficking via a GRASP-dependent unconventional secretion pathway. Cell *146*, 746–760.

Geering, K. (2005). Function of FXYD proteins, regulators of Na, K-ATPase. J. Bioenerg. Biomembr. *37*, 387–392.

George, C.H., Kendall, J.M., and Evans, W.H. (1999). Intracellular trafficking pathways in the assembly of connexins into gap junctions. J. Biol. Chem. *274*, 8678–8685.

Gheorghiade, M., van Veldhuisen, D.J., and Colucci, W.S. (2006). Contemporary use of digoxin in the management of cardiovascular disorders. Circulation *113*, 2556–2564.

Giordano, S., Sherman, L., Lyman, W., and Morrison, R. (1992). Multiple molecular weight forms of basic fibroblast growth factor are developmentally regulated in the central nervous system. Dev. Biol. *152*, 293–303.

Görlich, D., Prehn, S., Hartmann, E., Kalies, K.U., and Rapoport, T.A. (1992). A mammalian homolog of SEC61p and SECYp is associated with ribosomes and nascent polypeptides during translocation. Cell *71*, 489–503.

Graziani, I., Doyle, A., Sterling, S., Kirov, A., Tarantini, F., Landriscina, M., Kumar, T.K.S., Neivandt, D., and Prudovsky, I. (2009). Protein folding does not prevent the nonclassical export of FGF1 and S100A13. Biochem. Biophys. Res. Commun *381*, 350–354.

Grieve, A.G., and Rabouille, C. (2011). Golgi bypass: skirting around the heart of classical secretion. Cold Spring Harb Perspect Biol *3*.

Haas, M., Wang, H., Tian, J., and Xie, Z. (2002). Src-mediated inter-receptor cross-talk between the Na+/K+-ATPase and the epidermal growth factor receptor relays the signal from ouabain to mitogen-activated protein kinases. J. Biol. Chem *277*, 18694–18702.

Hamlyn, J.M., Blaustein, M.P., Bova, S., DuCharme, D.W., Harris, D.W., Mandel, F., Mathews, W.R., and Ludens, J.H. (1991). Identification and characterization of a ouabain-like compound from human plasma. Proc. Natl. Acad. Sci. U.S.A. *88*, 6259–6263.

Hasler, U., Crambert, G., Horisberger, J.D., and Geering, K. (2001). Structural and functional features of the transmembrane domain of the Na,K-ATPase beta subunit revealed by tryptophan scanning. J. Biol. Chem. *276*, 16356–16364.

Hieber, V., Siegel, G.J., Fink, D.J., Beaty, M.W., and Mata, M. (1991). Differential distribution of (Na, K)-ATPase alpha isoforms in the central nervous system. Cell. Mol. Neurobiol. *11*, 253–262.

Hundal, H.S., Marette, A., Mitsumoto, Y., Ramlal, T., Blostein, R., and Klip, A. (1992). Insulin induces translocation of the alpha 2 and beta 1 subunits of the Na+/K(+)-ATPase from intracellular compartments to the plasma membrane in mammalian skeletal muscle. J. Biol. Chem. *267*, 5040–5043.

Jackson, A., Tarantini, F., Gamble, S., Friedman, S., and Maciag, T. (1995). The release of fibroblast growth factor-1 from NIH 3T3 cells in response to temperature involves the function of cysteine residues. J. Biol. Chem. *270*, 33–36.

Kaplan, J.H. (2002). Biochemistry of Na,K-ATPase. Annu. Rev. Biochem. *71*, 511–535.

Kastrup, J.S., Eriksson, E.S., Dalbøge, H., and Flodgaard, H. (1997). X-ray structure of the 154-amino-acid form of recombinant human basic fibroblast growth factor. comparison with the truncated 146-amino-acid form. Acta Crystallogr. D Biol. Crystallogr. *53*, 160–168.

Keller, M., Rüegg, A., Werner, S., and Beer, H.-D. (2008). Active caspase-1 is a regulator of unconventional protein secretion. Cell *132*, 818–831.

Kockskämper, J., Gisselmann, G., and Glitsch, H.G. (1997). Comparison of ouabain-sensitive and -insensitive Na/K pumps in HEK293 cells. Biochim. Biophys. Acta *1325*, 197–208.

Landriscina, M., Bagalá, C., Mandinova, A., Soldi, R., Micucci, I., Bellum, S., Prudovsky, I., and Maciag, T. (2001). Copper induces the assembly of a multiprotein aggregate implicated in the release of fibroblast growth factor 1 in response to stress. J. Biol. Chem. *276*, 25549–25557.

Langer, G.A. (1977). Relationship between myocardial contractility and the effects of digitalis on ionic exchange. Fed. Proc. *36*, 2231–2234.

Lavoie, L., Levenson, R., Martin-Vasallo, P., and Klip, A. (1997). The molar ratios of alpha and beta subunits of the Na+-K+-ATPase differ in distinct subcellular membranes from rat skeletal muscle. Biochemistry *36*, 7726–7732.

Lee, M.C.S., Miller, E.A., Goldberg, J., Orci, L., and Schekman, R. (2004). Bi-directional protein transport between the ER and Golgi. Annu. Rev. Cell Dev. Biol. *20*, 87–123.

Lemas, M.V., Hamrick, M., Takeyasu, K., and Fambrough, D.M. (1994). 26 amino acids of an extracellular domain of the Na,K-ATPase alpha-subunit are sufficient for assembly with the Na,K-ATPase beta-subunit. J. Biol. Chem. *269*, 8255–8259.

Liang, M., Cai, T., Tian, J., Qu, W., and Xie, Z.-J. (2006). Functional characterization of Src-interacting Na/K-ATPase using RNA interference assay. J. Biol. Chem *281*, 19709–19719.

Liang, M., Tian, J., Liu, L., Pierre, S., Liu, J., Shapiro, J., and Xie, Z.-J. (2007). Identification of a pool of non-pumping Na/K-ATPase. J. Biol. Chem *282*, 10585–10593.

Lippincott-Schwartz, J., Yuan, L.C., Bonifacino, J.S., and Klausner, R.D. (1989). Rapid redistribution of Golgi proteins into the ER in cells treated with brefeldin A: evidence for membrane cycling from Golgi to ER. Cell *56*, 801–813.

Liu, J., and Shapiro, J.I. (2007). Regulation of sodium pump endocytosis by cardiotonic steroids: Molecular mechanisms and physiological implications. Pathophysiology *14*, 171–181.

Liu, J., Liang, M., Liu, L., Malhotra, D., Xie, Z., and Shapiro, J.I. (2005). Ouabain-induced endocytosis of the plasmalemmal Na/K-ATPase in LLC-PK1 cells requires caveolin-1. Kidney Int. *67*, 1844–1854.

Lopez-Castejon, G., and Brough, D. (2011). Understanding the mechanism of IL-1β secretion. Cytokine Growth Factor Rev. *22*, 189–195.

Lutsenko, S., and Kaplan, J.H. (1993). An essential role for the extracellular domain of the Na,K-ATPase beta-subunit in cation occlusion. Biochemistry *32*, 6737–6743.

Lytton, J. (1985). Insulin affects the sodium affinity of the rat adipocyte (Na+,K+)-ATPase. J. Biol. Chem. *260*, 10075–10080.

Maclean, L.M., O'Toole, P.J., Stark, M., Marrison, J., Seelenmeyer, C., Nickel, W., and Smith, D.F. (2012). Trafficking and release of Leishmania metacyclic HASPB on macrophage invasion. Cell. Microbiol. *14*, 740–761.

Malik, N., Canfield, V.A., Beckers, M.C., Gros, P., and Levenson, R. (1996). Identification of the mammalian Na,K-ATPase 3 subunit. J. Biol. Chem. *271*, 22754–22758.

McGrail, K.M., Phillips, J.M., and Sweadner, K.J. (1991). Immunofluorescent localization of three Na,K-ATPase isozymes in the rat central nervous system: both neurons and glia can express more than one Na,K-ATPase. J. Neurosci. *11*, 381–391.

McNeil, P.L., Muthukrishnan, L., Warder, E., and D'Amore, P.A. (1989). Growth factors are released by mechanically wounded endothelial cells. J. Cell Biol. *109*, 811–822.

Meunier, S., Navarro, M.G.-J., Bossard, C., Laurell, H., Touriol, C., Lacazette, E., and Prats, H. (2009). Pivotal role of translokin/CEP57 in the unconventional secretion versus nuclear translocation of FGF2. Traffic *10*, 1765–1772.

Mignatti, P., Morimoto, T., and Rifkin, D.B. (1992). Basic fibroblast growth factor, a protein devoid of secretory signal sequence, is released by cells via a pathway independent of the endoplasmic reticulum-Golgi complex. J. Cell. Physiol. *151*, 81–93.

Mohan, S.K., Rani, S.G., and Yu, C. (2010). The heterohexameric complex structure, a component in the non-classical pathway for fibroblast growth factor 1 (FGF1) secretion. J. Biol. Chem *285*, 15464–15475.

Morth, J.P., Pedersen, B.P., Buch-Pedersen, M.J., Andersen, J.P., Vilsen, B., Palmgren, M.G., and Nissen, P. (2011). A structural overview of the plasma membrane Na+,K+-ATPase and H+-ATPase ion pumps. Nat. Rev. Mol. Cell Biol. *12*, 60–70.

Möskes, C., Burghaus, P.A., Wernli, B., Sauder, U., Dürrenberger, M., and Kappes, B. (2004). Export of Plasmodium falciparum calcium-dependent protein kinase 1 to the parasitophorous vacuole is dependent on three N-terminal membrane anchor motifs. Mol. Microbiol. *54*, 676–691.

Mouta Carreira, C., Landriscina, M., Bellum, S., Prudovsky, I., and Maciag, T. (2001). The comparative release of FGF1 by hypoxia and temperature stress. Growth Factors *18*, 277–285.

Moy, F.J., Seddon, A.P., Böhlen, P., and Powers, R. (1996). High-resolution solution structure of basic fibroblast growth factor determined by multidimensional heteronuclear magnetic resonance spectroscopy. Biochemistry *35*, 13552–13561.

Muesch, A., Hartmann, E., Rohde, K., Rubartelli, A., Sitia, R., and Rapoport, T.A. (1990). A novel pathway for secretory proteins? Trends Biochem. Sci. *15*, 86–88.

Murakami, M., and Simons, M. (2008). Fibroblast growth factor regulation of neovascularization. Curr. Opin. Hematol *15*, 215–220.

Muth, T.R., Dunbar, L.A., Cortois-Coutry, N., Roush, D.L., and Caplan, M.J. (1997). Sorting and trafficking of ion transport proteins in polarized epithelial cells. Curr. Opin. Nephrol. Hypertens. *6*, 455–459.

Neufeld, G., Mitchell, R., Ponte, P., and Gospodarowicz, D. (1988). Expression of human basic fibroblast growth factor cDNA in baby hamster kidney-derived cells results in autonomous cell growth. J. Cell Biol. *106*, 1385–1394.

Neupert, W., and Herrmann, J.M. (2007). Translocation of proteins into mitochondria. Annu. Rev. Biochem. *76*, 723–749.

Nickel, W. (2005). Unconventional Secretory Routes: Direct Protein Export Across the Plasma Membrane of Mammalian Cells. Traffic *6*, 607–614.

Nickel, W. (2007). Unconventional secretion: an extracellular trap for export of fibroblast growth factor 2. J. Cell. Sci *120*, 2295–2299.

Nickel, W. (2010). Pathways of unconventional protein secretion. Curr. Opin. Biotechnol. *21*, 621–626.

Nickel, W., and Rabouille, C. (2009). Mechanisms of regulated unconventional protein secretion. Nat. Rev. Mol. Cell Biol *10*, 148–155.

Nickel, W., and Wieland, F.T. (1998). Biosynthetic protein transport through the early secretory pathway. Histochem. Cell Biol. *109*, 477–486.

Nickel, W., Tournaviti, S., Pietro, E.S., Terjung, S., Schafmeier, T., Wegehingel, S., Ritzerfeld, J., Schulz, J., Smith, D.F., and Pepperkok, R. (2009). Reversible phosphorylation as a molecular switch to regulate plasma membrane targeting of acylated SH4 domain proteins. Traffic *10*, 1047–1060.

Noguchi, S., Mishina, M., Kawamura, M., and Numa, S. (1987). Expression of functional (Na+ + K+)-ATPase from cloned cDNAs. FEBS Lett. *225*, 27–32.

Noguchi, S., Mutoh, Y., and Kawamura, M. (1994). The functional roles of disulfide bonds in the beta-subunit of (Na,K)ATPase as studied by site-directed mutagenesis. FEBS Lett. *341*, 233–238.

Núñez-Durán, H., Riboni, L., Ubaldo, E., Kabela, E., and Bárcenas-Ruiz, L. (1988). Ouabain uptake by endocytosis in isolated guinea pig atria. Am. J. Physiol. *255*, C479–485.

Okamura, H., Yasuhara, J.C., Fambrough, D.M., and Takeyasu, K. (2003). P-type ATPases in Caenorhabditis and Drosophila: implications for evolution of the P-type ATPase subunit families with special reference to the Na,K-ATPase and H,K-ATPase subgroup. J. Membr. Biol. *191*, 13–24.

Olesen, C., Picard, M., Winther, A.-M.L., Gyrup, C., Morth, J.P., Oxvig, C., Møller, J.V., and Nissen, P. (2007). The structural basis of calcium transport by the calcium pump. Nature *450*, 1036–1042.

Ornitz, D.M., and Itoh, N. (2001). Fibroblast growth factors. Genome Biol. *2*, REVIEWS3005.

Palasis, M., Kuntzweiler, T.A., Argüello, J.M., and Lingrel, J.B. (1996). Ouabain interactions with the H5-H6 hairpin of the Na,K-ATPase reveal a possible inhibition mechanism via the cation binding domain. J. Biol. Chem. *271*, 14176–14182.

Peng, L., Martin-Vasallo, P., and Sweadner, K.J. (1997). Isoforms of Na,K-ATPase alpha and beta subunits in the rat cerebellum and in granule cell cultures. J. Neurosci. *17*, 3488–3502.

Penuela, S., Bhalla, R., Gong, X.-Q., Cowan, K.N., Celetti, S.J., Cowan, B.J., Bai, D., Shao, Q., and Laird, D.W. (2007). Pannexin 1 and pannexin 3 are glycoproteins that exhibit many distinct characteristics from the connexin family of gap junction proteins. J. Cell. Sci. *120*, 3772–3783.

Pestov, N.B., Adams, G., Shakhparonov, M.I., and Modyanov, N.N. (1999). Identification of a novel gene of the X,K-ATPase beta-subunit family that is predominantly expressed in skeletal and heart muscles. FEBS Lett. *456*, 243–248.

Pike, L.J. (2008). The challenge of lipid rafts. The Journal of Lipid Research *50*, S323–S328.

Poulsen, L.R., López-Marqués, R.L., McDowell, S.C., Okkeri, J., Licht, D., Schulz, A., Pomorski, T., Harper, J.F., and Palmgren, M.G. (2008). The Arabidopsis P4-ATPase ALA3 localizes to the golgi and requires a beta-subunit to function in lipid translocation and secretory vesicle formation. Plant Cell *20*, 658–676.

Presta, M., Dell'Era, P., Mitola, S., Moroni, E., Ronca, R., and Rusnati, M. (2005). Fibroblast growth factor/fibroblast growth factor receptor system in angiogenesis. Cytokine Growth Factor Rev. *16*, 159–178.

Prudovsky, I., Tarantini, F., Landriscina, M., Neivandt, D., Soldi, R., Kirov, A., Small, D., Kathir, K.M., Rajalingam, D., and Kumar, T.K.S. (2008). Secretion without Golgi. J. Cell. Biochem *103*, 1327–1343.

Prudovsky, I., Kumar, T.K.S., Sterling, S., and Neivandt, D. (2013). Protein-phospholipid interactions in nonclassical protein secretion: problem and methods of study. Int J Mol Sci *14*, 3734–3772.

Qian, S., Wang, W., Yang, L., and Huang, H.W. (2008). Structure of transmembrane pore induced by Bax-derived peptide: evidence for lipidic pores. Proc. Natl. Acad. Sci. U.S.A. *105*, 17379–17383.

Qu, C., Gardner, P., and Schrijver, I. (2009). The role of the cytoskeleton in the formation of gap junctions by Connexin 30. Exp. Cell Res. *315*, 1683–1692.

Rabouille, C., Malhotra, V., and Nickel, W. (2012). Diversity in unconventional protein secretion. J. Cell. Sci. *125*, 5251–5255.

Ramirez-Ortega, M., Maldonado-Lagunas, V., Melendez-Zajgla, J., Carrillo-Hernandez, J.F., Pastelín-Hernandez, G., Picazo-Picazo, O., and Ceballos-Reyes, G. (2006). Proliferation and apoptosis of HeLa cells induced by in vitro stimulation with digitalis. Eur. J. Pharmacol. *534*, 71–76.

Rapoport, T.A. (1992). Transport of proteins across the endoplasmic reticulum membrane. Science *258*, 931–936.

Rayne, F., Debaisieux, S., Yezid, H., Lin, Y.-L., Mettling, C., Konate, K., Chazal, N., Arold, S.T., Pugnière, M., Sanchez, F., et al. (2010a). Phosphatidylinositol-(4,5)-bisphosphate enables efficient secretion of HIV-1 Tat by infected T-cells. EMBO J *29*, 1348–1362.

Rayne, F., Debaisieux, S., Bonhoure, A., and Beaumelle, B. (2010b). HIV-1 Tat is unconventionally secreted through the plasma membrane. Cell Biol. Int *34*, 409–413.

Renko, M., Quarto, N., Morimoto, T., and Rifkin, D.B. (1990). Nuclear and cytoplasmic localization of different basic fibroblast growth factor species. J. Cell. Physiol. *144*, 108–114.

Rescher, U., and Gerke, V. (2008). S100A10/p11: family, friends and functions. Pflugers Arch. *455*, 575–582.

Sáez, A.G., Lozano, E., and Zaldívar-Riverón, A. (2009). Evolutionary history of Na,K-ATPases and their osmoregulatory role. Genetica *136*, 479–490.

Salm, F., Cwiek, P., Ghosal, A., Lucia Buccarello, A., Largey, F., Wotzkow, C., Höland, K., Styp-Rekowska, B., Djonov, V., Zlobec, I., et al. (2013). RNA interference screening identifies a novel role for autocrine fibroblast growth factor signaling in neuroblastoma chemoresistance. Oncogene *32*, 3944–3953.

Sasada, R., Kurokawa, T., Iwane, M., and Igarashi, K. (1988). Transformation of mouse BALB/c 3T3 cells with human basic fibroblast growth factor cDNA. Mol. Cell. Biol. *8*, 588–594.

Sato, Y., and Rifkin, D.B. (1988). Autocrine activities of basic fibroblast growth factor: regulation of endothelial cell movement, plasminogen activator synthesis, and DNA synthesis. J. Cell Biol. *107*, 1199–1205.

Scarborough, G.A. (1999). Structure and function of the P-type ATPases. Curr. Opin. Cell Biol. *11*, 517–522.

Schaeffer, E.M., and Schwartzberg, P.L. (2000). Tec family kinases in lymphocyte signaling and function. Curr. Opin. Immunol. *12*, 282–288.

Schäfer, T., Zentgraf, H., Zehe, C., Brügger, B., Bernhagen, J., and Nickel, W. (2004a). Unconventional secretion of fibroblast growth factor 2 is mediated by direct translocation across the plasma membrane of mammalian cells. J. Biol. Chem *279*, 6244–6251.

Schäfer, T., Zentgraf, H., Zehe, C., Brügger, B., Bernhagen, J., and Nickel, W. (2004b). Unconventional secretion of fibroblast growth factor 2 is mediated by direct translocation across the plasma membrane of mammalian cells. J. Biol. Chem *279*, 6244–6251.

Scheiner-Bobis, G., and Farley, R.A. (1994). Subunit requirements for expression of functional sodium pumps in yeast cells. Biochim. Biophys. Acta *1193*, 226–234.

Schiera, G., Proia, P., Alberti, C., Mineo, M., Savettieri, G., and Di Liegro, I. (2007). Neurons produce FGF2 and VEGF and secrete them at least in part by shedding extracellular vesicles. J. Cell. Mol. Med. *11*, 1384–1394.

Schlessinger, J., Plotnikov, A.N., Ibrahimi, O.A., Eliseenkova, A.V., Yeh, B.K., Yayon, A., Linhardt, R.J., and Mohammadi, M. (2000). Crystal structure of a ternary FGF-FGFR-heparin complex reveals a dual role for heparin in FGFR binding and dimerization. Mol. Cell *6*, 743–750.

Schoner, W., and Scheiner-Bobis, G. (2007). Endogenous and exogenous cardiac glycosides and their mechanisms of action. Am J Cardiovasc Drugs *7*, 173–189.

Schotman, H., Karhinen, L., and Rabouille, C. (2008). dGRASP-mediated noncanonical integrin secretion is required for Drosophila epithelial remodeling. Dev. Cell *14*, 171–182.

Schulz, J.T., and Cantley, L.C. (1988). CV-1 cell recipients of the mouse ouabain resistance gene express a ouabain-insensitive Na,K-ATPase after growth in cardioactive steroids. J. Biol. Chem. *263*, 624–632.

Schweigerer, L., Neufeld, G., Friedman, J., Abraham, J.A., Fiddes, J.C., and Gospodarowicz, D. (1987). Capillary endothelial cells express basic fibroblast growth factor, a mitogen that promotes their own growth. Nature *325*, 257–259.

Seelenmeyer, C., Stegmayer, C., and Nickel, W. (2008). Unconventional secretion of fibroblast growth factor 2 and galectin-1 does not require shedding of plasma membrane-derived vesicles. FEBS Lett *582*, 1362–1368.

Seghezzi, G., Patel, S., Ren, C.J., Gualandris, A., Pintucci, G., Robbins, E.S., Shapiro, R.L., Galloway, A.C., Rifkin, D.B., and Mignatti, P. (1998). Fibroblast growth factor-2 (FGF-2) induces vascular endothelial growth factor (VEGF) expression in the endothelial cells of forming capillaries: an autocrine mechanism contributing to angiogenesis. J. Cell Biol. *141*, 1659–1673.

Shamraj, O.I., and Lingrel, J.B. (1994). A putative fourth Na+,K(+)-ATPase alpha-subunit gene is expressed in testis. Proc. Natl. Acad. Sci. U.S.A. *91*, 12952–12956.

Shao, S., and Hegde, R.S. (2011). Membrane protein insertion at the endoplasmic reticulum. Annu. Rev. Cell Dev. Biol. *27*, 25–56.

Sheng, Z., Lewis, J.A., and Chirico, W.J. (2004). Nuclear and nucleolar localization of 18-kDa fibroblast growth factor-2 is controlled by C-terminal signals. J. Biol. Chem *279*, 40153–40160.

Shin, J.T., Opalenik, S.R., Wehby, J.N., Mahesh, V.K., Jackson, A., Tarantini, F., Maciag, T., and Thompson, J.A. (1996). Serum-starvation induces the extracellular appearance of FGF-1. Biochim. Biophys. Acta *1312*, 27–38.

SKOU, J.C. (1957). The influence of some cations on an adenosine triphosphatase from peripheral nerves. Biochim. Biophys. Acta *23*, 394–401.

Stegmayer, C., Kehlenbach, A., Tournaviti, S., Wegehingel, S., Zehe, C., Denny, P., Smith, D.F., Schwappach, B., and Nickel, W. (2005). Direct transport across the plasma membrane of mammalian cells of Leishmania HASPB as revealed by a CHO export mutant. J. Cell. Sci *118*, 517–527.

Steringer, J.P., Bleicken, S., Andreas, H., Zacherl, S., Laussmann, M., Temmerman, K., Contreras, F.X., Bharat, T.A.M., Lechner, J., Muller, H.-M., et al. (2012). PI(4,5)P2 Dependent Oligomerization of Fibroblast Growth Factor 2 (FGF2) Triggers the Formation of a Lipidic Membrane Pore Implicated in Unconventional Secretion. The Journal of Biological Chemistry.

Sweadner, K.J., and Rael, E. (2000). The FXYD gene family of small ion transport regulators or channels: cDNA sequence, protein signature sequence, and expression. Genomics *68*, 41–56.

Tang, X., Halleck, M.S., Schlegel, R.A., and Williamson, P. (1996). A subfamily of P-type ATPases with aminophospholipid transporting activity. Science *272*, 1495–1497.

Taverna, S., Ghersi, G., Ginestra, A., Rigogliuso, S., Pecorella, S., Alaimo, G., Saladino, F., Dolo, V., Dell'Era, P., Pavan, A., et al. (2003). Shedding of membrane vesicles mediates fibroblast growth factor-2 release from cells. J. Biol. Chem. *278*, 51911–51919.

Taxis, C., Vogel, F., and Wolf, D.H. (2002). ER-golgi traffic is a prerequisite for efficient ER degradation. Mol. Biol. Cell *13*, 1806–1818.

Temmerman, K., Ebert, A.D., Müller, H.-M., Sinning, I., Tews, I., and Nickel, W. (2008). A direct role for phosphatidylinositol-4,5-bisphosphate in unconventional secretion of fibroblast growth factor 2. Traffic *9*, 1204–1217.

Tokhtaeva, E., Clifford, R.J., Kaplan, J.H., Sachs, G., and Vagin, O. (2012). Subunit isoform selectivity in assembly of Na,K-ATPase α-β heterodimers. J. Biol. Chem. *287*, 26115–26125.

Torrado, L.C., Temmerman, K., Müller, H.-M., Mayer, M.P., Seelenmeyer, C., Backhaus, R., and Nickel, W. (2009). An intrinsic quality-control mechanism ensures unconventional secretion of fibroblast growth factor 2 in a folded conformation. J. Cell. Sci *122*, 3322–3329.

Trudel, C., Faure-Desire, V., Florkiewicz, R.Z., and Baird, A. (2000). Translocation of FGF2 to the cell surface without release into conditioned media. J. Cell. Physiol *185*, 260–268.

Turner, N., and Grose, R. (2010). Fibroblast growth factor signalling: from development to cancer. Nat Rev Cancer *10*, 116–129.

Vescovi, A.L., Reynolds, B.A., Fraser, D.D., and Weiss, S. (1993). bFGF regulates the proliferative fate of unipotent (neuronal) and bipotent (neuronal/astroglial) EGF-generated CNS progenitor cells. Neuron *11*, 951–966.

Walter, P., Ibrahimi, I., and Blobel, G. (1981). Translocation of proteins across the endoplasmic reticulum. I. Signal recognition protein (SRP) binds to in-vitro-assembled polysomes synthesizing secretory protein. J. Cell Biol. *91*, 545–550.

Wang, Y., and Becker, D. (1997). Antisense targeting of basic fibroblast growth factor and fibroblast growth factor receptor-1 in human melanomas blocks intratumoral angiogenesis and tumor growth. Nat. Med. *3*, 887–893.

Xie, Z., and Cai, T. (2003). Na+-K+--ATPase-mediated signal transduction: from protein interaction to cellular function. Mol. Interv *3*, 157–168.

Yezid, H., Konate, K., Debaisieux, S., Bonhoure, A., and Beaumelle, B. (2009). Mechanism for HIV-1 Tat insertion into the endosome membrane. J. Biol. Chem. *284*, 22736–22746.

Yoo, J.-S., Moyer, B.D., Bannykh, S., Yoo, H.-M., Riordan, J.R., and Balch, W.E. (2002). Non-conventional trafficking of the cystic fibrosis transmembrane conductance regulator through the early secretory pathway. J. Biol. Chem. *277*, 11401–11409.

Yoshimura, S.H., Iwasaka, S., Schwarz, W., and Takeyasu, K. (2008). Fast degradation of the auxiliary subunit of Na+/K+-ATPase in the plasma membrane of HeLa cells. J. Cell. Sci *121*, 2159–2168.

Young, T.S., Ahmad, I., Yin, J.A., and Schultz, P.G. (2010). An enhanced system for unnatural amino acid mutagenesis in E. coli. J. Mol. Biol. *395*, 361–374.

Zahler, R., Brines, M., Kashgarian, M., Benz, E.J., Jr, and Gilmore-Hebert, M. (1992). The cardiac conduction system in the rat expresses the alpha 2 and alpha 3 isoforms of the Na+,K(+)-ATPase. Proc. Natl. Acad. Sci. U.S.A. *89*, 99–103.

Zamofing, D., Rossier, B.C., and Geering, K. (1988). Role of the Na,K-ATPase beta-subunit in the cellular accumulation and maturation of the enzyme as assessed by glycosylation inhibitors. J. Membr. Biol. *104*, 69–79.

Zehe, C., Engling, A., Wegehingel, S., Schäfer, T., and Nickel, W. (2006). Cell-surface heparan sulfate proteoglycans are essential components of the unconventional export machinery of FGF-2. Proc. Natl. Acad. Sci. U.S.A *103*, 15479–15484.

Zhang, J., Lee, M.Y., Cavalli, M., Chen, L., Berra-Romani, R., Balke, C.W., Bianchi, G., Ferrari, P., Hamlyn, J.M., Iwamoto, T., et al. (2005). Sodium pump alpha2 subunits control myogenic tone and blood pressure in mice. J. Physiol. (Lond.) *569*, 243–256.

Zhang, J.D., Cousens, L.S., Barr, P.J., and Sprang, S.R. (1991). Three-dimensional structure of human basic fibroblast growth factor, a structural homolog of interleukin 1 beta. Proc. Natl. Acad. Sci. U.S.A. *88*, 3446–3450.

Zhu, X., Komiya, H., Chirino, A., Faham, S., Fox, G.M., Arakawa, T., Hsu, B.T., and Rees, D.C. (1991). Three-dimensional structures of acidic and basic fibroblast growth factors. Science *251*, 90–93.

6 Appendix

6.1 Abbreviations

%	percent
°C	degree Celsius
3’	three prime
5’	five prime
α	alpha
β	beta
A	alanine
ABC-transporter	ATP-binding cassette-transporters
Acb1	acyl-CoA-binding protein
A-domain	actuator domain
ADP	adenosine diphosphate
APC	allophycocyanin
ArfI	ADP-ribosylation factor (small GTPase)
ATP	adenosine triphosphate
ATP1A1	α-subunit isoform 1, of the Na^+/K^+-ATPase
ATPase	adenosine triphosphatase
B	bound
BCA	bicinchoninic acid
BFA	brefeldin A
bp	base pairs
BSA	bovine serum albumin
Ca^{2+}	calcium ion
cAMP	cyclic adenosine monophosphate
cDNA	complementary deoxyribonucleic acid
CFTR	cystic fibrosis transmembrane conductance regulator
CGN	*cis*-Golgi network
CHO	chinese hamster ovary
cm	centimeter
CMV	cytomegalovirus
CO_2	carbon dioxide
CoA	coenzyme A
COP	coat protein
C-terminal	carboxy-terminal
CUPS	compartments for unconventional protein secretion

CV	column volumes
D	aspartate
D_2O	deuterated water
Da	dalton
DMEM	Dulbecco's modified eagle medium
DMSO	dimethyl sulphoxide
DNA	deoxyribonucleic acid
dNTPs	desoxyribonucleotide triphosphatedox
dox	doxycycline
DTT	1,4-Dithio-D,L-threitol
E. coli	*Escherichia coli*
EDTA	ethylenediaminetetraacetic acid
en route	on the way
ER	endoplasmic reticulum
ERAD	ER-associated degradation
ESCRT	endosomal sorting complex
et al.	*at alii* (and others)
EtBr	ethidium bromide
f	femto
FACS	fluorescence-activated cell sorting
FCS	fetal calf serum
FGF	fibroblast growth factor
FGFR	fibroblast growth factor receptor
g	gram
GAPDH	glyceraldehyde 3-phosphate dehydrogenase
GFP	green fluorescent protein
GRASP	Golgi reassembly and stacking protein
GST	glutathione-s-transferase
GTP	guanosine triphosphate
h	hour
H^+	proton
HEK	human embryonic kidney
HeLa	Henrietta Lacks (human epithelial cell line derived from cervical cancer cells)
HeLa S3	derivate of HeLa cell line
HIV-1	human immunodeficiency virus type 1
HMW	high molecular weight
HSPGs	heparan sulfate proteoglycans
IPTG	isopropyl β-D-1-thiogalactopyranoside

IRES	internal ribosome entry site
k	kilo
K	lysine
K^+	potassium ion
kb	kilobase
kDa	kilodalton
KCl	potassium chloride
KH_2PO_4	potassium dihydrogen phosphate (KH_2PO_4)
l	liter
LB	lysogeny broth
LMW	low molecular weight
LTRs	long terminal repeats
m	milli
M	molar
m/z	mass-to-charge ratio
MCAT / MT	murine cationic amino acid transporter
MDCK	Madin Darby canine kidney
$MgCl_2$	magnesium chloride
min	minutes
mRNA	messenger RNA
n	nano
N	asparagine
Na^+	sodium ion
N-domain	nucleotide binding domain
N-glycosylation	asparagine-linked glycosylation
N-terminal	amino terminal
Na^+/K^+-ATPase	sodium-potassium pump / sodium-potassium ATPase
Na_2HPO_4	sodium hydrogen phosphate
NaCl	sodium chloride
Ni	nickel
NLS	nuclear localization signal
nm	nanometer
NP-40	nonidet P40
O- linked glycosylation	oxygen-linked glycosylation
o/n	overnight
$PI(4,5)P_2$	phosphatidylinositol-4,5-bisphosphate
$PI(3,4,5)P_3$	phosphatidylinositol-3,4,5-triphosphate
PAGE	polyacrylamide gel electrophoresis
PBS	phosphate buffer saline

PCR	polymerase chain reaction
P-domain	phosphorylation domain
PMFS	phenylmethylsolfonyl fluorid
psi	pressure per square inch
Q	glutamine
R	arginine
rcf	relative centrifugal force
RNA	ribonucleic acid
RNAi	RNA interference
rpm	rounds per minute
RT	room temperature
rtTA	reverse tetracycline-responsive transcriptional activator
s	second
SDS	sodium dodecyl sufate
siRNA	small interfering RNA
SRP	signal-recognition particle
T	threonine
Tat	trans-activator of transcription
TGN	*trans*-Golgi network
TRE	tet-response element
t-SNAR	soluble N-ethylmaleimide sensitive factor attachment protein receptor on the target membrane
u	unit
UB	unbound
UV	ultraviolet
VEGF	vascular endothelial growth factor
v/v	percent volume per volume
v/w	percent weight per volume
µ	micro
W	tryptophan
Y	tyrosine

6.2 Comprehensive analysis of the HDX data

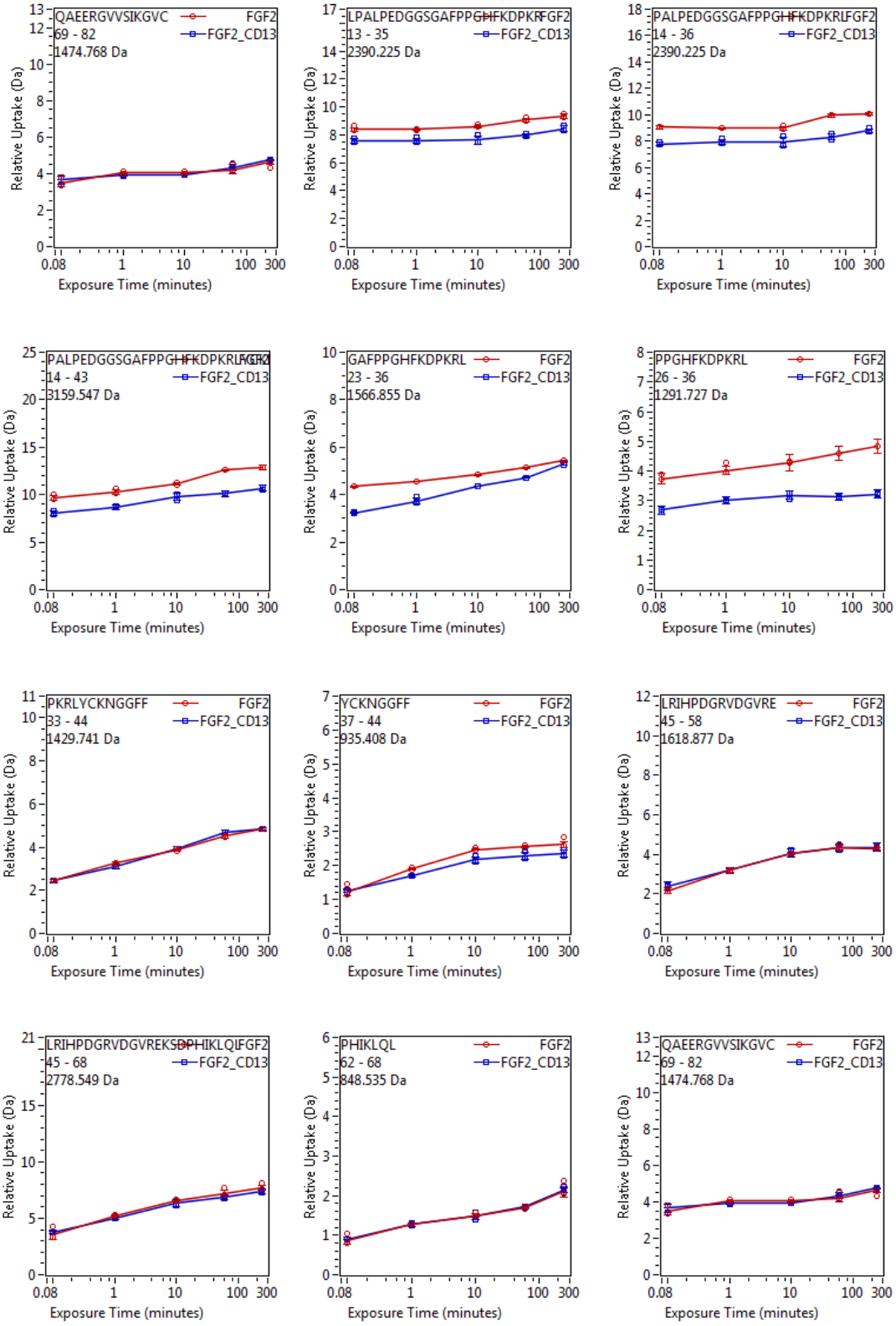

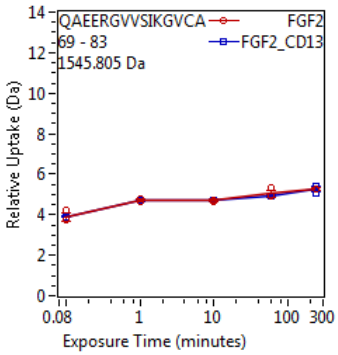
QAEERGVVSIKGVCA
69 - 83
1545.805 Da
FGF2
FGF2_CD13
Relative Uptake (Da)
Exposure Time (minutes)

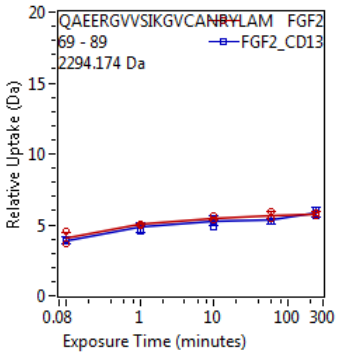
QAEERGVVSIKGVCANRYLAM
69 - 89
2294.174 Da
FGF2
FGF2_CD13
Relative Uptake (Da)
Exposure Time (minutes)

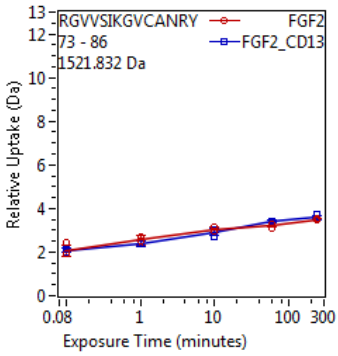
RGVVSIKGVCANRY
73 - 86
1521.832 Da
FGF2
FGF2_CD13
Relative Uptake (Da)
Exposure Time (minutes)

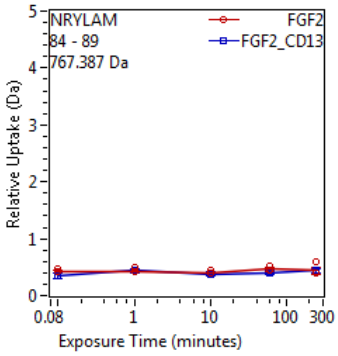
NRYLAM
84 - 89
767.387 Da
FGF2
FGF2_CD13
Relative Uptake (Da)
Exposure Time (minutes)

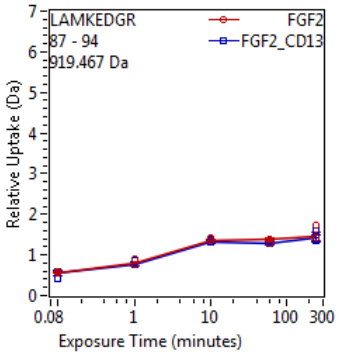
LAMKEDGR
87 - 94
919.467 Da
FGF2
FGF2_CD13
Relative Uptake (Da)
Exposure Time (minutes)

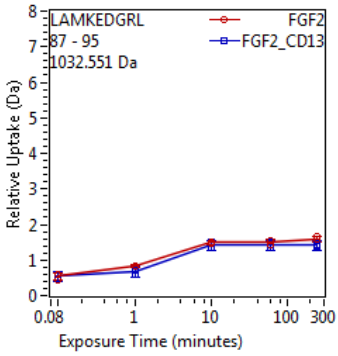
LAMKEDGRL
87 - 95
1032.551 Da
FGF2
FGF2_CD13
Relative Uptake (Da)
Exposure Time (minutes)

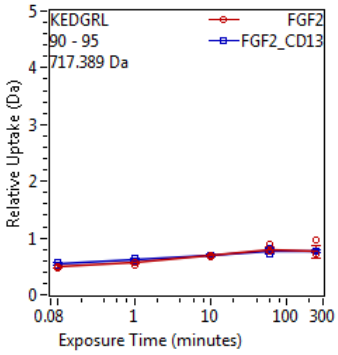
KEDGRL
90 - 95
717.389 Da
FGF2
FGF2_CD13
Relative Uptake (Da)
Exposure Time (minutes)

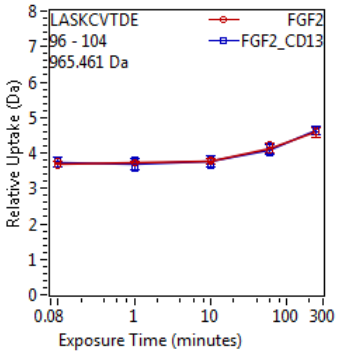
LASKCVTDE
96 - 104
965.461 Da
FGF2
FGF2_CD13
Relative Uptake (Da)
Exposure Time (minutes)

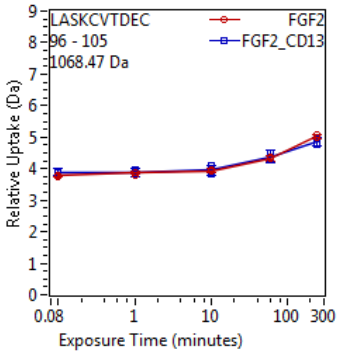
LASKCVTDEC
96 - 105
1068.47 Da
FGF2
FGF2_CD13
Relative Uptake (Da)
Exposure Time (minutes)

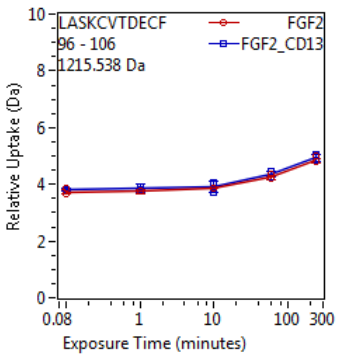
LASKCVTDECF
96 - 106
1215.538 Da
FGF2
FGF2_CD13
Relative Uptake (Da)
Exposure Time (minutes)

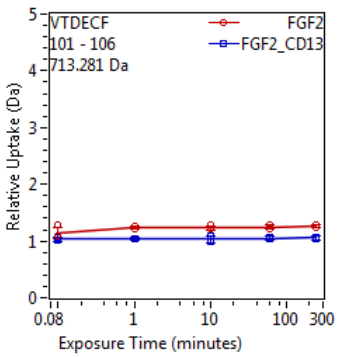
VTDECF
101 - 106
713.281 Da
FGF2
FGF2_CD13
Relative Uptake (Da)
Exposure Time (minutes)

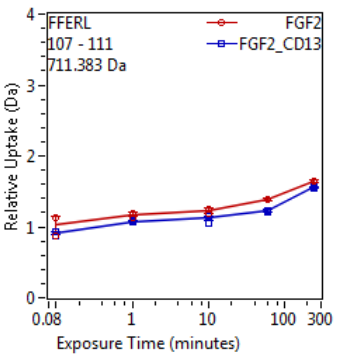
FFERL
107 - 111
711.383 Da
FGF2
FGF2_CD13
Relative Uptake (Da)
Exposure Time (minutes)

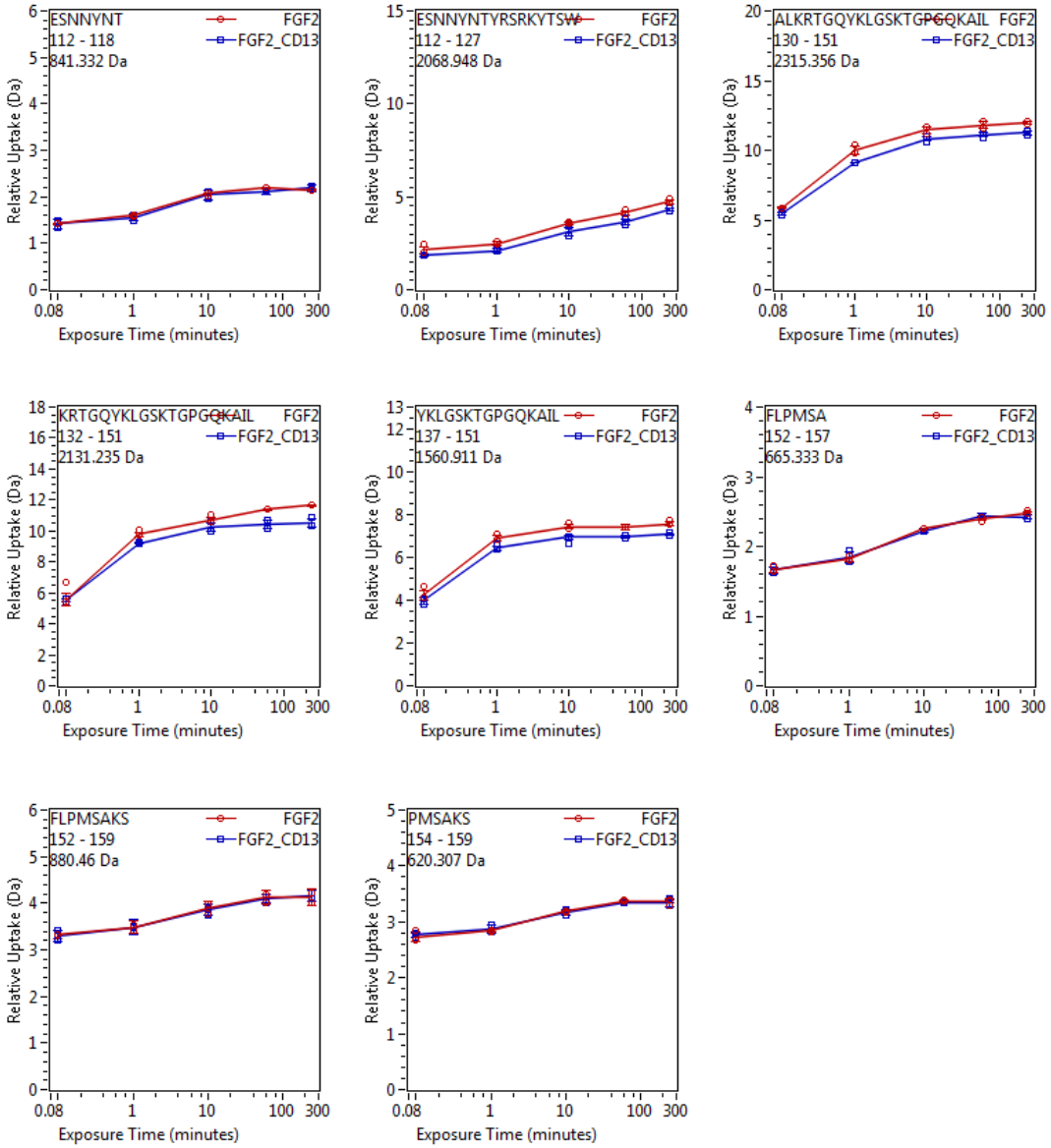

Figure 43: Total analysis of the HDX experiment of FGF2 without and in complex with hisCD1-3. FGF2 was analyzed either separately or in complex with hisCD1-3 subjected to HDX. FGF2 was analyzed alone (red) or in complex with hisCD1-3 (blue). For both reactions proteins were incubated for 1 h at RT before the continuous labeling with D_2O was initiated. Samples were taken at the following time points: 10 s, 1 min, 10 min, 1 h and 4 h and immediately afterwards subjected to pepsin digestion, peptide separation and mass spectrometry. The colored regions show peptides that have incorporated less deuterium because FGF2 was incubated together with hisCD1-3.

6.3 Publications

Ernst, A.M., Zacherl, S., Herrmann, A., Hacke, M., Nickel, W., Wieland, F.T., and Brügger, B. (2013). Differential transport of Influenza A neuraminidase signal anchor peptides to the plasma membrane. FEBS Lett. *587*, 1411–1417.

Steringer, J.P., Bleicken, S., Andreas, H., Zacherl, S., Laussmann, M., Temmerman, K., Contreras, F.X., Bharat, T.A.M., Lechner, J., Muller, H.-M., et al. (2012). PI(4,5)P2 Dependent Oligomerization of Fibroblast Growth Factor 2 (FGF2) Triggers the Formation of a Lipidic Membrane Pore Implicated in Unconventional Secretion. J. Biol. Chem.

6.4 Acknowledgements

I am deeply grateful to Prof. Dr. Walter Nickel for giving me another chance to conduct my PhD thesis. I am very thankful that I got the opportunity to undertake my PhD studies in his lab on this interesting project and especially for his patience, help, encouragement and guidance throughout my PhD. I very much appreciated his positive attitude towards science during this time.

I want to thank Prof. Dr. Oliver Fackler and Prof. Dr. Thomas Söllner for scientific advices during this thesis and to Prof. Dr. Sabine Strahl and Dr. Vytaute Starkuviene-Erfle for being my examiners.

Many thanks, to all collaborators that contributed a lot to the progression of my PhD. Many thanks to Prof. Dr. John Engen, who offered me the opportunity to learn HDX within his lab and especially to Dr. Roxana Iacob and Dr. Thomas Wales for amazing subversion and constant help. Many thanks, to Dr. Joe Lewis who made it possible to conduct the AlphaScreen in his lab and a special thanks to Dr. Peter Sehr with all the theoretical and experimental assistance.

Moreover, I am indebted very much to Sabine Wegehingel and Dr. Hans-Michael Müller with their continuous help during the past few years all these years to make this PhD thesis possible. Many thanks, to all members in the lab that accompanied me during this time. I enjoyed it very much to have spent all these hours with you in the lab, with many scientific but also amusing discussions and thank you all for the encouragement during this time! Many thanks to Georg Weidmann, who made the start of my PhD very easy, to Giuseppe La Venuta for endless philosophic and profound scientific discussions, to Julia Steringer who was always willing to help me with any scientific questions and to share many joyful hours with me at the ski trip. Not forgetting to mention Helena Weber with her never-ending patience and help with all the corrections and Tao Wang who was always full of surprises.

Special thanks, to all my friends who continuously supported me whenever there was need and to Giuliano, who always believed in me.

Der größte Dank gehört meinen Eltern die mich immer unterstützt haben während all der Zeit in meinem Studium, meiner Doktorarbeit und überhaupt in meinem Leben. Ohne Euch wäre das nicht möglich gewesen. Danke!